PROCESSING OF ULTRA-HIGH MOLECULAR WEIGHT POLYETHYLENE (UHMWPE) WITH REGULAR AND SPECIAL INJECTION MOLDING TECHNOLOGIES

By

Galip Yilmaz

A dissertation submitted in partial fulfillment of the requirements for the degree of

Doctor of Philosophy

(Mechanical Engineering)

University of Wisconsin–Madison

2020

Date of final oral examination: 17th January 2020

This dissertation is approved by the following members of the Final Oral Committee:

Lih-Sheng Tom Turng, Professor, Department of Mechanical Engineering

Majid Sarmadi, Professor, School of Human Ecology

Shaoqin Gong, Professor, Department of Biomedical Engineering

Frank Pfefferkorn, Professor, Department of Mechanical Engineering

Pavana Prabhakar, Assistant Professor, Department of Civil and Environmental Engineering

ACKNOWLEDGEMENTS

Foremost, I would like to express my deepest gratitude to my advisor, Professor Lih-Sheng (Tom) Turng for his enduring direction, guidance, and encouragement. His unique positive attitude and support will be always appreciated. It has been an honor and a privilege working in his research group.

I would like to acknowledge my Ph.D. committee: Professor Majid Sarmadi, Professor Shaoqin (Sarah) Gong, Professor Frank Pfefferkorn, and Professor Pavana Prabhakar for their great instruction and precious time.

I'd like to thank my current and former laboratory colleagues: Dr. Thomas Ellingham, Dr. Hrishikesh Kharbas, Dr. Yiyan Peng, Dr. Jason McNulty, Dr. Yiyang Xu, Dr. Sebastian Goris, Dr. Roberto Monroy, Abrahan Bechara, Stefanie Glas, and Huaguang Yang for all the help, training, and suggestions.

I would like to thank Chris Lacey for her great work on editing my thesis and journal papers, as well as helping me with my presentation skills. I'd also like to thank George Petry at the Morgridge Fab Lab and Anna Kiyanova at the Soft Materials Laboratory for their training and for helping me with whatever I needed.

I would also like to acknowledge the Celanese Corporation for their donation of materials and their technical support. I also gratefully appreciate the support from the Wisconsin Institute for Discovery (WID), the Kuo K. and Cindy F. Wang Professorship, the College of Engineering, and the Office of Vice Chancellor for Research and Graduate Education at the University of Wisconsin–Madison. Finally, I am thankful to SABIC for generously supporting my research.

ABSTRACT

In this work, the processing of a unique ultra-high molecular weight polyethylene (UHMWPE) polymer, in both powder and pellet form, using both regular and special injection molding techniques, was investigated in an effort to mass produce this high-grade specialty polymer. The goals of this study were to (i) improve the processability of UHMWPE, (ii) enhance the mechanical performance and overall quality of the molded parts, and (iii) develop an in-depth understanding of how the supercritical fluid (SCF), machine configuration, mold compression, mold insulating techniques, and process conditions affect the flow behavior and final quality of the injection molded UHMWPE.

In the first study, two common atmospheric gases in their supercritical states—namely, nitrogen (scN_2) and carbon dioxide ($scCO_2$)—were used as processing aids in a special full-shot, high-pressure microcellular injection molding (MIM) process for processing UHMWPE pellets. The mechanical properties in terms of tensile strength, Young's modulus, and elongation-at-break of the SCF-loaded samples were examined. The thermal and rheological properties of regular and SCF-loaded samples were also analyzed using differential scanning calorimetry (DSC) and parallel-plate rheometry, respectively. It was found that the processing of UHMWPE with both gases effectively reduced the thermal degradation of the material and the injection pressure, compared to regular injection molding, while still retaining the mechanical properties of the resin.

In the second part, a follow-up study was conducted on conventional injection molding (IM), along with the special full-shot, high-pressure microcellular injection molding (MIM) using UHMWPE in pellet form. A relatively complicated and thin-walled mold design was used to produce box-shaped parts with varying wall thickness. Although different processing settings

were tested in order to eliminate persistent short shot issues, only high-pressure MIM processing was able to fill parts completely. Furthermore, not only did high-pressure MIM processing effectively promote the processability of UHMWPE, it also reduced the very high injection pressure requirement and the high part shrinkage issues associated with the IM samples.

In the third study, UHMWPE powder was processed using injection molding (IM) and injection–compression molding (ICM). The processing parameters of feeding the powders were optimized to ensure proper dosage and to avoid damaging UHMWPE's molecular structure. Dynamic mechanical analysis (DMA) and Fourier-transform infrared spectroscopy (FTIR) tests confirmed that the thermal and oxidative degradation of the material was minimized but crosslinking was induced during molding. Tensile tests and impact tests showed that the ICM samples were superior to the IM samples. A delamination skin layer was formed on the IM sample surfaces, while it was absent in the ICM samples, thus suggesting two different flow behaviors between IM and ICM during the packing phase.

The delamination layer defect was the subject of the fourth study as one of the main challenges of UHMWPE molding. The delamination layer hampers UHMWPE's two key properties: wear resistance and impact strength. A mold insulation method was employed to eliminate the formation of the delamination layer. The working principle of the method was to reduce the cooling rate and the shear stress of the polymer while improving polymer chain "interdiffusion" across the entangled chain bundles during the injection filling stage via a low thermal conductivity mold coating (e.g., epoxy coating). This method yielded molded parts free of delamination by delaying skin cooling during filling and packing. Therefore, it produced parts with enhanced mechanical properties, excellent impact strength, and improved surface quality.

TABLE OF CONTENT

LIST OF FIGURES

LIST OF TABLES

1. INTRODUCTION

1.1. Introduction of UHMWPE

Polyethylene (PE), the most common engineering polymer, is simply comprised of basic ethylene monomers. However, its simplicity is only cognitive. Its physical structure is very complex and can be arranged in an almost infinite number of ways to create one of the widest ranges of products [1], [2]. As a linear homopolymer polyethylene, ultra-high molecular weight polyethylene (UHMWPE) holds a special place among other PE grades. It has an extremely high molecular weight, typically more than 1 million g/mol, that yields many favorable properties for industrial and medical applications. However, its high molecular weight adversely affects its melt processability because of its extremely high viscosity and highly entangled molecular structure [3], [4]. The resistance of UHMWPE against corrosive chemicals, wear, and impact forces is very high and far exceeds that of many other polymers, including other PE grades. This resistance, based on its high molecular weight and the resulting structure, opens up various applications for UHMWPE [5], [6]. Some other prominent properties of UHMWPE include a low friction coefficient, self-lubricating behavior, a very low service temperature, and noise dampening properties [4].

1.2. Processing Methods of UHMWPE

After its commercialization in the 1950s, UHMWPE has been used in two particular applications: high-performance fibers and artificial joint bearings for orthopedic applications [4], [7]. Figure 1.1 shows some advanced and specialized products typically made of UHMWPE.

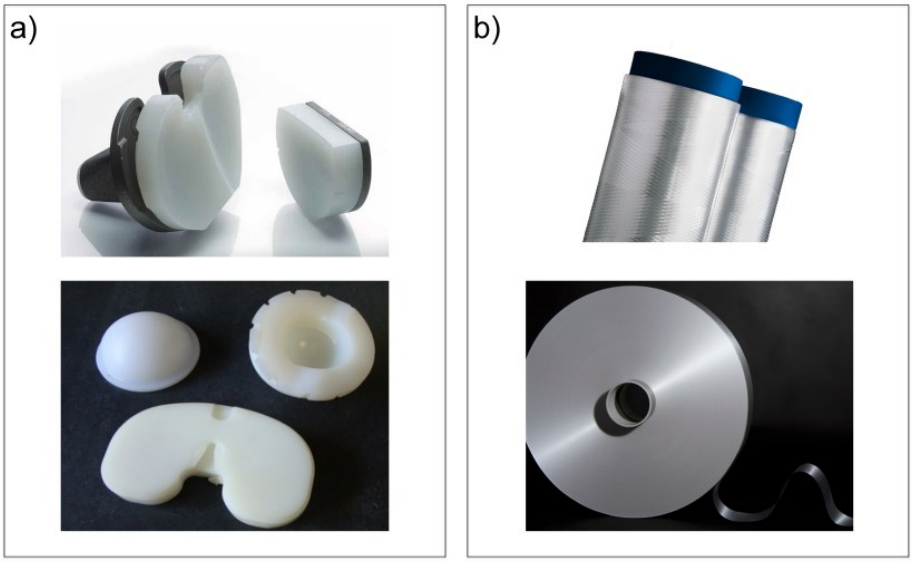

Figure 1.1. Applications of UHMWPE: (a) orthopedic implants in the medical field [8] and (b) high-strength fibers and film for in the industrial field applications [9].

1.2.1. Gel-Processing

Two conventional methods have been developed and employed to process UHMWPE for these applications [3]. The first method, called "gel-processing," is usually encountered in fiber or film making. Various solvents, such as decalin, are used to disentangle the UHMWPE chains and to increase its processability. However, large amounts of solvent, up to 90%, are needed for effective processing [10], [11]. There are some methods that have been suggested for lower solvent usage, such as 20% and even lower [7], [11]; however, none of these methods are practical for injection molding because even a small amount of latent solvent may ruin UHMWPE's mechanical properties [12]. Lastly, solvent cleaning and recovery processes are not economical for injection-molded parts because of the relatively large thickness of the molded parts (>1 mm) compared to the characteristic thickness of a fiber (<50 μm), thus making it difficult to clean and remove the solvent [13].

1.2.2. Ram Extruding and Compression Molding

The second conventional processing method for UHMWPE uses high-pressure ram extruding or compression molding at relatively small shear rates. This method can be seen in orthopedic implant manufacturing. These approaches may not be practical in injection molding because the shear rate for injection molding is very high [3], [14]. In injection molding, the material is forced through a small gate into the cavity at relatively high flow rates and then cooled quickly. If the shear rate or flow rate is reduced in injection molding, larger pressure values reaching conventional machine limits or short shots may result from premature freezing [15], [16]. Nevertheless, if appropriate part designs, machine parameter settings, and proper injection molding machines and technologies are used, it is possible to successfully injection mold UHMWPE. We will explore this further in this study.

1.2.3. Emerging Processing Methods of UHMWPE

Besides these conventional methods, there are some novel studies aimed at developing easily processable UHMWPE based on the synthesis of nascent powders with lower entanglement densities of the polymer chains. Some polymer synthesis techniques based on reducing polymerization temperatures and lowering monomer pressures have been developed to produce less entangled polymers [17]–[20]. To the best of our knowledge, none of these synthesized materials has been scaled up from the laboratory to the industrial scale. One of the drawbacks of this type of UHMWPE is its tendency to entangle when heated above its melting point [21]. Nevertheless, these methods could still be promising for improving UHMWPE processing in the future.

1.2.4. Processing UHMWPE with Supercritical Fluid (SCF) as a Plasticizer

Supercritical fluid (SCF) can be used in UHMWPE during melt processing as a reversible plasticizer. SCF is simply a gas that has been highly pressurized and heated beyond its so-called critical temperature and critical pressure. These critical points are unique for each gas. For example, the critical temperature and pressure for CO_2 are 31 °C and 7.37 MPa, respectively, and for N_2 they are –147 °C and 3.39 MPa, respectively [22]. SCFs are unique in that they exhibit liquid behavior when dissolved in solid substances but have the high diffusivity of a gas [22], [23]. Depending on the weight percentage of SCF used, they can reduce the viscosity of the polymer melt and change the flow behavior [24]. SCFs also act as reversible plasticizers because they can leave the polymer matrix simply by diffusing out after processing is complete. Furthermore, SCFs are advantageous because they can eliminate tedious solvent handling and all post-processing operations [25]–[27].

1.3. Injection Molding of UHMWPE Powder and Pellets

UHMWPE is commonly available in powder form, although many typical PE resins are provided in pellet form [28]. This is because the UHMWPE synthesis process produces a powder and its thermal and viscoelastic properties obstruct the economical pelleting process [29]. Nevertheless, relatively costly and special pelleting processes have been developed and commercialized to sinter UHMWPE powder into pellet form [30], [31]. Figure 1.2 shows an image of UHMWPE powder and pellet resins and their SEM images. The pellet resin (GUR® 5129) in Figure 1.2 (c) is being produced and commercialized based on some patents [28], [29], [31]. Figure 1.2 (d) shows an SEM image of the surface of one of the UHMWPE pellets. It seems that the fine particles of the UHMWPE were bonded by a polymer matrix, which was

most likely a low molecular weight PE used as a binder of the UHMWPE powder particles (Figure 1.2 (d)) as described in the patent literature [28], [29]. The main motivation for creating pellets is to overcome the difficulties associated with handling and processing powders for processes or machines used in injection molding. However, the scope of the processing method in this study is meant to be applicable to both forms as long as the correct machine, processing parameters, and mold design is used.

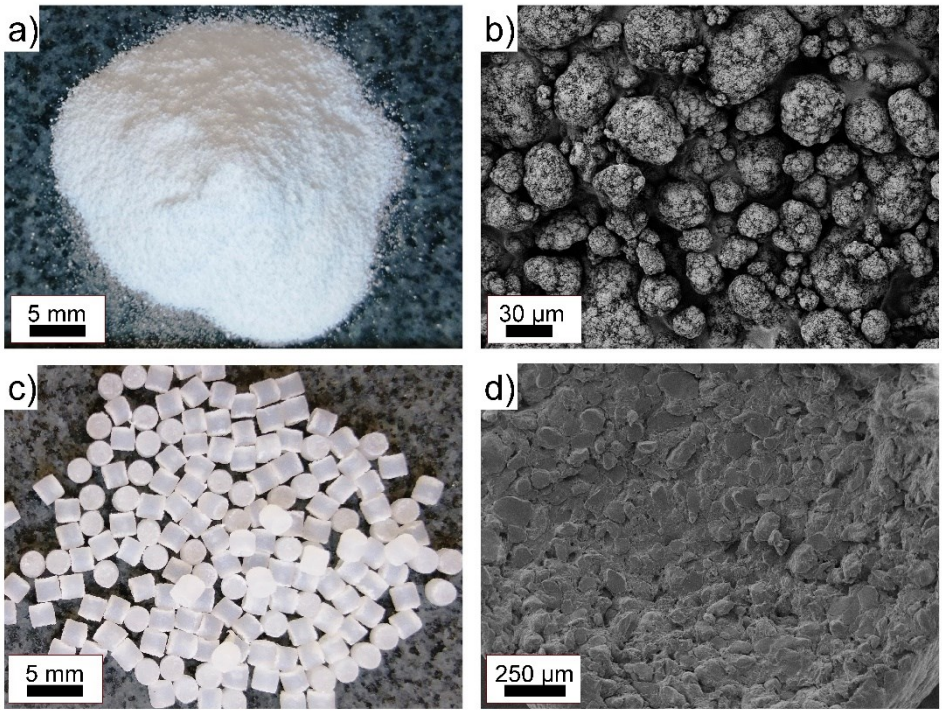

Figure 1.2. UHMWPE powder and pellet resin types: (a) photograph of powder resin, (b) SEM image of a powder pile, (c) photograph of pellet resin, and (d) SEM image of the surface of a single pellet.

Plastic injection molding technology is the most versatile and economical manufacturing method when a complex part design is needed at high manufacturing rates [32]. To the best of our knowledge, the literature that focuses on the injection molding of UHMWPE in pellet form is limited to a few studies [33]. This might be due to the difficulty of processing UHMWPE and the limited quantity and higher cost of obtaining injection molding grades of UHMWPE in pellet

form. Alternatively, powder resins are easy to find and well-known for some applications. However, processing and handling powders in injection molding is very difficult, which may explain why there are so few attempts at using UHMWPE powder resins in injection molding in the literature [16], [34]. One of the disadvantages of powder resin is the dusting of fine particles (Figure 1.2 (b)), which is a main concern during the transfer and handling of plastic powder resins. Another problem is the proper feeding of the fine powder material into the injection molding barrel, which is delicate and specific to the processing conditions and machine types. However, UHMWPE powder resins might be preferable to pellets because they can be more economical and easier to compound prior to injection molding.

1.4. Rheological Properties of UHMWPE

When the temperature is raised above the melting point, most engineering thermoplastics, such as high-density polyethylene (HDPE), show a typical transition from elastic behavior to viscous behavior. However, when the molecular weight is above 500,000 g/mol, this transition is obstructed by the high degree of entanglement of the polymer chains, which restricts the molecular motion of the chains [4]. Figure 1.3 shows the molecular weight of UHMWPE and other PEs on a logarithmic scale. The molecular weight of HDPE ranges from 50,000 to 250,000 g/mol, while paraffin wax (PW) is usually lower than 1,000 g/mol [4]–[6]. This comparison helps to illustrate how high the molecular weight of UHMWPE is compared to other grades of PE.

The flow mechanics and rheological properties of the UHMWPE melt are greatly influenced by its extreme molecular weight. The typical flow behavior of many engineering polymers in the channel of the mold is characterized by so-called “fountain flow” behavior. When the polymer

melt touches the cold mold surface, it builds a growing solid layer (frozen layer) during mold filling. Meanwhile, the flowing hot core advances through the narrowing center due to the growing solid frame. The melt velocity becomes faster at the center and has zero velocity at the solid–melt interface [35]. At the melt front, a combination of shear and extensional flows continuously force the fluid elements from the center core to the mold wall, creating an outward trajectory that is commonly referred as "fountain flow" behavior until the filling cycle is complete.

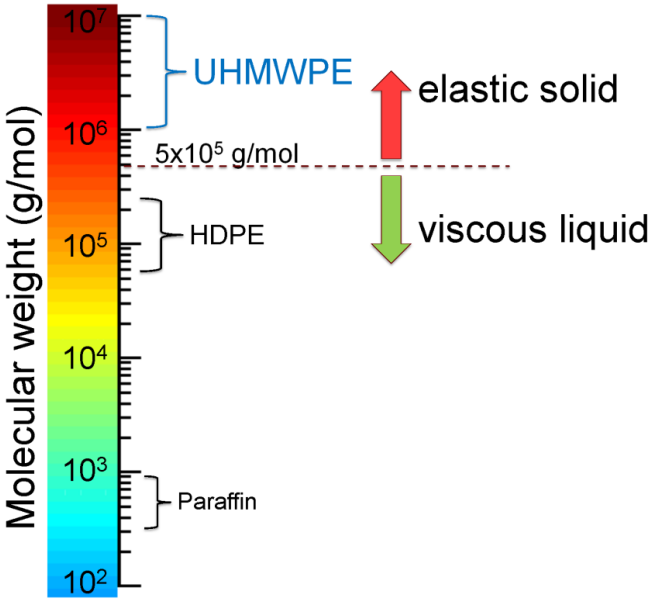

Figure 1.3. Schematic molecular weight comparison of UHMWPE to other PE grades.

However, with UHMWPE, even at a temperature well above its melting point, the flow does not completely demonstrate the fountain flow behavior, especially at the beginning of mold filling. In particular, it has been observed that the UHMWPE melt does not stick to the mold surface easily and instead tends to exhibit so-called "plug flow" behavior. In this type of flow, the velocity of the melt is assumed to be constant across the mold thickness direction. Another strange behavior of UHMWPE is that the melt enters the mold cavity as a porous material that

looks like popcorn due to severe melt fracture instead of as a continuous and progressive melt. For example, in the literature, Gorden et al. [16] described a method of manufacturing UHMWPE porous parts by canceling the packing cycle. Their method was simply based on melt fracture without the use of any blowing agents or foaming additives. If solid parts are needed, the packing cycle of injection molding can be applied to compress and consolidate this porous structure.

1.5. Thermal Degradation of Melt-Processed UHMWPE

UHMWPE is thermally stable, although melt processing at high shear rates can cause undesirable thermal degradation that can severally affect UHMWPE's properties, such as the its wear and impact resistance, as well as its other mechanical properties. Therefore, the injection molding process should be carefully employed to avoid any severe thermal degradation. Additionally, the final products should be monitored to correct for any unacceptable thermal degradation.

1.6. Summary

In summary, UHMWPE is a material with high impact strength, wear resistance, self-lubrication, and chemical inertness that has great commercial potential if its processing challenges such as high viscosity, lack of fluidity, delamination layer, difficulty in handling powder form, can be overcome. Injection molding is one of the most widely used and efficient polymer processing methods, and as such, the ability to effectively injection mold UHMWPE would enable it to be used in a variety of important applications across a wide number of industries. This thesis has explored various solutions to these processing challenges and has

thereby opened the door for UHMWPE to be injection molded, thus enabling it to be utilized across a wide array of industry sectors for a variety of applications.

2. IMPROVED PROCESSABILITY AND THE PROCESSING–STRUCTURE–PROPERTIES RELATIONSHIP OF ULTRA-HIGH MOLECULAR WEIGHT POLYETHYLENE VIA SUPERCRITICAL NITROGEN AND CARBON DIOXIDE IN INJECTION MOLDING

2.1. Abstract

The processability of injection molding ultra-high molecular weight polyethylene (UHMWPE) was improved by introducing supercritical nitrogen (scN_2) or supercritical carbon dioxide ($scCO_2$) into the polymer melt, which decreased its viscosity and injection pressure while reducing the risk of degradation. When using the special full-shot option of microcellular injection molding (MIM), it was found that the required injection pressure decreased by up to 30% and 35% when $scCO_2$ and scN_2 were used, respectively. The mechanical properties in terms of tensile strength, Young's modulus, and elongation-at-break of the SCF-loaded samples were examined. The thermal and rheological properties of regular and SCF-loaded samples were analyzed using differential scanning calorimetry (DSC) and parallel-plate rheometry, respectively. The results showed that the temperature dependence of UHMWPE was very low, suggesting that increasing the processing temperature is not a viable method for reducing injection pressure or improving processability. Moreover, the use of scN_2 and $scCO_2$ with UHMWPE and MIM retained the high molecular weight, and thus the mechanical properties, of the polymer, while regular injection molding led to signs of degradation.

2.2. Introduction

Ultra-high molecular weight polyethylene (UHMWPE) is a linear homopolymer polyethylene that possesses many desirable solid-state characteristics [3]. When comparing

UHMWPE to well-known polyethylene grades such as high-density polyethylene (HDPE), its distinct properties are directly associated with its ultra-high molecular weight, which ranges from 1–6 million g/mol, compared to 0.05–0.25 million g/mol for HDPE [4], [5], [15]. Owing to its ultra-high molecular weight, UHMWPE has many high-performance properties, including high abrasion resistance, high toughness and fiber modulus, great chemical inertness, low friction coefficient, self-lubrication behavior, very low service temperature, noise dampening, and more.

As a result, UHMWPE has found successful applications in many industrial and medical sectors. For example, it has been employed in high-performance fiber products, artificial joint prosthesis, bearings, bumpers, and the sliding parts of production lines [4], [7], [36]. Its chemical inertness, low friction, and wear-resistant features make it a useful material for parts where lubricants could cause contamination or maintenance problems, such as in food and medical applications [3], [37].

However, the ultra-high molecular weight that yields these desirable properties and applications also hinder the fabrication of UHMWPE by standard polymer processing methods, such as injection molding (IM), as it requires a very high processing pressure due to its high melt viscosity and lack of fluidity [3], [4], [38].

In the plastics processing industry, injection molding is one of the most important processes due to its wide range of processable materials, ready-to-use final products, capability to make complex parts, short cycle time, and high degree of automation [32]. It is estimated that injection molding is used to process approximately one-third of all thermoplastic materials, with the process encompassing around one-half of all plastic processing equipment [14].

At present, only a few UHMWPE grades in granular form are available for injection molding. Its original powder form is unsuitable for injection molding, even when using specially designed screws for powder resins. Due to its high viscosity, molding UHMWPE requires high injection rates and injection pressures (values such as 110 MPa compared to 55–70 MPa for most polymers) [15], [39]. Although the special grades of UHMWPE allow for injection molding, a further understanding of their behavior is necessary to take advantage of all of the potential benefits and achieve optimal and reliable processing conditions. Moreover, if the processing of UHMWPE is not performed properly, the product quality can suffer due to thermal degradation.

Given its processing challenges, research literature on the injection molding of UHMWPE remains scarce. To the best of our knowledge, injection molding of UHMWPE is limited to Kuo's work [33], [40]. In these studies, the injection molding of UHMWPE, process optimization for improved mechanical properties, and tribological characteristics were investigated.

There are two well-known approaches for successfully fabricating UHMWPE parts: (1) using high-pressure settings or (2) reducing the viscosity via solvents [3]. Solvents, including mineral oil, paraffin wax, decalin, and xylene, have been used successfully to process UHMWPE [7]. However, some tedious post-processing operations are necessary to clean parts and reclaim and recycle the solvents. Also, the high pressures required for processing increases tool wear and manufacturing costs.

An effective method for overcoming the high viscosity of UHMWPE is by using supercritical fluid (SCF) as a plasticizer. A compressed atmospheric gas, such as N_2 or CO_2 above its critical temperature and pressure values (cf. Table 2.1), is referred to as an SCF. An

SCF exhibits the density of a liquid but has the high diffusivity and low viscosity of a gas. This specific phase allows not only accurate metering and pumping as a liquid, but also an increased diffusion rate into the polymer as a gas [22], [23].

Once SCF is diffused into the polymer melt evenly, it can reduce the viscosity and the glass transition temperature of the polymer depending on the weight percentage of SCF used [24]. The physical effect that SCF has on UHMWPE can be described by two mechanisms. The first and dominant mechanism is the increased free volume among entangled polymer chains. The secondary mechanism is decreased chain entanglement due to the dilution of the polymer via the addition of the dissolved SCF [41]. The SCF also acts as a reversible plasticizer because it can leave the polymer matrix simply by diffusing out after processing is complete or when the thermodynamic instability is triggered due to changes in pressure or temperature. However, there are some drawbacks of SCFs, such as the need for high-pressure equipment. Nonetheless, SCF is still commonly used with favorable results because it can eliminate tedious solvent handling and all post-processing operations [25]–[27].

In this study, atmospheric gases, which are less expensive and unregulated—namely, N_2 and CO_2, were used in their supercritical state [22]. Several studies have been done on the plasticizing effects of supercritical CO_2 in various polymer processing methods [26], [27], [41]–[44]. Wilding et al. showed that the effect of supercritical CO_2 on viscosity intensifies as the molecular weight of the linear PE grade increases [45]. This suggests that the viscosity of UHMWPE can be reduced effectively via SCF. Moreover, supercritical N_2 has received some attention as an alternative to CO_2 for processing, especially for polyethylenes like LDPE [46]. In practice, injection molding using supercritical N_2 as a foaming agent is more common because it yields a finer and denser foamed microstructure [25], [47]. The main advantage of N_2 over CO_2

is that the back pressure required to keep N_2 in its supercritical state is much lower (~54%) than the back pressure required for CO_2 [23]. A higher back pressure requires a longer dosage time, which is undesirable. On the other hand, the estimated maximum gas solubility of CO_2 is almost four times higher than N_2 in PE at 200 °C [22]. Therefore, CO_2 may have more potential to modify the melt properties when a higher amount of SCF is needed.

One of the commercially available technologies used to introduce SCF into the polymer is the microcellular injection molding (MIM) process. In this process, SCF is first dosed and injected into the injection molding barrel and mixed with the polymer melt during the dosage cycle. Thanks to the properties of SCFs, it diffuses to form small gas bubbles and eventually dissolves in the polymer matrix, thus creating a so-called "single-phase polymer–SCF solution" [22], [23], [48]. As the high- pressure polymer–SCF solution enters the mold cavity, a sudden pressure drop causes the nucleation of bubbles, which expand to create a foamed product without the need for a packing cycle. This is because the expanding gas bubbles increase the volume of the foamed polymer, which compensates for material shrinkage as it cools, and thus fills the entire mold cavity [49]–[51]. The main usage of the MIM process is to create very fine and lightweight polymer foams with a typical average cell size of 3–100 μm [23], [52] and a cell density of over 10^6 cells/cm^3.

Occasionally, solid products instead of foamed ones can also be produced while utilizing SCF in the MIM process. This process option is called high-pressure foam injection molding (FIM) [53]. In this case, the entire mold cavity is filled with a full shot volume's worth of material and then packing pressure is applied to suppress gas expansion and re-dissolve the gas into the polymer melt. In high-pressure FIM, the cells may or may not be eliminated completely

depending on the processing parameters, such as the pressure in the cavity, SCF content, temperature, and polymer type [53], [54].

In this study, the high-pressure foam injection molding option of the MIM process was used to produce solid parts rather than foamed ones in the UHMWPE injection molding experiments. Utilization of the plasticizing effect of supercritical N_2 and CO_2 was the aim. After the injection cycle, packing pressure was applied to block cell nucleation and re-solubilize the escaping gas. The injection molding of foamed UHMWPE parts using MIM was found to be a more involved project than their solid counterparts and remains an active on-going research subject. Herein, the processability in terms of injection pressure values and mold filling behavior of tensile bars, tensile properties, rheological properties, DSC data, and microstructure in forms of micro-computed tomography (μCT) images of the solid samples will be presented.

2.3. Materials and Methods

An injection molding grade of UHMWPE resin (GUR® 5129) was provided by Celanese Corporation (Irving, TX, USA). It had a viscosity average molecular weight of 4.7 million g/mol and a density of 0.93 g/cm^3. Industrial grade carbon dioxide (CO_2) and nitrogen (N_2) were purchased from Airgas (Greenville, SC, USA) and used as the SCF source for MIM.

2.3.1. Methods

A MIM-equipped injection molding machine, Arburg Allrounder 320S, with a 25 mm diameter screw, was used to introduce scCO_2 and scN_2 into the melt. Here, the main purpose was to make a solid part rather than a foamed product by applying sufficient packing pressure to compress the full-size melt and suppress foaming. One critical requirement for the injection molding of UHMWPE is that the compression ratio of the screw must be less than 2.5:1, and

preferably 2:1, due to the absence of melt flow based on the ISO 1133 standard. The compression ratio of the injection molding screw can be defined as the ratio of the feed section channel depth to the metering section channel depth [14]. The machine used in this study had a 2.5:1 compression ratio. Table 2.1 shows the injection molded sample types and SCF loading percentages used in this study. The percent of SCF loading used was determined experimentally to introduce a high and controllable amount of SCF.

Table 2.1. Sample name and SCF loading percent.

Sample Name	**SCF**	**Critical points**	**Loading % by Weight**
Regular	N/A	N/A	0
CO_2 sample	CO_2	31 °C, 7.37 MPa	1.5
N_2 sample	N_2	-147 °C, 3.40 MPa	1.5

Table 2.2. Processing parameters used in injection molding.

Processing Parameters	**Units**	**Value**
Injection speed	cm^3/s	80
Injection vol.	cm^3	17.2
Cooling time	s	25
Back pressure	MPa	Regular: 0.5 N_2: 5 CO_2: 8
Packing pressure	MPa	110
Packing time	s	7
Nozzle temp.	°C	260
Mold temp.	°C	80

The processing parameters used for injection molding are listed in Table 2.2 and were set according to the material's molding recommendations and the machine type used. The back pressure was adjusted for each gas to keep the SCF in its supercritical state.

An aluminum mold designed and machined in-house was used to produce ASTM Type I tensile bars with a 2 mm thick fan gate. Figure 2.1 shows the mold cavity and the sprue location, which was located on top of the fan gate without a runner to minimize additional pressure requirements. Prior to any characterization experiments, the injection molded UHMWPE samples were stored for at least one week to allow the dissolved gas to completely diffuse out.

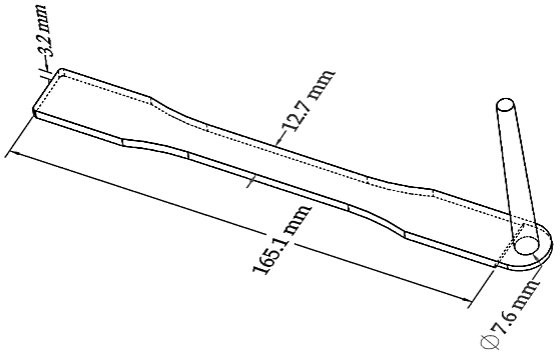

Figure 2.1. Schematic of the injection molded specimen ASTM D638 Type I tensile bar mold cavity with its sprue.

2.3.2. Differential Scanning Calorimetry

Differential scanning calorimetry (DSC) was conducted according to the ASTM F2625-10 (2016) standard test method on a TA Instruments Q20 (New Castle, DE, USA) to measure the enthalpy of fusion, percent crystallinity, and the melting point of the UHMWPE samples. The procedure was applied from ambient temperature to 200 °C, with a heat/cool/heat cycle at a 10 °C/min scanning rate. Four tests for each type of sample were performed with a weight range of 5 to 8 mg. Test samples were cut from the middle of the tensile bar. The enthalpy of melting per sample mass was normalized against the theoretical enthalpy of melting of 100% crystalline

polyethylene to calculate the percentage of crystallinity in the test sample. The standard equation was used as follows,

$$\%\ Crystallinity = 100 \times \frac{\Delta H_s}{\Delta H_f} \quad (1)$$

where ΔH_s was the sample's heat of fusion per unit mass during the freezing transition. The heat of fusion of 100% crystalline UHMWPE, ΔH_f = 289.3 J/g, was used in the calculation [55].

2.3.3. Rheology

A stress-controlled rheometer, TA Instruments AR 2000ex, was used to measure the complex viscosity of the samples. Tests were conducted with 25 mm diameter parallel plates with a 1 mm gap. Samples were cut from the tensile test bars, then compression molded at 200 °C for 10 s at 1 mm thickness. When room temperature was reached, the samples were punched into 25 mm diameter disks. First, a stress sweep test was run to determine the linear viscoelastic region and 0.5% strain was selected for the following tests. Frequency sweep tests were conducted from 0.01 Hz to 100 Hz at a temperature of 260°C. For temperature dependency analyses, temperature ramp tests were run from 180°C to 280°C at two different frequencies, 0.1 Hz and 100 Hz, respectively. The temperature dependence of the materials was calculated using the following equation [56],

$$m(T) = m_o \cdot exp[-a(T - T_o)] \quad (2)$$

where $m(T)$ is the consistency index, m_o is the consistency index at the reference temperature, T_o, a is the temperature dependence or sensitivity coefficient, and T is the temperature at which the viscosity was measured.

2.3.4. Micro-Computed Tomography (μCT)

To examine if any bubbles formed in the samples, μCT scans were conducted with an industrial type Metrotom 800 μCT system from Carl Zeiss AG (Oberkochen, Germany). The scanning power was set at 32 kV and 120 μA for a 5 μm spot and voxel size. Image processing was performed using ImageJ software from the National Institutes of Health, US.

2.3.5. Tensile Tests

Tensile testing of the samples was performed on an Instron 5967 (Norwood, MA, USA) with a 30 kN load cell using ASTM D638-03 Type I tensile specimens. At least five samples of each type were tested with a crosshead speed of 50 mm/min as recommended in the standard. Before testing, all samples were examined with transmitted light to check for any remaining bubbles. Samples with defects were excluded. Moreover, the samples were weighed and compared to each other to eliminate any odd samples. A few samples were one standard deviation away from the mean and were also excluded.

2.3.6. Tensile Bar Images and Injection Pressure Measurements

To examine the mold-filing behavior of UHMWPE melt, the injection volume was reduced by 20% and the holding stage was canceled so that the injection pressure reduction and the effect of dissolved SCF on the shape of the short shots could be observed. Pressure data were collected at least five times for each injection speed setting from 10 cm^3/s to the maximum machine injection speed of 80 cm^3/s in 10 cm^3/s increments. All samples were weighed each time to ensure that the same amount of material was injected within 0.1 g.

2.4. Results and Discussion

2.4.1. Differential Scanning Calorimetry

The first and second heating DSC graphs of the neat and injection molded (regular, CO_2, and N_2) samples can be seen in Figure 2.2, and the data derived from the DSC test is reported in Table 2.3 and Table 2.4 for the first and second heating tests, respectively.

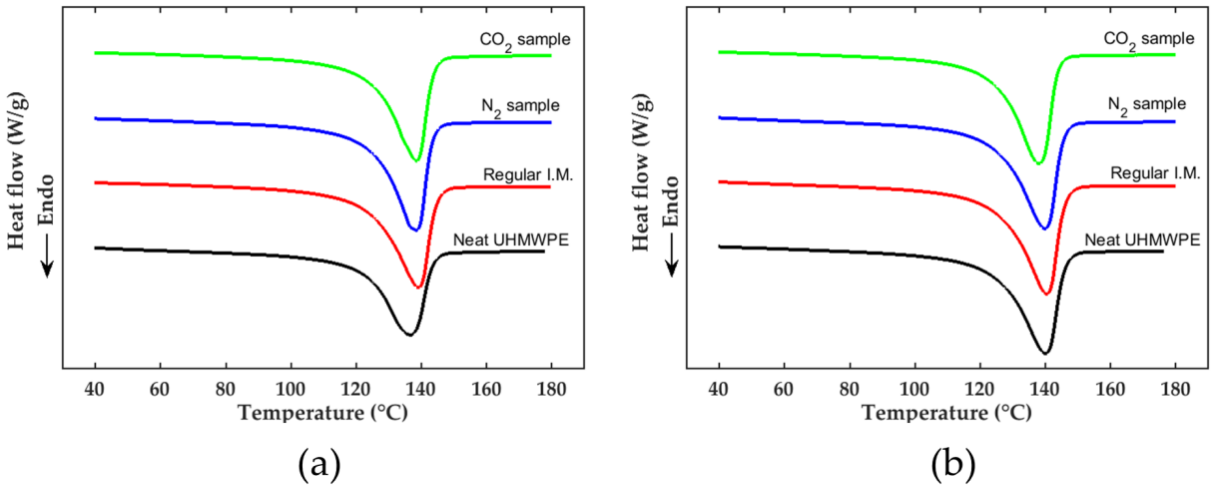

Figure 2.2. (a) The first heating and (b) the second heating of DSC graphs of the injection molded samples and neat UHMWPE.

In Figure 2.2 (a), the first heating curves for all injection molded samples seemed identical and showed a higher melting point than the neat sample. It is known that different thermomechanical (temperature–pressure) histories, as well as material degradation, can alter the first heating thermograms. The distinct factor in the thermal history of the injection molded samples is expected to be the presence of scN_2 and $scCO_2$ during processing. However, the degree of crystallinity (% crystallinity) of the samples tabulated in Table 2.3 was similar within the standard deviation. The degree of crystallinity of the neat sample was much less than the injection molded samples, likely due to a different thermomechanical history from its production process.

Table 2.3. The average thermal behavior of injection molded samples obtained from the first heating thermograms.

Sample	**T_m (°C)**	**ΔH_s**	**% Crystallinity**
Neat	136.9 ± 0.1	142.4 ± 1.9	49.2 ± 0.7
Regular	139.5 ± 0.4	158.2 ± 3.2	54.7 ± 1.1
N_2 sample	138.7 ± 1.0	161.1 ± 2.7	55.7 ± 0.8
CO_2 sample	138.6 ± 0.7	159.6 ± 2.2	55.1 ± 0.9

The difference between the regular and SCF-loaded injection molded samples was smaller than the standard error for each of them, thus indicating that SCF did not have a clear effect on the thermal properties. Even so, the N_2 and CO_2 samples had slightly higher-than-average degrees of crystallinity as compared to the regular sample: 1.0% more for the N_2 samples and 0.4% more for the CO_2 samples. This behavior might have been due to the slightly increased molecular mobility and higher packing pressure on the N_2 and CO_2 samples. As mentioned earlier, scN_2 and $scCO_2$ can reduce the viscosity of the polymer by increasing the free volume between polymer chains. Therefore, it is expected to enhance the crystallization kinetics and degree of crystallinity. In addition, lower flow resistance on the polymer should transfer more pressure during the packing cycle. On the other hand, the foaming and melt fracture mechanisms during the filling stage caused some gas to escape and vent out just before the packing stage. This lowered the amount of SCF in the melt during the cooling phase and the packing cycle, which decreased crystallization in these phases.

Since the crystal structure is very rigid compared to the amorphous structure, a higher degree of crystallinity usually increases the Young's modulus of the final product [57]. As will be seen later, the Young's modulus in the tensile tests in this study followed the results of the DSC tests.

In the absence of SCF, the degree of crystallinity for the regular sample was slightly lower than for the SCF samples. Meanwhile, the average melting points were similar among the samples.

Because the second heating had the same thermal history, the second heating thermograms should reflect the thermal degradation of the material rather than the processing history. It is known that a lower molecular weight PE, namely HDPE, tends to have a higher degree of crystallinity. The data in Table 2.4 show that all injection molded samples had slightly higher degrees of crystallinity than neat UHMWPE, although there were no significant differences in degrees of crystallinity or melting points among the injection molded samples.

Table 2.4. The average thermal behavior of injection molded samples obtained from the second heating thermograms.

Sample	**T_m (°C)**	**ΔH_s**	**% Crystallinity**
Neat	139.8 ± 0.6	166.7 ± 0.7	57.6 ± 0.2
Regular	140.3 ± 0.9	167.7 ± 2.7	58.0 ± 0.8
N_2 sample	140.2 ± 0.8	169.8 ± 1.5	58.7 ± 0.5
CO_2 sample	139.7 ± 1.2	167.6 ± 1.9	57.9 ± 0.6

Yasuniwa et al. reported that, although the melting point of the PE grades increased linearly with the molecular weight, above 10^6 g/mol, the change was insignificant [58]. The results in our study agree with this finding. While the melting points of all injection molded samples were similar, the rheology and mechanical test results to be discussed below showed that the regular sample had a lower viscosity and tensile properties than the SCF samples.

One possible source of error in the DSC tests could stem from an uneven molecular weight distribution in the final product. Within the injection molding barrel, thermal degradation mainly

occurs on the surface of the barrel rather than on the screw root. Once the material enters the cavity, material degradation takes place where the temperature (due to viscous heating) or stress (due to shear and elongational flows) is highest. Although four tests for each type of sample were performed, the degraded material may not have been distributed and dispersed evenly within the main matrix.

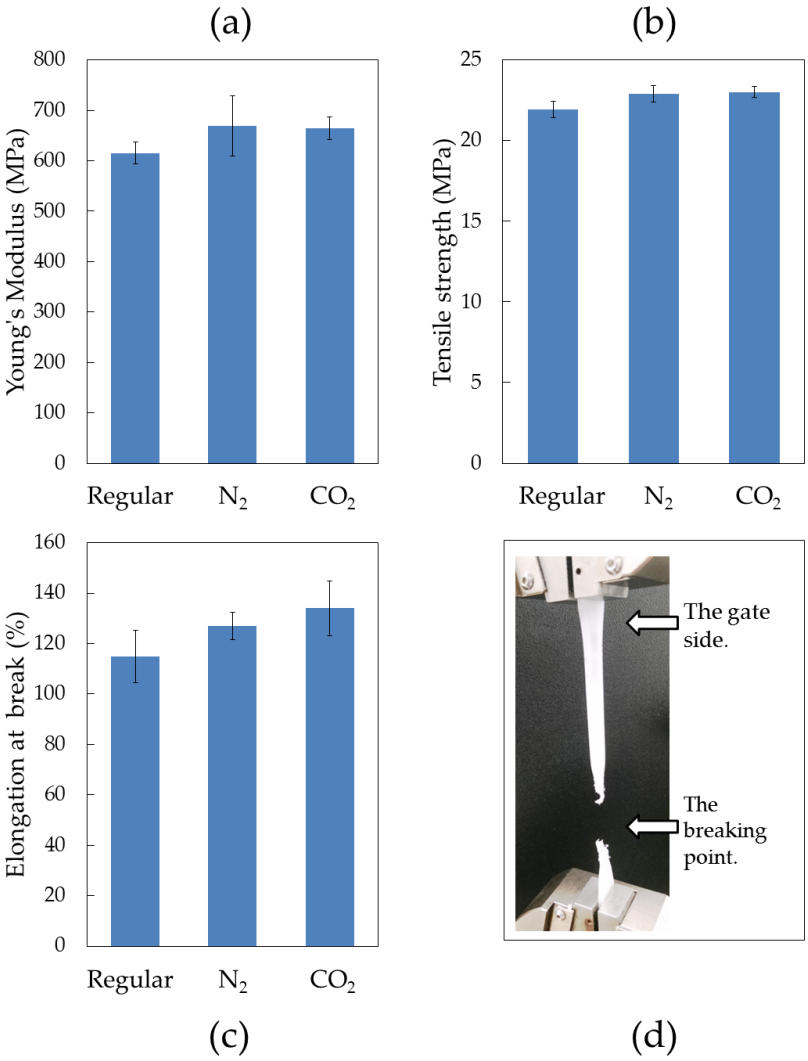

Figure 2.3. (a–c) Mechanical properties of UHMWPE samples and (d) an image of the breaking point.

2.4.2. Mechanical Properties

The bar graphs in Figure 2.3 (a)–(c) show the mechanical properties of the injection molded samples. The same data are also tabulated in Table 2.5. The Young's moduli of the N_2 and CO_2 samples increased slightly from 8% to 9% compared to the regular sample. A similar slight increase was also observed for tensile strength, with about 1 MPa of difference.

The largest improvement was observed on the elongation-at-break. The N_2 sample had a 12% elongation-at-break increase and the CO_2 sample had a 19% elongation-at-break increase, indicating that the samples with super-critical gas deformed more before fracturing than the regular sample.

During the mechanical tests, all parts ruptured in the same thin section on the side farthest from the gate (cf. Figure 2.3 (d)). Elongation-at-break was mainly determined by the weakness of this point. This weakness was attributed to relatively low pressure at that point along the part during the packing cycle, as the pressure during the packing phase decreased from the gate to the end of the part. The dominant role of the melt pressure on the mechanical properties of injection molded parts is a well-known phenomenon [59], [60]. However, melt pressure values across the same part do not vary much for low viscosity materials. Here, the reason might be that the high viscosity of the UHMWPE caused a relatively high pressure variance, which resulted in weakness at the indicated far-end location on the tensile bar. While the N_2 samples exhibited a slightly higher Young's modulus, the CO_2 samples had higher values in terms of elongation-at-break and toughness. But the differences between the N_2 and CO_2 samples were within the standard variation. The reason for this might have been that both gases had similar physical effects on the flow behavior.

Table 2.5. Tensile properties of injection molded samples.

Samples	Young's Modulus (MPa)	Elongation at Break (%)	Tensile Strength (MPa)	Toughness (J/m^3)
Regular	615.2 ± 21.4	115 ± 10	21.9 ± 0.5	64.4 ± 7.1
N_2 samples	669.6 ± 59.9	127 ± 5	22.9 ± 0.5	73.2 ± 4.0
CO_2 samples	664.0 ± 22.7	134 ± 11	23.0 ± 0.3	77.8 ± 8.4

2.4.3. Rheology

UHMWPE is normally selected as a material for its excellent impact strength and wear resistance based on its ultra-high molecular weight. This high molecular weight must be preserved to an acceptable level after thermal processing via a process like injection molding. The molecular weight of the final product should be checked to determine whether the process was successful or not. Due to the high molecular weight of UHMWPE and the difficulty of accessing a suitable solvent for the gel permeation chromatography (GPC) device, the molecular weight of the neat and injection molded samples were analyzed in an indirect way by examining the change in melt viscosity. Moreover, a better understanding of the rheological characteristics of UHMWPE may help design processing parameters. Figure 2.4 (a) displays the complex viscosity of neat and injection molded UHMWPE samples.

In the tested frequency range in Figure 2.4 (a), all UHMWPE samples fit the Power-Law model with a strong shear-thinning behavior and without a zero-shear rate Newtonian viscosity plateau. At the lowest frequency tested, 0.01 Hz, the complex viscosity of neat UHMWPE corresponded to 2.553 x 10^6 Pa·s. Regular injection molded UHMWPE samples processed without any SCF had a complex viscosity of 1.324 x 10^6 Pa·s, which was about 48% lower. On

the other hand, the viscosities of the N_2 and CO_2 samples were closer to the neat sample, with an 18% reduction for N_2 samples and a 12% reduction for CO_2 samples. This viscosity reduction was likely due to material degradation as a result of viscous heating, especially during the recovery or dosage cycles and the injection molding process.

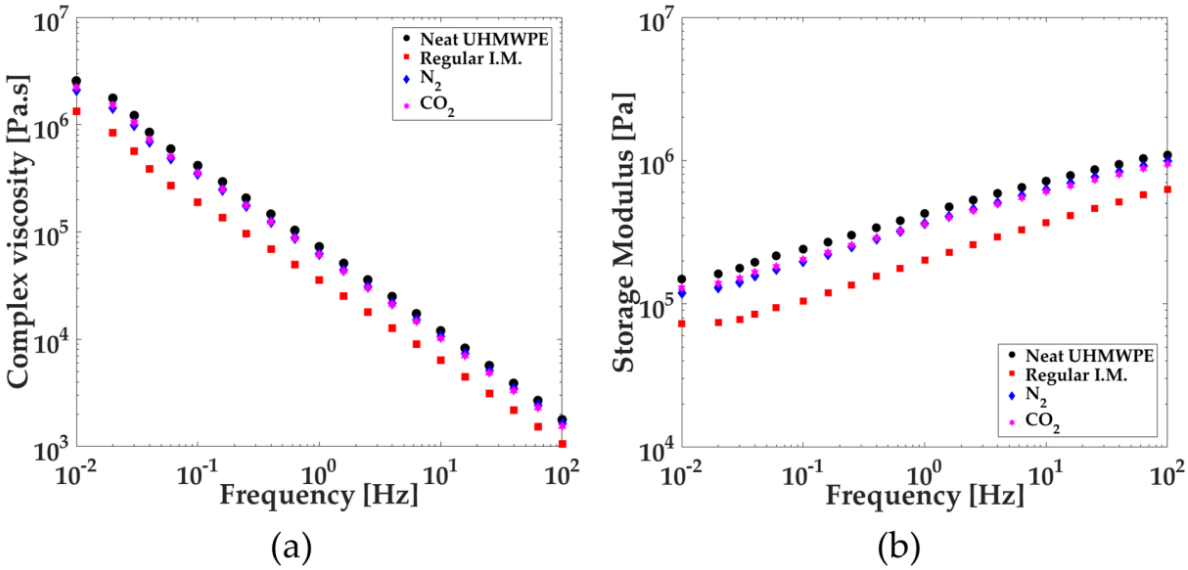

Figure 2.4. (a) Complex viscosity versus frequency. (b) Storage modulus versus frequency.

Thermal degradation lowers the molecular weight and broadens its distribution by breaking the polymer chains. Although increasing the amount of low-molecular-weight chains in the polymer typically improves flowability, it degrades the impact strength and wear resistance of the final products [56], [61]. Based on our experimental observations, the thermal degradation of UHMWPE was minimized with proper machine and mold selection, such as using a smaller compression-ratio screw, small volume part, and a larger gate. Independent of this, the rheological results suggested that SCF helped minimize the thermal degradation of UHMWPE.

Figure 2.4 (b) shows the storage moduli of neat and injection molded UHMWPE samples. It can be seen that the storage moduli of the N_2 and CO_2 samples behaved similarly to the viscosity

results, showing only a slight decrease compared to the neat sample, whereas the regular injection molded sample displayed a comparatively large decrease. Equation 3 shows the expression of viscous heating upon shear deformation.

$$\dot{Q}_{VH} = \eta \dot{\gamma}^2 \tag{3}$$

In the above equation, $\dot{Q}_{VH}$ is the rate of viscous heating, η represents the shear viscosity, and $\dot{\gamma}$ is the shear deformation rate [56], [61]. Thermal degradation of a material that occurs during processing is largely the result of the viscous heating. Although all samples except the neat sample were produced using the same processing parameters, the viscous heating might have been lower for the N_2 and CO_2 samples due to the plasticizing effect of the SCF, which lowers viscosity [24], [62].

The temperature dependence of the UHMWPE viscosity should be understood for successful manufacturing. For this purpose, a temperature sweep test was performed and reported in Figure 2.5 at two frequencies (0.1 Hz and 100 Hz). Only a small temperature dependence was observed for the UHMWPE viscosity, as shown by the slope of the data points in Figure 2.5 for both frequencies tested. The temperature sweep tests suggested that increasing the temperature of the UHMWPE melt for processing ease was not an effective way of decreasing the viscosity of the polymer, despite its common practice.

When temperature dependence, based on the temperature dependence relationship presented in Equation 2, was compared among common thermoplastics (PS, HDPE, LDPE, PP, PA66, PC, and PVC), from a general standpoint, the smallest temperature dependence coefficient, *a*, was reported as 0.002 $°C^{-1}$ for HDPE [56]. According to the same model, the temperature dependence coefficient of UHMWPE was calculated as 0.001 $°C^{-1}$, about half that of HDPE's dependence.

Low temperature dependence for a polymer can be a desirable property for a reliable injection molding process. Therein, the polymer can maintain its viscosity within stable limits, despite factors like viscous heating or varying zone temperatures along the barrel. However, having a lower temperature dependence shifts the focus to the resistance to flow which regardless of the melt temperature, becomes the major impediment in processing UHMWPE.

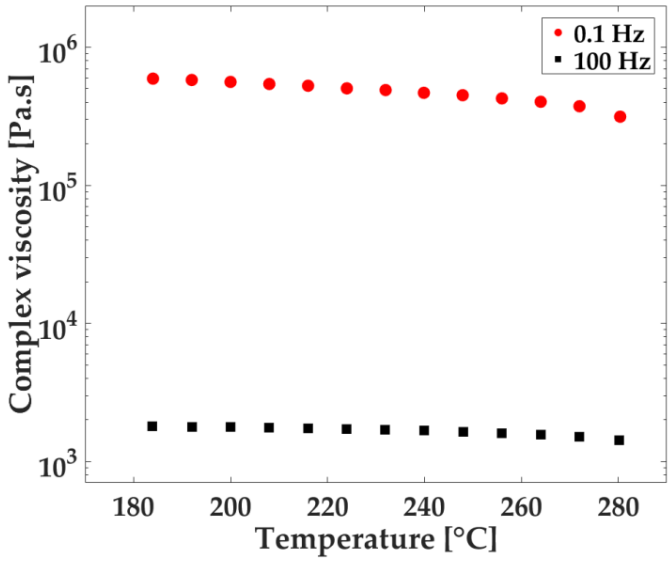

Figure 2.5. Complex viscosity versus temperature.

2.4.4. Tensile Bar Images and Injection Pressure Measurements

Images of complete and short-shot injection molded UHMWPE parts are shown in Figure 2.6 (a)–(b). The gate location was on the right side of the parts. Although the appearance of the complete parts in Figure 2.6 (a) was identical for all sample types, the short-shot images in Figure 2.6 (b) showed a unique difference in flow behavior between the regular injection molded samples and the SCF samples. It is well-known that many engineering plastics exhibit so-called "fountain flow" behavior [35]. However, in Figure 2.6 (b), it can be seen that the UHMWPE melt failed to demonstrate fountain flow behavior. This was because the material slipped at the

mold surface as a result of its high viscosity and very low friction properties as well as the severe melt fracture that occurred as the melt entered the cavity under high stress. As a result, the flow front of the regular short-shot sample formed an irregular porous structure that became less porous near the gate. This might have been due to the huge pressure near the gate region where the part transitioned from a porous-like structure to a continuous-like structure. That is, the high-pressure development in the gate area caused the polymer to form a solid structure near the gate of the regular injection molded part. Interestingly, it was observed that the N_2 and CO_2 samples in Figure 2.6 (b) filled the entire cavity with a completely porous-like, foam-like structure, even near the gate side, as a result of gas expansion and venting. Such a porous structure was later compacted into solid-like parts (cf. Figure 2.6 (a)) through packing pressure during the packing stage.

Figure 2.7 shows the injection pressure values versus flow rate on a linear scale axis. There was a noticeable decrease between the regular injection molded and SCF-loaded samples. The N_2 samples yielded slightly lower pressure values compared to the CO_2 samples.

The shapes of the curves, especially from moderate to high flow rates, seemed linear. For the 80 cm^3/s flow rate used to create the injection molded samples, the average pressure reduction was about 30% for CO_2 samples and 35% for the N_2 samples. This pressure reduction might have been due to the viscosity reduction effects of the dissolved SCF in the polymer melt. Previous studies have reported this effect for scN_2 and $scCO_2$ on various PE grades [45], [46], [62]. Other contributions to the pressure drop may have been that the material changed its flow behavior as demonstrated in Figure 2.6 (b). It seems that SCF decreased the material's tendency to agglomerate and stick to the mold surface, thus resulting in less pressure development.

Furthermore, the escaping high-pressure gas during the filling stage may have caused a lubrication effect and slipping between the UHMWPE part and the mold surface.

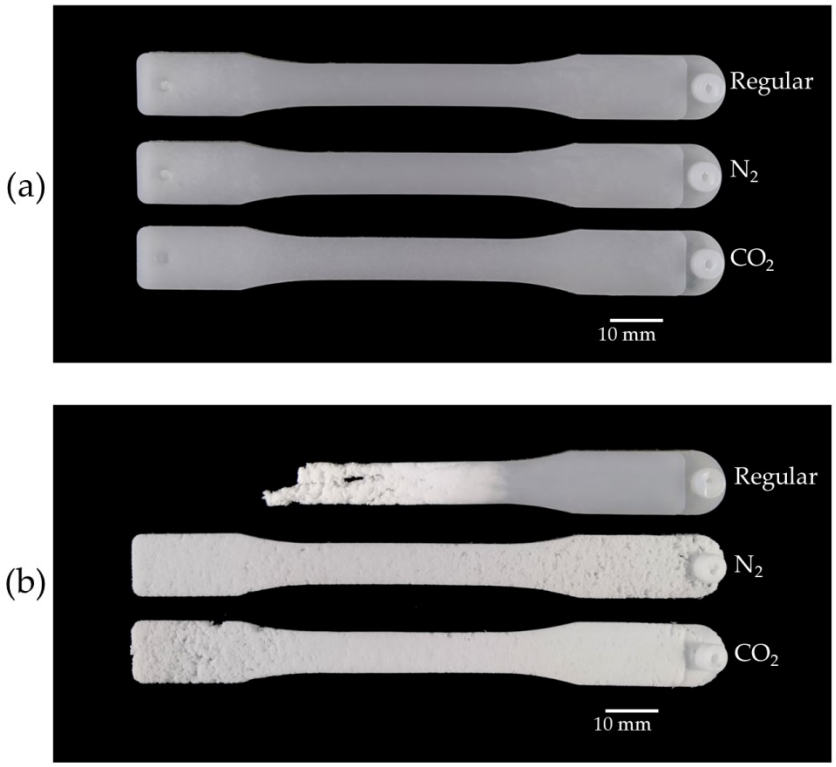

Figure 2.6. Images of injection molded UHMWPE samples: (a) complete parts, and (b) short-shot samples.

Another reason for the pressure reduction might have been undissolved gas bubbles in the screw chamber or emerging gas bubbles in the mold cavity, which may also explain why scN_2 reduced the pressure slightly more than $scCO_2$. In microcellular injection molding (MIM), until the injection cycle begins, it is assumed that finely distributed micro-gas bubbles completely dissolve in the polymer melt and create a single-phase solution. However, in practice, the single-phase polymer/ gas solution may not form completely at certain molding settings over a typical recovery time. As long as the back pressure is kept above the super critical pressure, the residual micro-bubbles will not affect the MIM process [23].

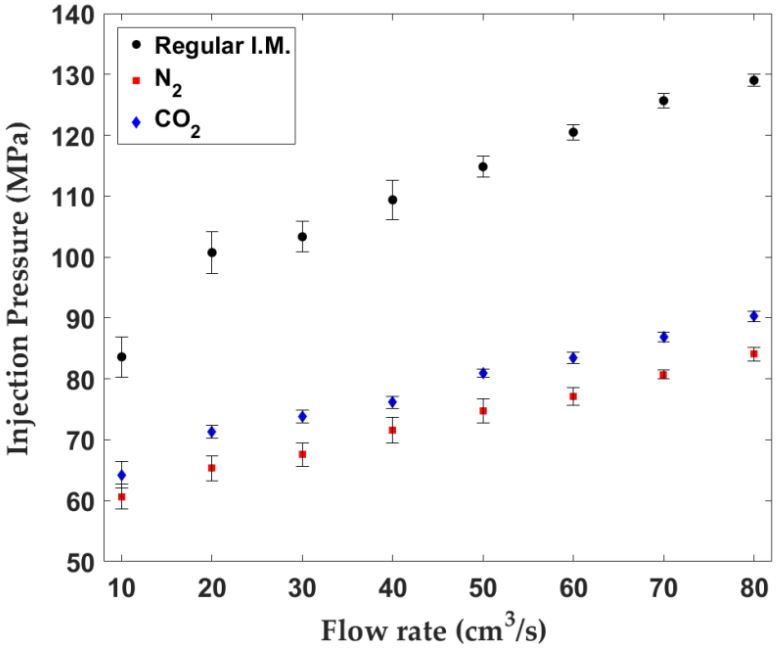

Figure 2.7. Injection pressure versus flow rate.

The gas solubility in polymers is a strong function of pressure and temperature. Based on our experimental observations, it was estimated that the residual microbubbles when scN_2 was used were more numerous than with the $scCO_2$ case because of the lower solubility of scN_2 in the UHMWPE melt. To the best of our knowledge, gas solubility and diffusion data are not available for UHMWPE. For one grade of HDPE, the gas solubility was reported as 1.2 wt% for scN_2 and 4.6 wt% for $scCO_2$ at 270 °C [23]. Similarly, as gas emerges from the polymer/gas solution during injection, numerous bubbles form due to thermodynamic instability. Since scN_2 has a lower solubility in UHMWPE, it will have a higher degree of supersaturation for scN_2 given the same gas loading at 1.5 wt% (cf. Table 2.1). Thus, more gas bubbles are expected to form for the N_2 samples. Either way, tiny bubbles with relatively negligible viscosity may reduce the average flow resistivity of the melt–gas mixture.

2.4.5. Micro-Computed Tomography (μCT)

Although μCT resolution (5 μm) is limited when compared to electron microscopy methods, as a nondestructive method, it enables us to scan large volumes conveniently instead of only a limited area of the fracture surface. It also allows one to effectively analyze and select the most representative cross-section images. μCT images of injection molded samples are shown in Figure 2.8.

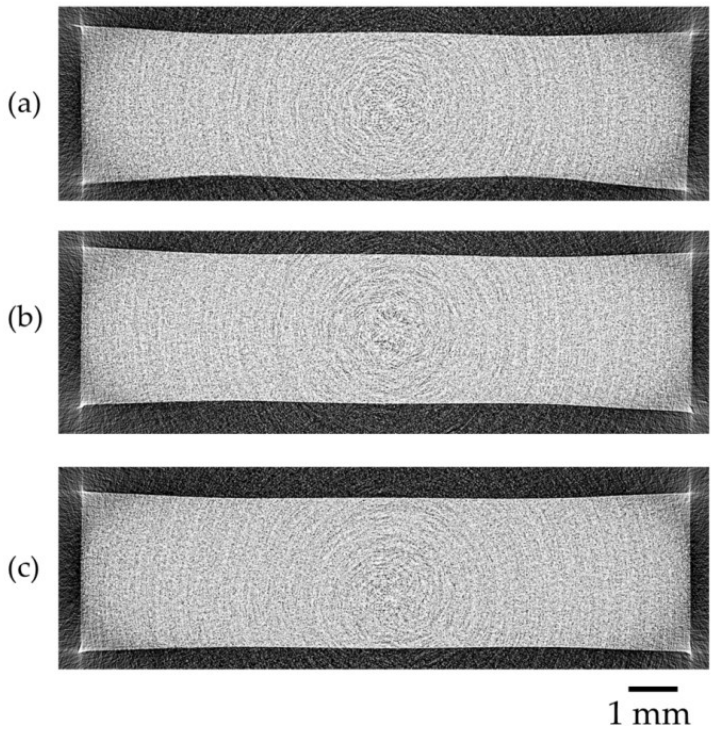

Figure 2.8. μCT images of injection-molded samples: (a) regular injection molded sample, (b) N_2 sample, and (c) CO_2 sample.

Remaining bubbles in injection molded parts can cause some cosmetic and mechanical defects. When SCF is used, remaining bubbles can be a challenge to eliminate. During cooling, the shrinkage of the polymer can create some random bubbles in the part. However, the injection molding images in Figure 2.6 (b) show that UHMWPE underwent foaming and allowed gas to emerge and escape. Even if there is a relatively small amount of gas remaining, it is easy to pack

the part and eliminate the bubbles for both N_2 and CO_2 samples, resulting in solid injection molded parts free of any residual bubbles as shown in Figure 2.8. In μCT images of all injection molded samples, the corners of the cross sections images demonstrated unexpectedly sharp and light colored edges. This might have been due to the exponential edge-gradient effect observed as a defect of the μCT mathematical reconstruction algorithm whenever long sharp edges of high contrast are encountered [63].

2.5. Conclusions

In summary, UHMWPE was processed via microcellular injection molding with supercritical N_2 or CO_2 as a reversible plasticizer and compared with regular injection molded samples. It was found that both scN_2 and $scCO_2$ reduced the required injection pressure for the chosen material flowrate during injection. The flow behavior was also found to be different when scN_2 and $scCO_2$ were used. UHMWPE failed to demonstrate typical fountain flow behavior; instead, it slipped on the mold surface. While DSC results showed a small difference in terms of the degree of crystallization and melting temperature among all samples, the rheological tests showed that the complex viscosity and storage modulus of the N_2 and CO_2 samples were closer to that of the neat sample and higher than the regular injection molded sample. This suggests that some thermal degradation may have occurred during processing, but scN_2 and $scCO_2$ helped reduce the overall degradation due to the plasticizing effect in the barrel and injection molding cycle. In addition, the rheological tests showed that increasing the melt temperature would not reduce the viscosity. From the mechanical tests, it was found that CO_2 samples had the most favorable elongation-at-break results while N_2 samples had the highest Young's modulus. Finally, μCT images showed that N_2 and CO_2 samples were free of any residual bubbles.

2.6. Acknowledgments

The authors gratefully acknowledge the support from the Wisconsin Institute for Discovery (WID), the Kuo K. and Cindy F. Wang Professorship, the College of Engineering, and Office of Vice Chancellor for Research and Graduate Education at the University of Wisconsin–Madison. The UHMWPE was generously donated by the Celanese Corporation (Irving, TX, USA).

3. PROCESSING OF ULTRA-HIGH MOLECULAR WEIGHT POLYETHYLENE (UHMWPE) INTO BOX-SHAPED PARTS WITH REGULAR AND SPECIAL INJECTION MOLDING TECHNOLOGIES

3.1. Abstract

Ultra-high molecular weight polyethylene (UHMWPE) in pellet form was injection molded into box-shaped parts using a specially designed mold by both conventional and special, high-pressure microcellular injection molding (MIM). Super critical nitrogen (scN_2) was utilized as the physical blowing agent or, more precisely, plasticizer, in MIM. It was found that persistent short shot issues associated with conventionally injection molded samples could be solved and complete parts can be injection molded when scN_2 was used. Furthermore, not only did scN_2 effectively promote processability of UHMWPE, it also reduced the very high injection pressure requirement and high part shrinkage issues.

3.2. Introduction

As a linear homopolymer polyethylene, ultra-high molecular weight polyethylene (UHMWPE) holds a special place among other PE grades. It has an extremely high molecular weight, typically more than 1 million g/mol, and possesses many favorable properties for industrial and medical applications. However, its high molecular weight adversely affects its melt processability because of its extremely high viscosity and highly entangled molecular structure [4].

Injection molding is preferred over other types of polymer processing methods for complex part designs and highly repeatable and automated manufacturing [14]. Strong competition, varied

customer demands, and fast-changing markets force molders to constantly improve their products, develop and apply new technologies, and bring new equipment and resins to the market [32]. Accordingly, costs of production equipment and design complexity keep increasing to meet these demands. Meanwhile, mold makers normally charge tens of thousands of dollars for professionally made molds [64]. Therefore, in-depth fundamental research is required to meet these challenges and reduce the costly trial-and-error approach typically used in injection molding, especially for emerging materials such as UHMWPE.

So far, most of the research that has investigated the molding behavior and resulting part quality of UHMWPE has been limited to simple geometries such as tensile bars and rectangular parts [65]–[67]. However, complex part designs, which are more representative of potential and targeted UHMWPE applications, will yield more useful information and in-depth understanding of UHMWPE's molding behavior.

Conventional injection molding of UHMWPE has been hampered by the lack of fluidity, short shots, and other molding difficulties resulting from the ultra-high molecular weight and molecular entanglement of UHMWPE. It has been reported that supercritical fluids (SCFs) could improve the moldability of UHMWPE [67]. In this study, scN_2 was chosen because it was found that scN_2 and $scCO_2$ had a similar effect on the processing of UHMWPE. Moreover, compared to CO_2, using N_2 in microcellular injection molding (MIM) requires 50% less back pressure, which is beneficial when a large dosage volume is required [22].

This study aims to utilize SCF to improve the injection molding of solid UHMWPE parts using more complicated molds and part designs. This effort will allow for the development of processing guidelines and engineering know–how for the injection molding of this unique

material. For this purpose, experiments of molding solid UHMWPE with and without scN_2 into a box-shaped mold were conducted. Herein, the images of injection molded parts, part weights, injection pressures, and percentage of linear shrinkage measurements will be presented.

3.3. Material and Equipment

UHMWPE resin (GUR® 5129) in pellet form was provided by the Celanese Corporation. It had an average molecular weight of 4.7 million g/mol and a density of 0.93 g/cm^3. An Arburg Allrounder 320S equipped with MIM technology was used to produce regular solid parts without scN_2 and special solid parts by first introducing scN_2 into the injection barrel to be dissolved into the melt and then by packing the melt in the cavity after the cavity is completely filled to suppress the foaming and force the emerging N_2 to dissolve back into the melt again.

Figure 3.1 shows a 3D model of the box-shaped part with overall dimensions of 100 × 75 × 45 mm. Intended to produce molded parts with severe shrinkage and warpage for research purposes, the design of the box-shaped part was intentionally flawed, with a decreasing thickness (from 3.5 mm to 2.0 mm in steps of 0.5 mm) on the shorter wall. The wider wall had a very small thickness of 1.25 mm. The thickness of the top wall of the box was 2.25 mm, as shown in the Figure 3.1.

Sample types produced in this study are tabulated in Table 3.1, together with major processing differences in scN_2 content, injection speed, and packing pressure. For the scN_2-laden MIM samples, the nitrogen content was fixed at 0.5 wt%, which is a commonly used SCF dosage in the MIM process.

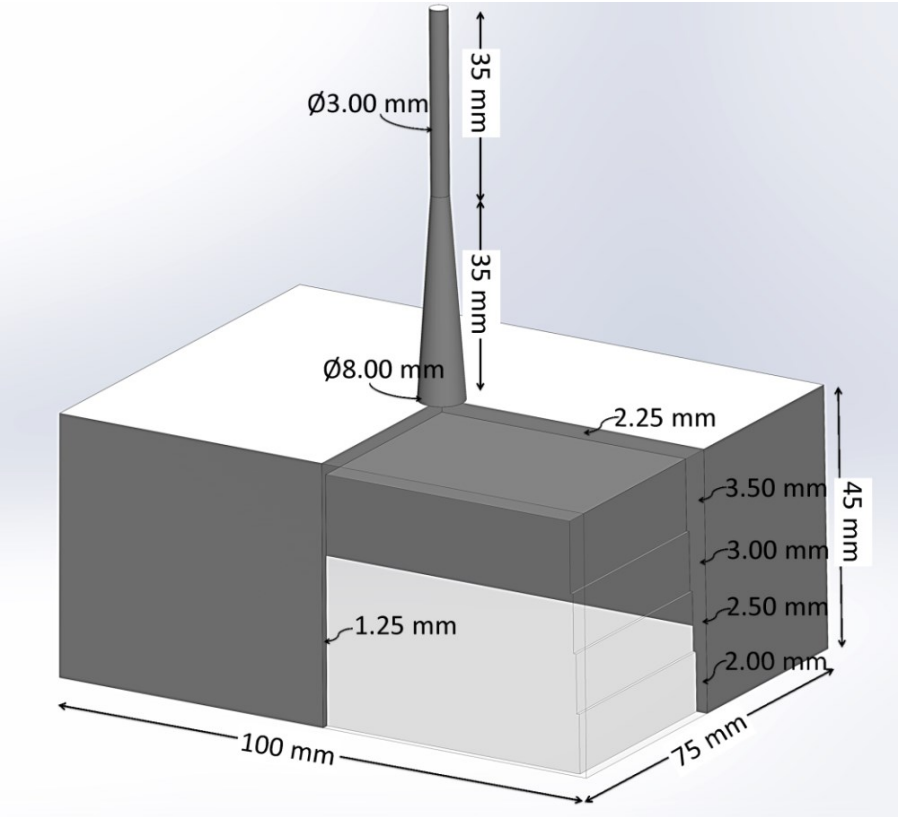

Figure 3.1. 3D model of the box part. A quarter of the part is cut away to show the variable wall thickness.

Table 3.1. Sample types and differences in relevant processing conditions.

Sample Name	**Condition**	**scN_2 Loading Weight %**	**Injection Speed (cm^3/s)**	**Packing Pressure (MPa)**
Regular	Regular injection molding as a reference sample	0	40	130
High-Q	Regular molding with a doubled flow speed (Q)	0	80	130
High-P	Regular molding with an increased packing pressure (P)	0	40	150
scN_2-laden	Similar conditions to the regular sample, but processed with scN_2	0.5	40	130

However, packing pressure was applied to the scN_2-laden samples so that the gas emerging from the polymer–gas mixture during filling would be forced to dissolve back into the polymer melt until the material was fully solidified. Eventually, the dissolved gas will diffuse out from the solidified parts. With this approach, scN_2-laden solid samples were produced.

Table 3.2. Processing parameters used in injection molding.

Processing Parameters	**Units**	**Value**
Injection volume	cm^3	53.5
Velocity to pressure switch over volume	cm^3	2
Cooling time	s	25
Packing time	s	7
Nozzle temp.	°C	255
Mold temp.	°C	80
Barrel temp. profile	°C	255-255-240-180-135-18

Processing parameters are always important, but for UHMWPE molding, they are crucial. Table 3.2 shows the rest of the processing parameters of the box part used in the preliminary study. A moderate injection speed (40 cm^3/s) and packing pressure (130 MPa) were used for the regular injection molded samples (cf. Table 3.1). A relatively high injection speed (80 cm^3/s) was set for the High-Q samples. The packing pressure was increased from 130 to 150 MPa (very close to machine's maximum injection pressure) for High-P samples. scN_2-laden samples had similar conditions to the regular samples, but with the addition of a 0.5 wt% gas dosage.

Table 3.3. Two-stage dosage of SCF for various molded samples.

Sample Type	**Number of Stages**	**Volume of Plasticated Melt (cm^3)**	**Back Pressure (MPa)**	**Screw Rotational Speed (rpm)**
Regular	Single stage	From 0 to 53.5	2.0	210
scN_2-laden	Stage 1	From 0 to 8.0	3.5	125
	Stage 2	From 8.0 to 53.5	6.0	210

One of the critical stages for successful MIM is the SCF dosage stage. In general, the melt pressure during the dosage stage is mainly dictated by the back pressure (BP), which ideally needs to be higher than the SCF critical point (3.4 MPa for N_2) to maintain the supercritical phase of the gas in the injection barrel. Moreover, a high rotational speed (rpm) is also needed for uniformly mixing the SCF with the polymer melt in the barrel [22], [23]. Unlike common thermoplastics, and due to its ultra-high molecular weight and entangled structure, UHMWPE melt is slow in absorbing the SCF. Thus, it requires a much higher SCF delivery pressure and a lower melt pressure in the injection barrel to allow for a sufficient amount of SCF to be injected into the melt. In addition, it needs a higher screw rpm to help mix the SCF with the polymer melt in the injection barrel. Therefore, we have developed a two-stage dosing strategy for UHMWPE. Processing parameters of the two-stage dosage strategy are tabulated in Table 3.3. In the first stage, SCF is injected into the injection barrel at low BP and rpm to ease SCF injection into the resistant UHMWPE melt. After SCF injection is completed and a relatively small amount of volume (8 cm^3) is plasticated, the second stage is run with high BP and rpm to finish the dosage process. During the second stage, proper mixing of SCF and a quick dosage time were achieved. For all cases studied, at least 5 molded samples were measured and averaged. The size for the

shrinkage data was measured with a caliper. The height of the samples was measured from the thick wall side due to the short shot problem seen on the thin walls.

3.4. Results

3.4.1. Mold Filling

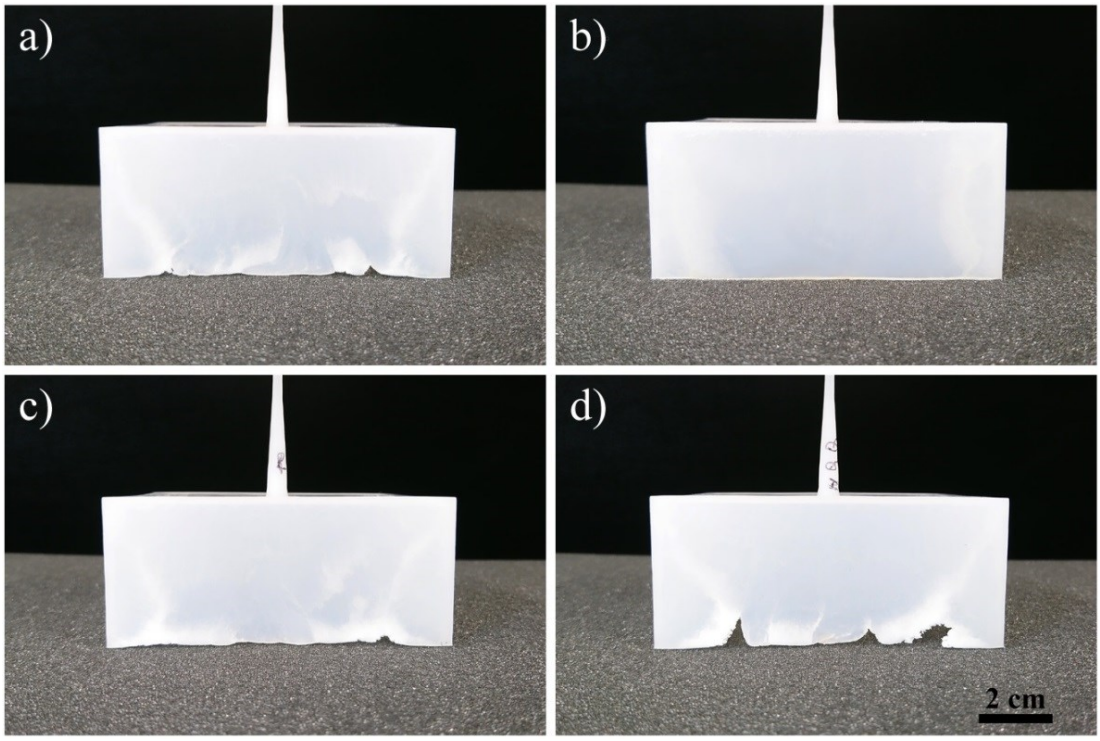

Figure 3.2. Sample Sample images: (a) Regular molded sample, (b) scN_2-laden sample, (c) High-P molded sample, and (d) High-Q molded sample.

Figure 3.2 shows the injection molded samples. The average weight %, which was normalized based on the average part weight of the scN_2-laden samples (37.01 g), can be seen in Figure 3.3. The edges of the thin walls of all samples, except the scN_2-laden sample, had short shot issues of various degrees. This is a known and expected problem of UHMWPE molding with thinner wall thicknesses (1.25 mm).

The regular injection molded samples weighed considerably lower, about 4% less than the scN_2-laden samples. Increasing the packing pressure from 130 MPa to 150 MPa (High-P) seemed to help the filling process by injecting more material under a higher packing pressure. However, the parts were still 3.7% lighter than the scN_2-laden samples. Therefore, High-P molded samples were unable to completely fill the mold, as can be seen in Figure 3.2 (c). The High-Q molded samples (one of them can be seen in Figure 3.2 (d)) interestingly even weighed 2.0% less than the regular molded samples, and 6.0% less than scN_2-laden samples, despite having two-times faster filling. This result was actually the opposite of conventional wisdom and intuition. The obvious reason why High-Q molded samples weighed even less than regular molded samples was likely due to the polymer leakage through the nozzle contact area and the clearance between other functional parts caused by the extreme pressure [15], [39]. For this box mold, the average injection pressure for most polymers typically ranged from 55–70 MPa. However, the average injection pressures for regular and High-Q molded UHMWPE samples were 153.4 MPa and 184.0 MPa, respectively. Based on our observation, the leakage was obvious when the injection pressure reached around 160 MPa, and some amount of polymer leaked depending on the pressure build-up. This also explains why the regular molded sample weighed slightly more than the High-Q molded samples. Therefore, controlling the injection pressure is very important for successfully molding UHMWPE. However, the leakage and pressure spike do not explain the whole story when we compare the weight of all molded samples.

Another reason for the High-Q samples' weight shortage could be the increased frictional force because of the high pressure and high flow speed of the sliding melt during the filling cycle. The frictional force between the melt and mold interface is simply a function of the

coefficient of friction and the normal force. However, the complicated tribological behavior of the UHMWPE melt on cold metal, especially for the injection molding process, is not well understood and has not been reported in the literature.

Among the sample types, only scN_2-laden samples were able to fill the cavity completely. When the thin-wall-edge scN_2-laden sample is examined in Figure 3.2 (b), it can be seen that its edge is flat on the bottom and also that it is the heaviest sample, as shown in Figure 3.3 (a). This not only indicates that the emerging gas was either vented or dissolved into the polymer completely, it also shows that there is a low surface friction due to the escaping scN_2 easing effect on the melt during the filling and packing cycles. The lowest injection pressure in Figure 3.3 (b) proves that the escaping N_2 reduced the frictional force between the melt and the mold surface.

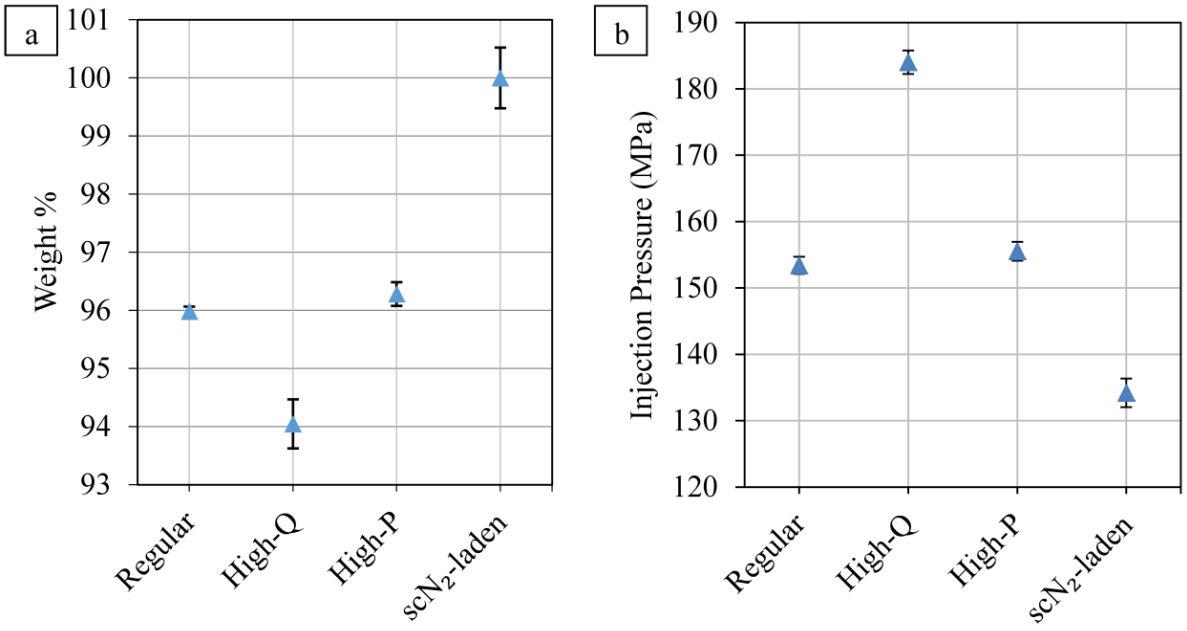

Figure 3.3. (a) Average weight % and (b) injection pressure.

Furthermore, it is well-known that the plasticizing effect of scN_2 lowers viscosity due to induced chain mobility. This effect may also contribute to the lower injection pressure [24]. In our early study, we found that SCFs yielded lower thermal degradation. By assuming that a majority of the thermal degradation occurred during the dosage and injection stages, the plasticizing effect of scN_2 will have had a considerable impact on the degradation behavior of UHMWPE and could have led to a lower injection pressure.

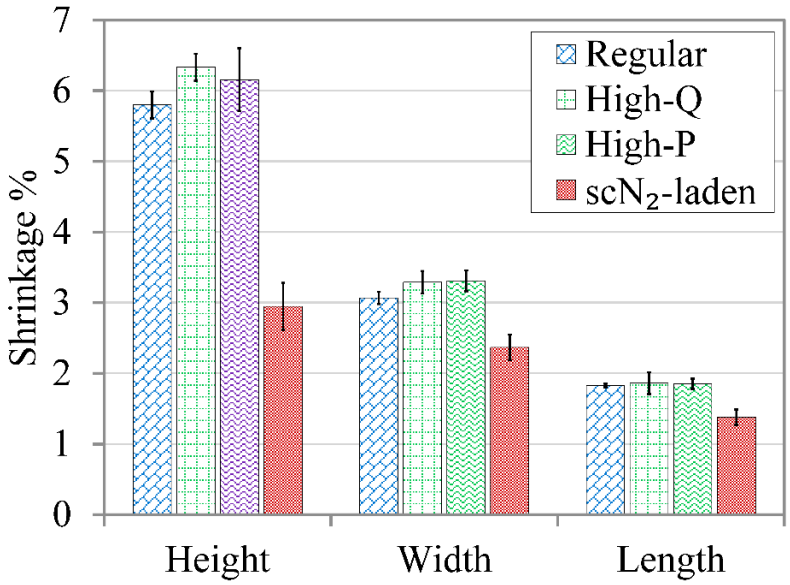

Figure 3.4. Shrinkage % of the samples.

3.4.2. Shrinkage Discussion

Shrinkage of the polymer is inevitable during cooling. To the best of our knowledge, there is no study that focuses on the shrinkage of injection molded UHMWPE. However, as a semi-crystalline polymer, UHMWPE tends to shrink a considerable amount. Figure 3.4 shows the linear shrinkage % based on the dimensions of the nominal box-shaped mold. All samples showed the highest shrinkage in the direction of the box's height. All samples, except scN_2-laden samples, showed approximately 6% shrinkage, which was considerably high for dimensional accuracy. The length and width shrunk relatively less than the height of the box. This was due to

the mold core restricting shrinkage in the width and length directions during cooling, while the height dimension had more freedom to shrink due to the lack of mold constraints. Compared to other samples, the scN_2-laden samples yielded less shrinkage in all directions. This was due to more material having been packed into the mold with the aid of the scN_2.

3.5. Conclusions

The results show that the injection molding of UHMWPE with scN_2 is a promising method. It helps solve the persistent and challenging problem of short shots when injection molding UHMWPE. It is also beneficial for improving the dimensional accuracy of the final part. Despite some interesting behaviors revealed by this preliminary study, it is hard to draw a complete conclusion on the relationships among filling speed, injection pressure, and sliding frictional force. Therefore, more research is needed to explore the optimum filling speed, mold temperature, and melt temperature settings to facilitate the proper mold filling of UHMWPE in injection molding.

3.6 Acknowledgment

The authors acknowledge the support of the Wisconsin Institute for Discovery (WID) and the Kuo K. and Cindy F. Wang Professorship at the University of Wisconsin–Madison. The authors would also like to thank the support of the SPE Milwaukee Education Foundation and Celanese Corporation for the material donations.

4. INJECTION AND INJECTION COMPRESSION MOLDING OF ULTRA-HIGH MOLECULAR WEIGHT POLYETHYLENE (UHMWPE) POWDER

4.1. Abstract

Ultra-high molecular weight polyethylene (UHMWPE) powder was processed using injection molding (IM) with different cavity thicknesses and injection-compression molding (ICM). The processing parameters of feeding the powders were optimized to ensure proper dosage and avoid jeopardizing the UHMWPE molecular structure. Dynamic mechanical analysis (DMA) and Fourier-transform infrared spectroscopy (FTIR) tests confirmed that the thermal and oxidative degradations of the material were avoided but crosslinking was induced during melt processing. Tensile tests and impact tests showed that the ICM samples were superior to those of IM. Increased cavity thickness and ICM were helpful for reducing the injection pressure and improving the mechanical properties due to effective packing of the material. Short shot molding showed that the UHMWPE melt did not exhibit the typical progressive and smooth melt front advancements. Due to its highly entangled polymer chains structure, it entered the cavity as an irregular porous-like structure, as shown by short shots and micro-computed tomography (μCT) scans. A delamination skin layer (around 300 μm thick and independent of cavity thickness) was formed on all IM sample surfaces while it was absent in the ICM samples, suggesting two different flow behaviors between IM and ICM during the packing phase.

4.2. Introduction

The principal characteristics of ultra-high molecular weight polyethylene (UHMWPE) that distinguishes it from other engineering polyethylene grades is its extremely high molecular weight, which is typically more than 1 million g/mol [4]. Its high molecular weight yields a high viscosity and molecular entanglement. This makes UHMWPE difficult to process due to viscous heating-related thermolysis, which causes material degradation. Nonetheless, if processed successfully, UHMWPE has the following superior properties in comparison with many other engineering polymers: one of the highest impact strengths, strong chemical inertness, and very low service temperatures. Moreover, UHMWPE can be distinguished by one of the lowest friction coefficients and its superior wear resistance [6], [68]. These properties lead UHMWPE to be considered a high-grade specialty polymer in many applications [4].

After its invention in the 1950s, UHMWPE became very popular for two particular applications: high-performance fibers and artificial joint bearings for orthopedics [4], [7]. However, its high resistance to flow, even at high temperatures, has limited its scope with common polymer processing methods [15]. Among them, injection molding will be the main theme of this study.

Injection molding is the most economical polymer processing technology when a relatively complicated design is required at high manufacturing rates. Many specialized methods of injection molding have been developed [14]. Among them, injection–compression molding (ICM) is a capable alternative for UHMWPE processing [40]. It is a well-known and effective technique for difficult-to-flow materials, such as polycarbonates, which are used for digital data discs and optical lenses [69].

ICM applies a compression action after the filling phase to pack the material by reducing the cavity thickness/volume via advancing the mold half or mold insert. ICM also reduces the injection pressure because of the enlarged cavity thickness during filling. Moreover, for material packing, ICM applies a more even pressure distribution across the surface of the part to compensate for shrinkage. This uniform pressure over the part length usually results in uniform material properties when compared with the packing cycle of regular injection molding. Some of the drawbacks of ICM, in general, include the following: increased capital costs and complexity of processing, stagnation of polymer melt flow over a thinner area (so-called hesitation mark) and, sometimes, limitations on part design [14].

Based on a survey of existing work, the scope of the literature—which focuses on the injection molding of pure UHMWPE rather than its blends—is limited to only a few studies [65], [67], and patent literature is comprised of only a couple of attempts regarding powder-type resin in injection molding [16], [34].

Lower molecular weight polyethylene grades are commonly supplied in pellet form by manufactures. Contrary to this, almost all grades of UHMWPE come in powder form because virgin resins during UHMWPE synthesis are obtained in powder form [28] and their thermal and viscoelastic properties hinder the pelleting process [29]. Nevertheless, a few grades of UHMWPE are commercially available in granule form. These grades are relatively costly because of the additional special pelleting processes needed to manufacture them [30], [31]. The fine powder of UHMWPE has very low friction and it does not feed or flow easily in the barrel. Although handling and processing of UHMWPE powder in injection molding are more troublesome compared to its pellet counterpart, it might be preferable because it could be more economical and easier for compounding prior to injection molding. For example, the powder

resin can be easily customized in-house for changing product requirements by dry mixing instead of subjecting the material to an extra thermal cycle like extrusion. It can be modified with a variety of additives such as stabilizers, color pigments, solid beads, and fibers. The study here is limited to powder resin; nevertheless, the method described is applicable to pellet grades as well.

The rheological properties of UHMWPE are quite unique, especially its flow behavior under high shear. Even at a temperature well above its melting point, UHMWPE maintains its rubber-like properties. In other words, it prevents the transition from elastic solid to viscous liquid (very low ratio of loss modulus to storage modulus) [70]. In contrast to the lower molecular weight polyethylene grades, when the molecular weight is above 500,000 g/mol, the entanglement degree, viscosity, and relaxation time of the polymer are considerably high and establish UHMWPE's rheological characteristics [4], [7], [67]. Moreover, the temperature dependence of UHMWPE was reported as one of the lowest among common engineering thermoplastics [67]. This suggests that further heating the material for better processability would not help processing, but would exacerbate thermal degradation.

In one of our previous studies [67], we found a unique flow behavior of UHMWPE, which is characterized by a lack of so-called fountain flow [35]. At the initial stage of mold filling, the UHMWPE melt enters the mold cavity as a porous material instead of a continuous melt because of severe melt fracture. Furthermore, in our previous study [67], we found that if a supercritical fluid (SCF) is used in the melt, it can effectively delay the transition from a porous-like structure to a solid-like structure. Therefore, a larger flow length-to-part thickness ratio can be used without a high-pressure jump. However, this process requires special equipment such as a microcellular injection molding machine to employ supercritical fluid.

Quality UHMWPE part entails excellent wear and impact resistance. However, thermal degradation and part delamination have to be minimized. When UHMWPE powder is used in injection molding, it is prone to the so-called delamination defect, which is a layer separation problem on the surface of the part [28], [34]. These layers can be easily peeled away from the core and ruin the wear and impact resistance of UHMWPE. Another main concern is that the injection molding process can degrade the UHMWPE [67].

In this study, we aimed to develop a successful processing technique for UHMWPE powder in injection molding and ICM. Herein, the tensile and impact properties of molded samples were characterized. Furthermore, DMA and FTIR tests were performed to analyze the effect of the processing conditions on the molecular structure, viscoelastic properties, and potential degradation of UHMWPE. The scanning electron microscope (SEM) was used to investigate the delamination layer formation. μCT scans were performed on molded samples to observe the microstructure and flow behavior of UHMWPE.

4.3. Methods and Experiments

4.3.1. Material

A UHMWPE powder resin (GUR® 4120) with a calculated molecular weight of 5.0 million g/mol (based on ISO 1628-3 standard) was obtained from the Celanese Corporation. It had a true density of 0.93 g/cm^3 and an apparent (bulk) density of about 0.45 g/cm^3. It also contained a corrosion stabilizer (CS); other than that, it was a pure grade. The UHMWPE powder was used as received from the company.

4.3.2. Injection Molding and Processing Conditions

A 350 kN injection molding machine (Arburg Allrounder 270A) with an 18 mm diameter screw was used. Table 4.1 tabulates the relevant machine properties.

Table 4.1. Injection molding machine properties.

Property	**Value**	**Property**	**Value**
Screw diameter	18 mm	*Max. dosage speed*	795 rpm
Compression ratio	2.0:1	*Max. back pressure*	35 MPa
Max. injection pressure	250 MPa	*Max. clamping force*	350 kN
Max. injection speed	76.0 cm^3/s	*Machine Type*	Hybrid

One of the critical screw properties for effectively processing high viscosity materials is the compression ratio (CR), which can be defined as the ratio of the feeding zone depth to the metering depth [14]. If the screw has a smaller CR, the material that goes forward in the barrel will experience less compression pressure. The machine used in this study had a 2.0:1 CR, which is lower than the typical range of 2.5:1 to 3.0:1 [14] but is desirable for UHMWPE powder. Another important screw property is the diameter of the screw. For UHMWPE processing, a smaller screw diameter is preferred even though it reduces the injection volume capacity of the machine. This is because the smaller diameter screw usually has more pressure capacity and precise temperature control. The last equipment feature that helps the processing of UHMWPE powder is cooling the feed throat of the barrel with water or compressed air. The powder material, even for slippery UHMWPE, can block the feed throat. The low temperature of the feed throat is not only useful for continuous powder flow (thus minimizing the chance of a hang-up of

the material) in the hopper, but it also prevents overheating in the feeding zone during continuous running wherein the material experiences a lot of compression and shear force [14], [30].

4.3.3. Mold Design and Sample Types

Figure 4.1 shows the design of the mold that has a rectangular 50.8 mm × 101.6 mm (2" × 4") shape and an adjustable cavity thickness via movable core in the thickness direction. The sample types and their details are tabulated in Table 4.2.

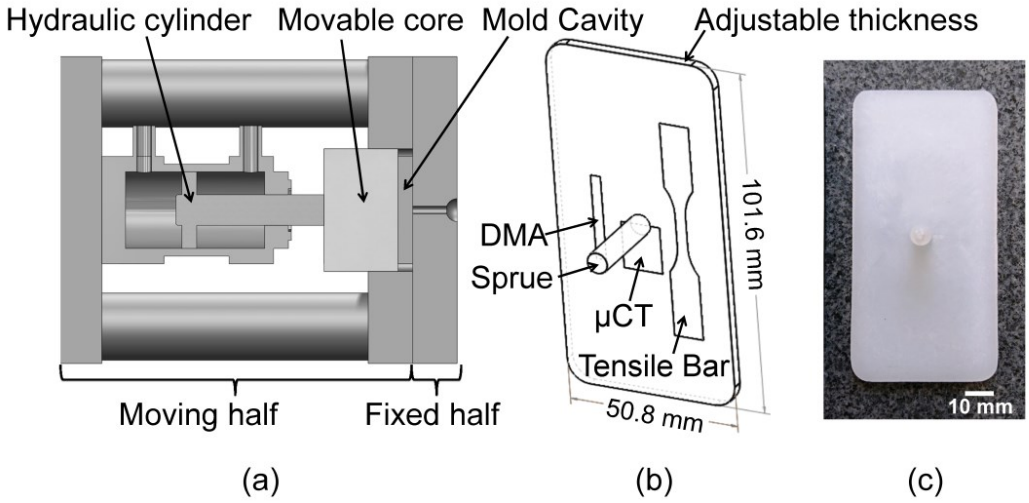

Figure 4.1. (a) Schematic of the ICM mold, (b) cavity geometry and test locations, and (c) an injection molded part.

In this paper, IM refers to all samples produced by injection molding with three different fixed cavity thicknesses (2.5 mm, 3.0 mm, and 3.5 mm). ICM refers either to injection–compression molding or samples produced with using it. When ICM was used, the core position and its movement were controlled with a hydraulic cylinder that was mounted on the moving side of the mold (Figure 4.1). The hydraulic cylinder was run through the standard core-pulling function of the machine.

Table 4.2. Injection molding sample types.

Sample	Method	Details
IM2.5	Injection into a fixed mold cavity thickness	2.5 mm fixed cavity thickness
IM3.0		3.0 mm fixed cavity thickness
IM3.5		3.5 mm fixed cavity thickness
ICM	Injection–compression molding	Injected into 6 mm mold and compressed to 3 mm cavity thickness
CM	Compression-molded sample for reference	No injection molding. Neat UHMWPE powders were pressed to a thickness of 3 mm at 230 °C for 3 min.

The final thickness of the ICM samples was adjusted based on the injection volume. There was no physical limit on the moving core. The core average speed was measured as 63 mm/s and the calculated cavity pressure was 16.7 MPa. The temperature of the hopper was adjusted slightly lower than room temperature at 18 °C. This was the lowest the machine setup could reach.

In one of our previous studies, it was found that the temperature dependence of UHMWPE was very low [67]. Therefore, the nozzle temperature was not a critical parameter for improving the injection process. While a higher melt temperature can improve the packing phase, it may delay material cooling in the mold, thus leading to an increased risk of thermal degradation. We chose a mild nozzle temperature of 235 °C that was well above the melting point of UHMWPE (132 °C). Processing parameters used in injection molding are listed in Table 4.3. A different set of experiments was performed on a mold with an ASTM Type 1 tensile bar cavity (165 mm length and 3 mm thickness) to address the effect of increasing the packing pressure on the formation of the delamination layer.

Table 4.3. Processing parameters used in injection molding.

Processing Parameters	Value
Injection speed	60 cm^3/s
Injection volume	IM2.5: 15 cm^3 IM3.0: 17 cm^3 IM3.5: 20 cm^3
Cooling time	20 s
Back pressure	4 MPa
Packing pressure and time for IM	90 MPa for 5 s
Compression pressure and time for ICM	17 MPa for 20 s
Temperature from hopper to nozzle	18–135–200–230–235 °C
Mold temperature	85 °C

All parameters were kept the same except for the packing pressure (see below) and the injection volume, which was adjusted to 14.2 cm^3 according to the mold volume. Three different packing pressures were used: 90 MPa, 120 MPa, and 150 MPa. The injection molded samples were clamped vertically on a milling vise. The samples were cut into 0.3 mm thick slices using a razor blade at different locations; namely, near the gate, in the middle of the part, and on the far side of the part. An optical microscope with a digital camera, Leica DM750, was used to image the edge of the parts that had a delamination layer.

4.3.4. Mechanical Test

Tensile properties of at least five samples for each sample type were measured according to the ASTM D638−14 standard on an Instron 5967 testing system with a 30 kN capacity load cell. A crosshead speed of 50 mm/min was selected based on the standard. Samples were punched to

an ASTM Type 5 sample shape with a die cutter. The sample location was selected at a distance of 12.7 mm from the center of the part in the lengthwise direction (cf. Figure 4.1 b).

4.3.5. Dynamic Mechanical Analysis (DMA)

A dynamic mechanical analyzer (DMA) (RSA III from TA instruments) was used to study the viscoelastic properties of samples in the tensile clamp mode. All samples (25 mm × 3 mm × 1 mm) were prepared using a milling machine from one surface to the cross-section dimensions (cf. Figure 4.1 b). The crosshead distance of the tensile clamps for all samples was 25 mm. All tests were run in dynamic temperature ramp mode at a constant frequency of 1 Hz and a constant strain of 1.0%, which was determined earlier by the strain sweep test to ensure linear viscoelastic properties. The temperature decreased from 150 °C to 60 °C at a cooling rate of 5 °C/min. The auto tension option of the instrument was selected with a constant static tension that was 10% greater than the maximum peak of the dynamic force to avoid possible buckling problems during the test.

4.3.6. Impact Test

At least five samples for each type were tested to determine the impact resistance according to the ASTM D256−10e1 plastics impact test standard. Samples were machined down to about 12.7 mm wide × 63.5 mm long. Samples were notched on one edge at a 45-degree angle and a 2.54 mm depth. Due to the high impact resistance of the samples at room temperature, they will not fracture with the impact tester. Therefore, specimens had to be cryogenically conditioned in liquid nitrogen at least 15 minutes before being attached to the impact tester. Tests were run immediately after attachment while the sample was partially submerged, with the notched cross

section in liquid nitrogen and the upper side open to the air to allow the pendulum to slide without obstruction from the nitrogen container.

For comparison, additional compression-molded (CM) samples were produced for the impact tests and DMA tests from neat powder resin in a hot press. The mold temperature was 230 °C and the compression time was 3 min at a pressure of 10 MPa.

4.3.7. Scanning Electron Microscopy (SEM)

Gold-spattered neat powder surface images and impact test fracture surface images were captured by Neo-Scope JCM-5000 and Zeiss LEO 1550VP scanning electron microscopes, respectively. Impact test samples were dried at 60 °C for 4 hours under vacuum before gold-sputter coating.

4.3.8. Micro-Computed Tomography (μCT)

A micro-computed tomography (μCT) system, Metrotom 800 of the Carl Zeiss Company, was used to image the inside of the samples non-destructively. All sample types and their intermediate flow patterns (short shots for IM samples and ICM samples before compression) were scanned. The resolution, x-ray tube voltage, and current of all scans were 8 μm, 85 KV, and 55 μA, respectively. The samples were located on the μCT stage to target a specific image area that was at the center of the thickness direction. The gate center was located in the middle of the top line of the image (cf. Figure 4.1 b).

4.3.9. Injection Pressure and Shot Weight Measurements

The first type of short shot of IM samples was produced by skipping the packing phase. Further reduction on the part weight for all sample types was achieved by reducing the injection

volume in 2 cm^3 increments until 40 to 50% weight reduction was reached. For all volume reduction steps, the injection pressure and the weight of at least 5 samples were measured. For each type of IM sample, the full shot weight was assumed as 100% and the weight % of the short shots was calculated based on the full shot weight of the related IM sample.

4.3.10. Dosage Study

A set of screw rotational speeds (rpm) from 100 to 400 rpm, at 100 rpm increments, was run for each back pressure (BP) setting: 4 MPa, 6 MPa, and 8 MPa. These ranges were selected based on a preliminary study. The feeding process was found to be unreliable when parameters beyond these ranges were used. For every data set, at least seven parts were injection molded. Meanwhile, screw torque data and dosage time were recorded from the machine. At a screw rotational speed of 100 rpm, 4 MPa and 6 MPa back pressure experiments were also excluded from the analysis because of inadequate material dosage. Energy consumption per unit mass is shown in Equation 1 and was calculated based on the measured torque and rpm settings. This equation was derived from the relationship between the motor torque and the motor power of the rotating action.

$$Energy\ consumption\ (J/g) = \frac{(time)(torque)(rpm)}{(Weight)}\frac{2\pi}{60} \quad (1)$$

4.3.11. Fourier-Transform Infrared (FTIR) Measurement

An FTIR spectrometer device, Bruker Tensor 27, was used in transmittance mode with a resolution of 4 cm^{-1} and in a wavenumber range of 4000–600 cm^{-1}. Control samples made of compression-molded powder were intentionally aged to have oxidative degradation in a convection oven for 30 and 60 min at 180 °C.

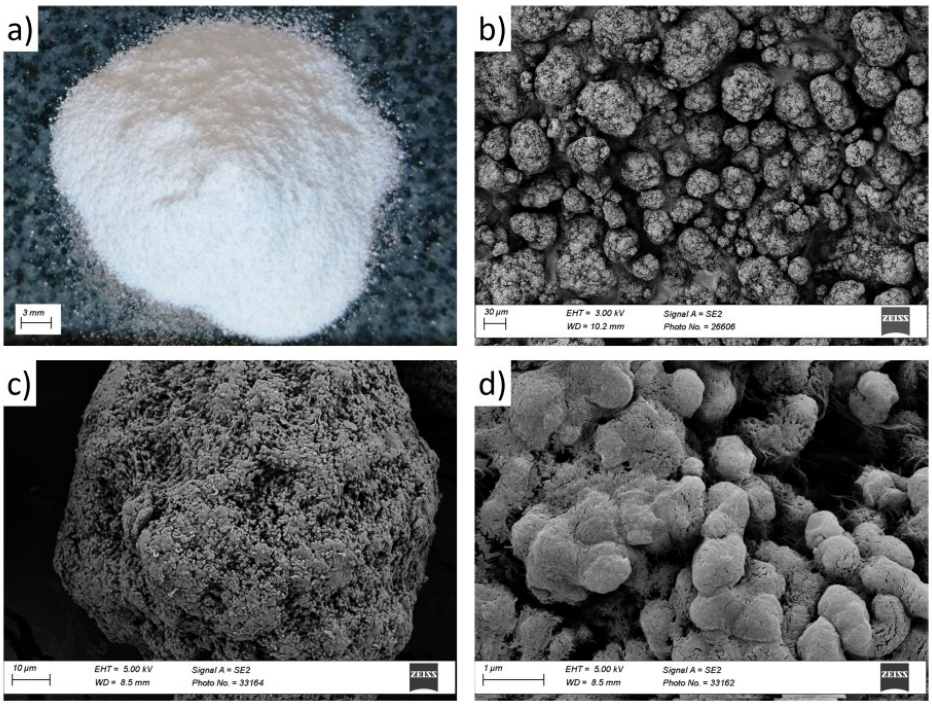

Figure 4.2. (a) Image of UHMWPE powder pile, (b) SEM of powder pile, (c) SEM of a single particle of powder, and (d) magnified surface morphology of a single particle of powder.

4.4. Results and Discussion

4.4.1. Feeding of UHMWPE

Figure 4.2 shows a microscopic image of the as-received UHMWPE powders and SEM images in increasing magnification. According to the material datasheet, the average particle size (d50) was reported as 120 µm. An SEM of the bulk powder can be seen in Figure 4.2 (b). The surface morphology of a single UHMWPE particle, which appears rough and textured, can be seen in Figure 4.2 (c). A higher magnification of the particle surface is shown in Figure 4.2 (d), where a lot of spherical bodies are attached to the powder particle with some fibrils on the back.

The screw rotational speed (rpm) and back pressure (BP) are two critical parameters for the proper feeding of the polymer in the barrel [14]. The feeding strategy in this study was a trade-

off between the shortest dosage time and the lowest energy consumption. This means that the energy and time should be consumed mainly on the feeding of the material rather than the damaging of the molecular structure. Therefore, the material is expected to be processed in the barrel more efficiently while reducing the risk of thermal degradation.

Table 4.4. Dosage time and energy consumption.

		Dosage Time (s)				**Energy Per Mass (J/g)**		
		4 MPa	*6 MPa*	*8 MPa*		*4 MPa*	*6 MPa*	*8 MPa*
The screw rotational speed (rpm)	*200 rpm*	3.57 ±0.11	3.45 ±0.04	3.52 ±0.11	*200 rpm*	70.36 ±3.95	77.18 ±2.29	86.53 ±2.07
	300 rpm	2.61 ±0.01	2.68 ±0.04	2.69 ±0.02	*300 rpm*	93.20 ±3.27	101.49 ±3.65	108.05 ±3.12
	400 rpm	2.11 ±0.03	2.21 ±0.02	2.23 ±0.02	*400 rpm*	121.28 ±6.57	127.26 ±7.39	135.49 ±6.12

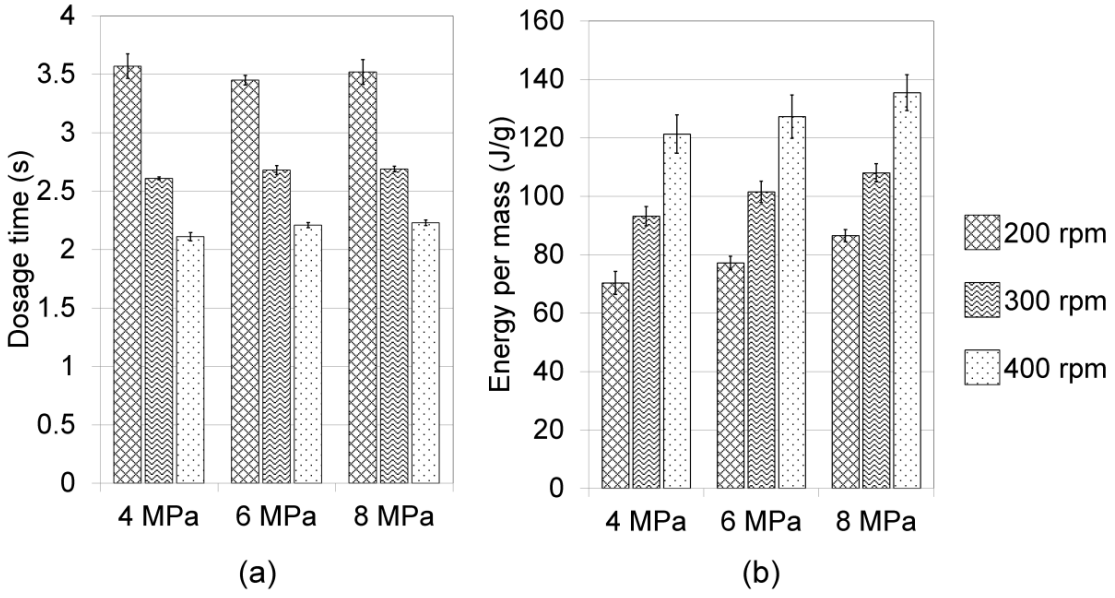

Figure 4.3. (a) Dosage time and (b) energy consumption based on screw rotation and back pressure.

Figure 4.3 shows the dosage time and the energy consumption per unit mass for a variety of rpm and BP settings; the same data are reported in Table 4.4. One can see that the dosage time and energy consumption have a slight dependency on the BP, while an obvious change in rotational speed increases the energy consumption and reduces the dosage time. In this study, settings of 300 rpm and 4 MPa were selected as the most reliable and efficient parameters to process UHMWPE powder.

4.4.2. Mechanical Properties

Figure 4.4 shows the representative tensile stress versus strain curves of each sample type, i.e., IM2.5, IM3.0, IM3.5, and ICM. An obvious improvement was seen. The average strain at break of ICM was 395%, while all IM samples similarly failed around 110% strain. Moreover, the tensile stress of the IM samples could not pass 20 MPa and tended to show a stress drop after yielding. Contrary to this, ICM samples showed strain hardening until failure.

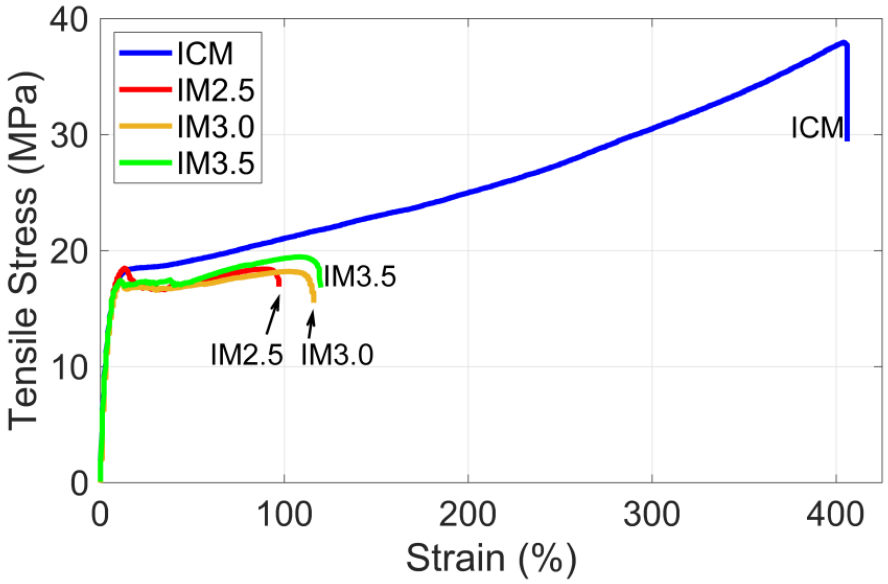

Figure 4.4. Tensile stress plots of representative samples for each sample type.

The bar graphs in Figure 4.5 show the average results of at least five samples for each sample type. This significant difference among the IM and ICM samples was attributed to whether a delamination defect existed on the surface of the parts. This layer caused early failure of the IM samples.

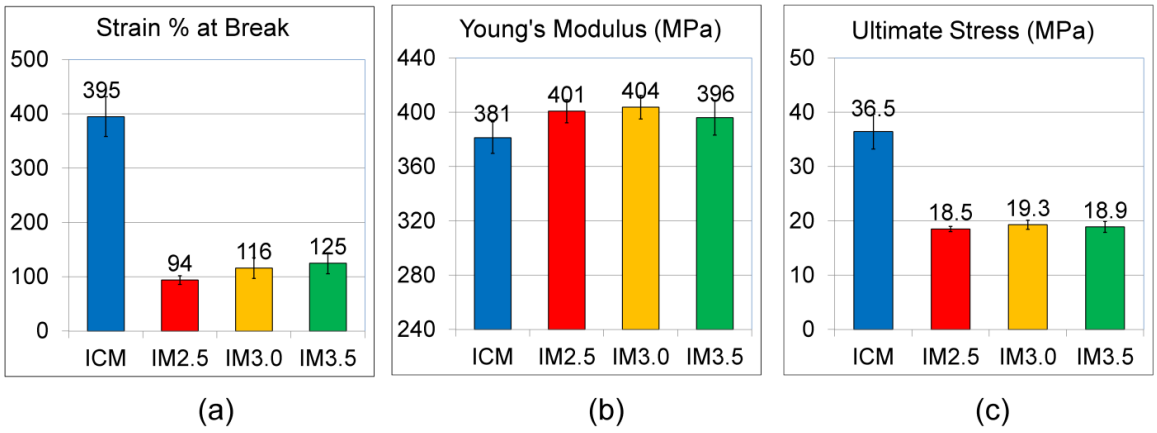

Figure 4.5. Bar graph of average mechanical properties: (a) strain % at break, (b) Young's modulus (MPa), and (c) ultimate tensile stress (MPa).

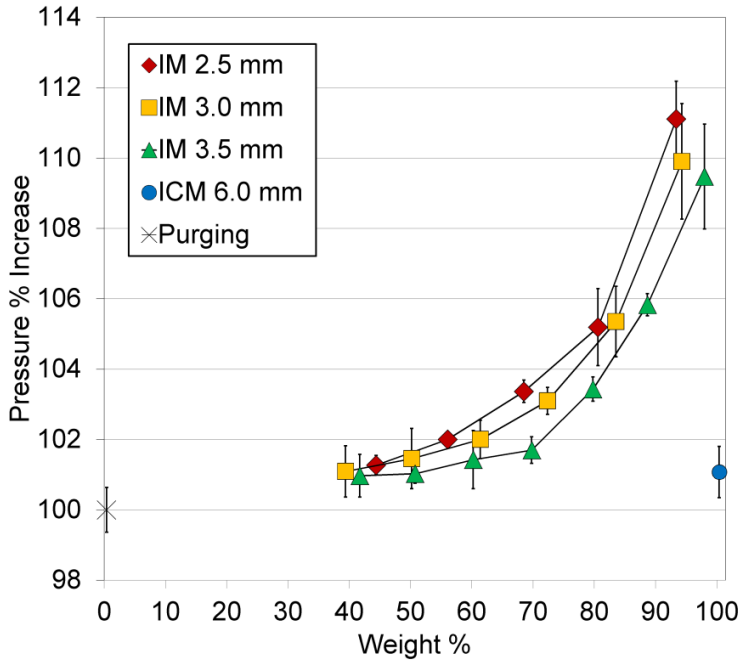

Figure 4.6. Injection pressure percent increase vs weight percent.

There was a slight improvement of strain at break with IM samples and increasing thickness, from 94% to 125%, as seen in Figure 4.5 (a). The Young's modulus of IM samples, as shown in Figure 4.5 (b), was quite similar (averaging around 400 MPa), while ICM samples had a Young's modulus of 381 MPa. This drop in modulus might be due to the lack of a brittle delamination layer. Two types of defects could be detected on the parts that caused early failure. The first and obvious defect was the delamination formation on the IM sample surfaces. The second defect might be the lack of enough packing pressure to properly fuse the porous UHMWPE melt. The ultimate tensile stress of the ICM samples was 36.5 MPa, while all of the IM samples failed below 20 MPa.

4.4.3. Mold-Filling Behavior and Injection Pressure Characteristics

Figure 4.6 shows the pressure percent increase versus weight percent. All of the pressure increase data were normalized based on the purging pressure (no mold filling), i.e., 100% pressure at 0% weight.

The purging pressure should represent the resistance of the material in the injection barrel regardless of any mold flow restriction. The ICM weight was assumed to be 100%, and the relative injection pressure was measured as 101% in reference to the purging pressure. All IM sample pressure values in Figure 4.6 showed an increase from 40% to 60% weight. Then the pressure was sharply increased and diverged from 60% to 98%. At this range, the cavity thickness effect was clear since the IM2.5 samples showed the highest pressure increase.

The μCT scans of short-shot IM samples with increasing shot weight percent are shown in Figure 4.7. As the shot weight percent increased, the degree of internal porosity decreased. This further confirmed that the UHMWPE melt entered the mold as an irregular porous structure and

then became less porous when more material was injected. In one of our previous studies, we reported a similar flow behavior for a different grade of UHMWPE in pellet form that also slipped on the mold surface and did not exhibit the typical fountain flow behavior [67].

The compression phase of some ICM samples was skipped to examine the sample formation without the compression action. For example, a melt fractured and highly porous structure of such a sample and its μCT scan are shown in Figure 4.8.

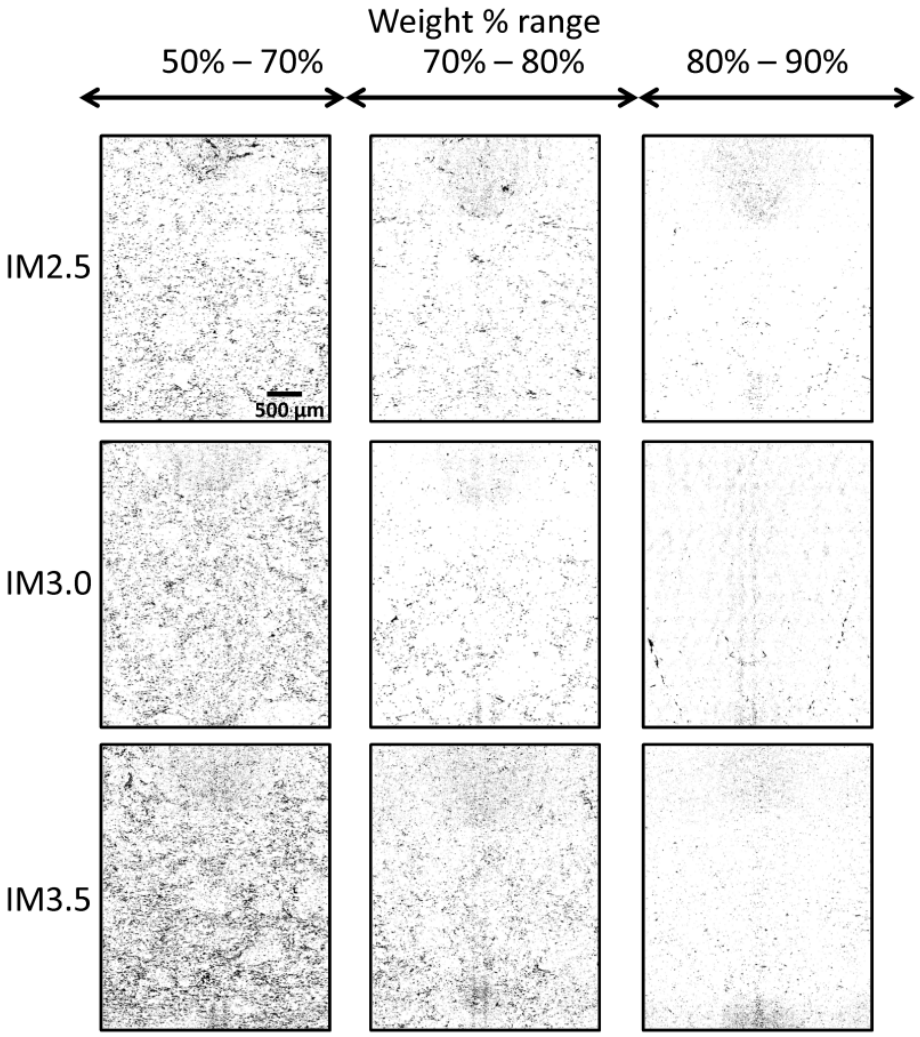

Figure 4.7. μCT scans of samples with different weight %.

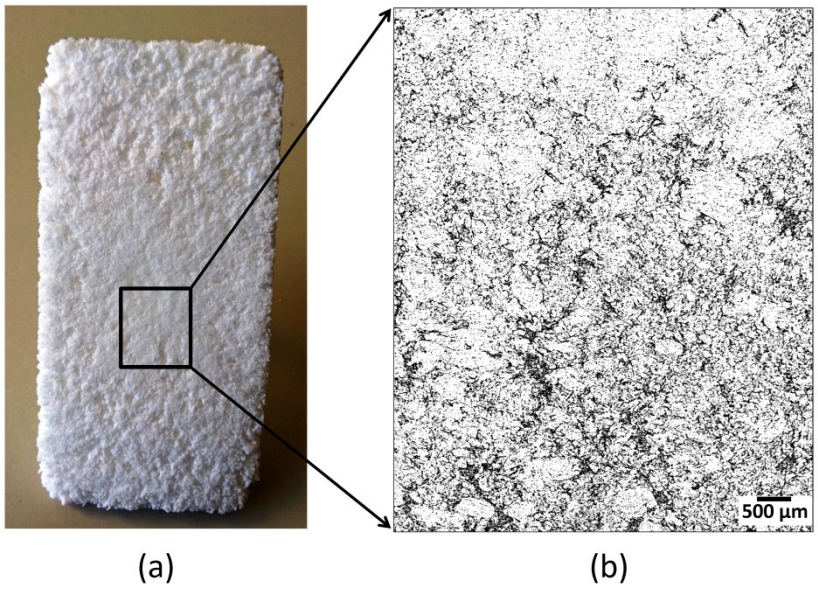

Figure 4.8. (a) Image of an ICM sample without the compression action and (b) µCT scan of the area as shown.

4.4.4. Oxidation and Thermal Degradation

During the processing of UHMWPE or under a prolonged aging process, the presence of oxygen may lead to oxidative degradation in the material that is detrimental to key properties such as wear resistance [71]. The oxidative degradation can be detected by FTIR as the transmittance of the peak at 1718 cm^{-1} [72]. The FTIR curves of the molded samples and two control samples aged for 30 minutes and 60 minutes at 180 °C are plotted in Figure 4.9. All samples showed a characteristic polyethylene curve as expected [73]. The image in Figure 4.9 (b) provides a subplot of the 1718 cm^{-1} area from 1850 to 1550 cm^{-1}. While aged samples exhibited an obvious peak around the wavenumber of oxidation, none of the IM or ICM samples exhibited a peak at that point. This suggests that the oxidation level in all molded samples was very low and was undetectable by FTIR. In the next section, the possible molecular level reduction due to thermally induced chain scission will be studied using DMA.

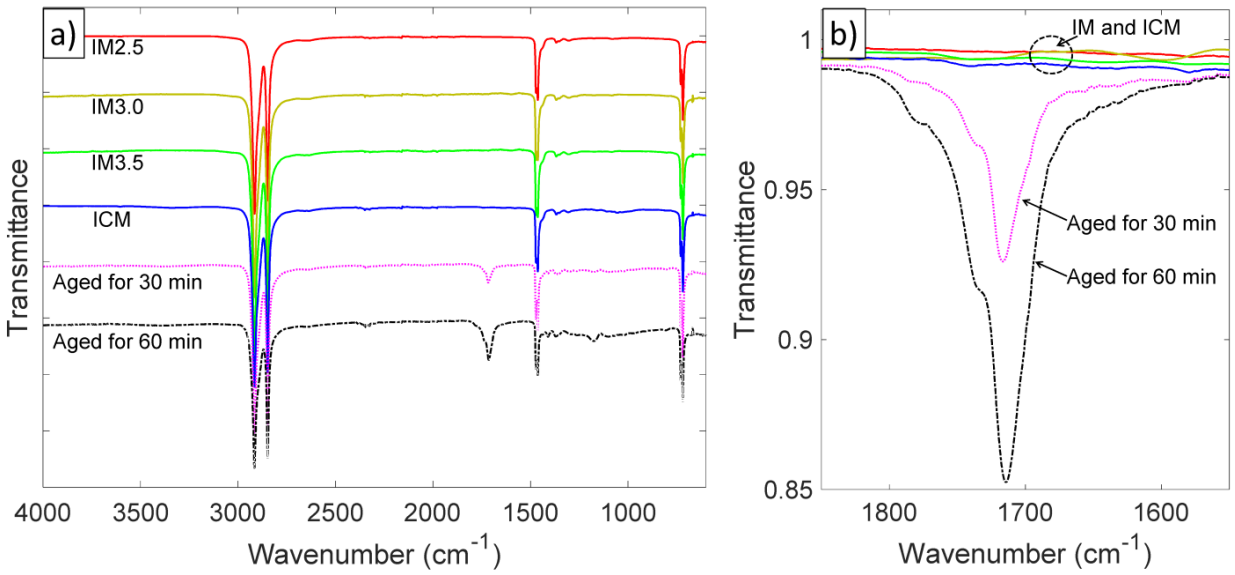

Figure 4.9. FTIR scans of UHMWPE samples: (a) range from 4000 to 600 cm^{-1}, and (b) transmittance at the carbonyl region.

4.4.5. Dynamic Mechanical Analysis (DMA)

Injection molded samples should be examined not only for oxidation but also molecular level reduction due to chain scission. Given the reported difficulties when using rotational rheometers [37], [70], DMA tests in tensile mode was employed to handle the high viscosity of UHMWPE over a wide range of temperatures (even at temperatures higher than its melting point) and elastic moduli without reaching the machine limits.

DMA results of CM, IM, and ICM samples in Figure 4.10 were plotted based on the average values of the samples. The average data the measurements for each sample type are illustrated in Figure 4.11. The upper level of the temperature was set at 150 °C, which was well above the melting point of UHMWPE.

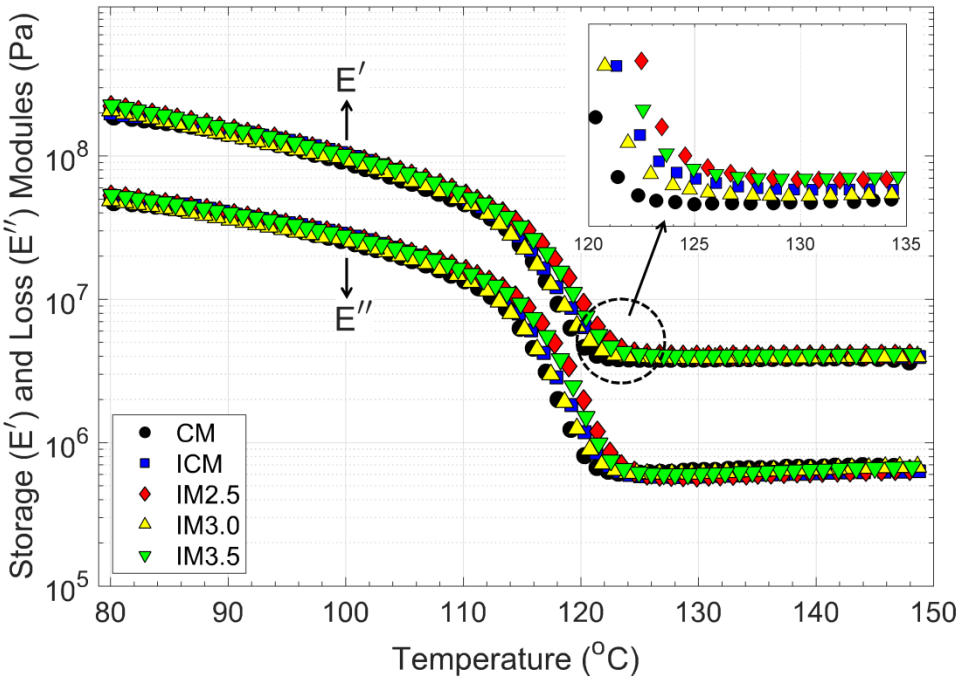

Figure 4.10. DMA results of CM and injection molded samples.

There was a typical softening decline in both the storage modulus (E') and the loss modulus (E") from the beginning until the temperature exceeded ~120 °C. Then the E' showed a relatively constant and less temperature-dependent region, the so-called rubber plateau. In this study, a temperature of 140 °C, which is above the melting point and in the rubber plateau region, was selected as a reference point for the DMA results. A higher level of the rubber plateau of E' indicates a higher molecular level or crosslinking of the polymer chains [74]. In Figure 4.11 (a), as expected, there was no significant difference among the E' of IM and that of the ICM samples (overall E' average of all samples, except the CM sample, was 4.00 ± 0.18 MPa). The average E' of the CM sample (3.88 ± 0.04 MPa) was slightly lower than that of the IM and ICM samples. At first, this might look counterintuitive. However, it is known that linear polyethylene tends to crosslink, which usually increases the melt viscosity and storage modulus of the polymer if there is no excessive thermal degradation [75], [76].

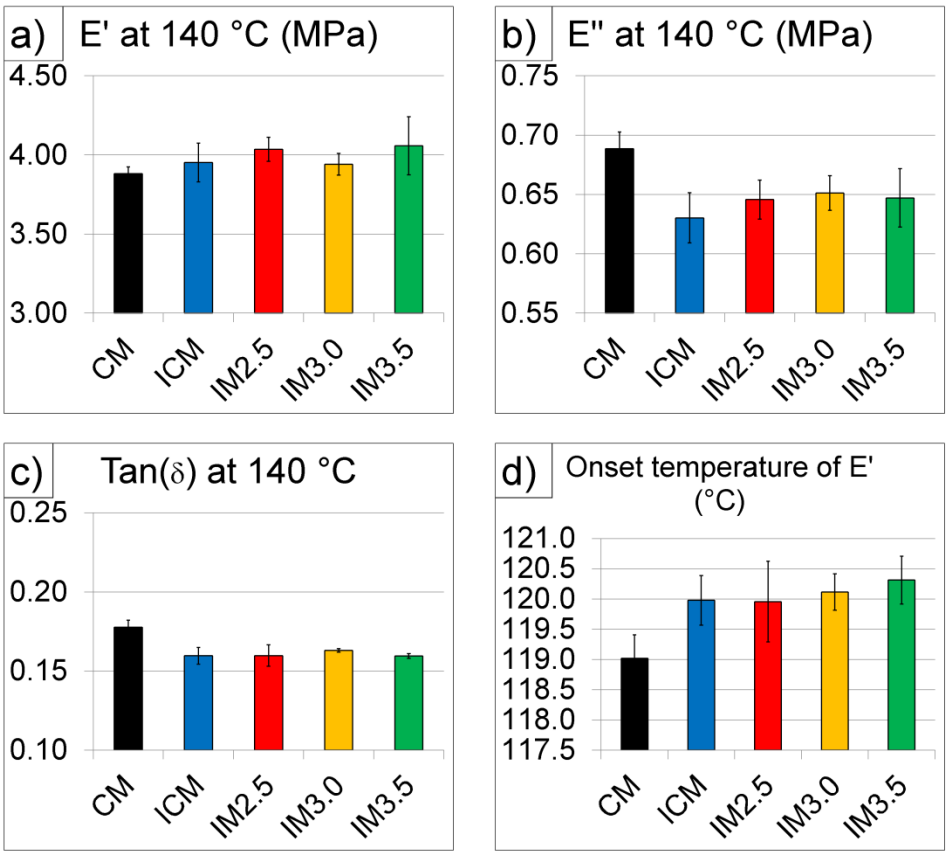

Figure 4.11. Average DMA results: (a) E' at 140 °C (MPa), (b) E" at 140 °C (MPa), (c) tan (δ) at 140 °C, and (d) onset temperature of E' (°C).

It has been reported that the experimental conditions may significantly affect the results of DMA of UHMWPE [77]. The sample volume changes when the sample melts due to the thermal expansion and increasing free volume in the melt. Therefore, as a dimensionless quantity, tan (δ) (the loss factor) might be a more reliable parameter in DMA to examine possible thermal degradation. Tan (δ) simply compares viscous and elastic behaviors based on the ratio of the loss modulus (E") to the storage modulus (E'). Figure 4.11 (c) shows the average tan (δ) measurements of the samples. The average tan (δ) of CM was higher than all other IM and ICM samples, which indicates that more elastic behavior was present in IM and ICM samples due to the possible crosslinking.

Another indication of crosslinking of the IM and ICM samples might be the higher onset temperature of E' at the starting point of the rubber plateau [74]. The close-up, inset image in Figure 4.10 shows that all of the IM and ICM samples have higher onset temperatures. The average onset temperature of the CM samples in Figure 4.11 (d) is about 1 °C lower than all other samples.

In general, IM and ICM samples exhibited similar behaviors in the DMA tests and no excessive thermal degradation. In addition, different injection volumes, injection pressures, mold thicknesses, ICM method, and also some minor noise factors did not have enough influence to cause a detectable difference on the DMA results within this study.

4.4.6. Impact Test

The exceptional impact strength of UHMWPE is one of its critical properties. An impact test was first intended to be performed at room temperature according to the ASTM D256−10e1 standard. However, none of the injection molded samples fractured. This suggested that a high molecular level was present, which was also indicated by the DMA results. In the literature, some modifications—such as milling a double notch on both sides with a narrower angle and using a higher pendulum capacity—were performed to incite fracture [78], [79]. However, UHMWPE behaves like a rubber under impact. Specimens tend to absorb energy by excessive bending and twisting rather than fracturing. Therefore, the reliability and repeatability of the test was still susceptible to errors. One convenient method that did not drastically depart from the ASTM standard was to perform the test well below the glass transition temperature of the UHMWPE (–122 °C). Thus, liquid nitrogen with a boiling point of about −195 °C was used to lower and control the test temperature.

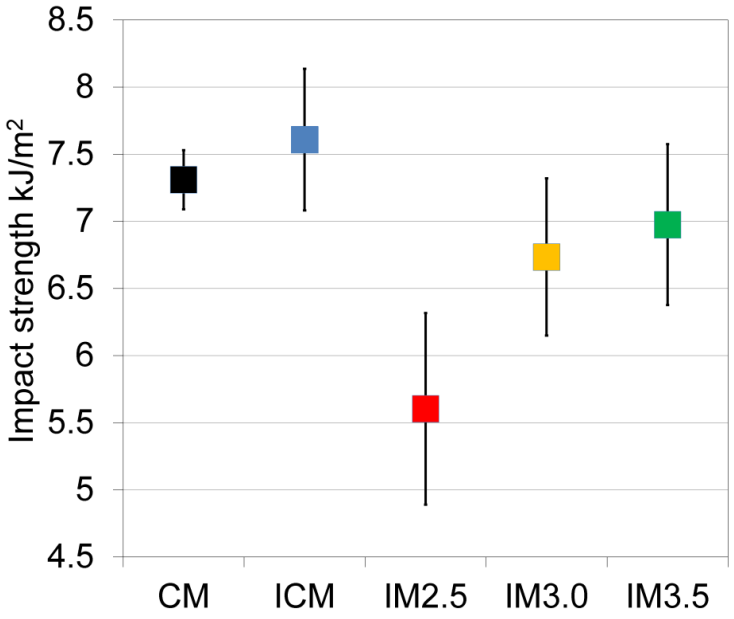

Figure 4.12. Impact strength plot of UHMWPE samples.

Figure 4.12 shows the impact strength plots of cryogenically treated UHMWPE samples. As a reference point, CM samples had average impact strength of 7.31 ± 0.22 kJ/m^2. ICM samples had a slightly higher impact strength, with a wider standard deviation, of 7.61 ± 0.53 kJ/m^2. It is known that different processing may affect the mechanical properties of UHMWPE differently due to different levels of reptation (also known as the time and pressure dependent diffusion) of the polymer chains [80]. In this study, ICM samples showed slightly higher impact strengths than the IM samples, which also agreed with the DMA results. The lower impact strength of IM samples may be attributed to the limited infusion packing of the material based on the fixed cavity thickness, which also explains why a 2.5 mm thickness leads to a lower impact strength. Another reason for the strength drop might be the brittle delamination layer on the surface of the IM samples. Nevertheless, the difficulty in fracturing all the molded samples at room temperature suggested that the proper injection molding process can prevent UHMWPE from experiencing significant thermal degradation.

Figure 4.13 shows SEM images of the fracture surfaces of impact-tested UHMWPE samples. The milled surfaces for the notch on the top edge and the surface layer can be seen on the left side. The CM and ICM samples in Figure 4.13 (a)–(b) lack the delamination layer due to the compression action on the surface.

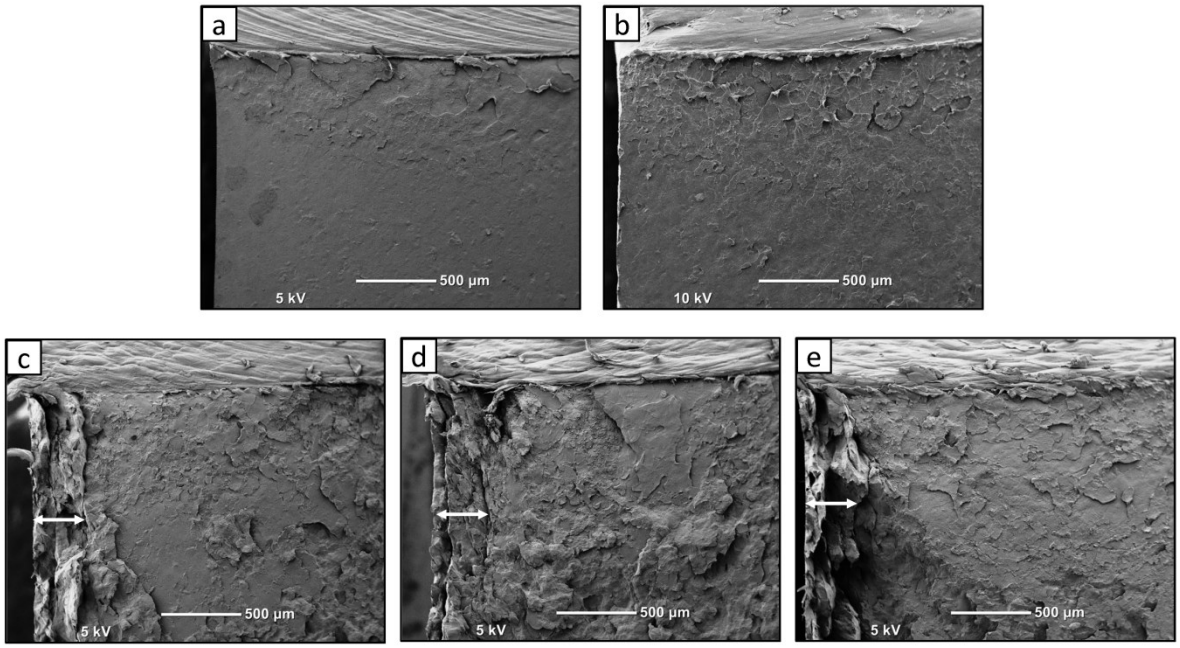

Figure 4.13. SEM images of samples: (a) CM, (b) ICM, and (c,d,e) injection molded samples IM2.5, IM3.0, and IM3.5. (Double arrow lines show the thickness of the delamination layers).

However, the IM samples in Figure 4.13 (c)–(e) have a characteristic delamination layer that includes two distinct sub-layers. The first is a thin sub-layer on the top and bottom surfaces, while a relatively thicker sub-layer was formed underneath the skin during the molding of UHMWPE. Although it is hard to measure the thickness of the delamination layer because of the wavy separation, it can be seen that the thickness of all IM samples is similar and around 300 µm. Namely, the thickness of the delamination layer does not show a dependency on the part thickness. The formation of the delamination layer is likely due to the material separation between the frozen layer and the highly entangled moving melt in the hot core of IM samples

during the packing phase. The gap-wise compression action in IMC is able to better fuse the frozen layer and the molten core.

4.4.7. The Relationship Between the Packing Pressure and the Formation of a Delamination Layer

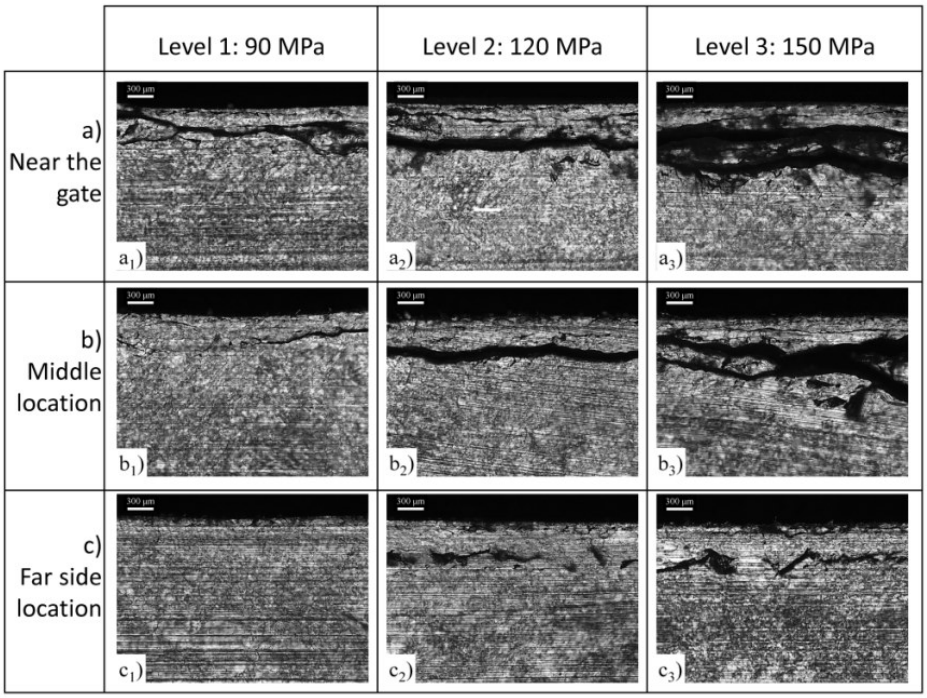

Figure 4.14. Optical microscope images of sliced samples based on different locations and different packing pressure settings. (a), (b), and (c) The images show the locations from the gate to the far side of the part. Subscript numbers 1 to 3 show the increasing packing pressure levels. The white scale bar on the left corner is equivalent to 300 µm. The flow direction is perpendicular to the page.

Although the ICM method eliminated the delamination layer, in regular injection molding, different parameter settings—such as the mold temperature, packing time, and packing pressure—can affect the delamination defect and should be investigated.

Using a higher mold temperature and longer packing time were not feasible in this case. This is because the mold temperature was already very high and at the suggested maximum.

Moreover, a packing time longer than 5 seconds had a negligible effect due to the gate freezing. However, higher packing pressure values are still applicable and can change the formation of a delamination layer on the skin.

Figure 4.14 shows the optical microscope images of the samples. The rows in the figure show the three different cross-sections, while the columns show the three different levels of packing pressure (90 MPa, 120 MPa, and 150 MPa). The flow direction is perpendicular to the page for all images. Please note that the straight horizontal lines in the images are scratch marks from the razor blade. The delamination layer formation from Figure 4.14 (a) to (c) seems to be decreasing, particularly at the lowest packing pressure of 90 MPa. Figure 4.14 (c_1) seems to be free of crack lines at the lowest pressure setting. The packing pressure through the part is estimated to be declining because of the solidifying material sticking to the mold surface. It is obvious that increasing the packing pressure was not able to suppress the delamination layer or reduce its thickness in conventional injection molding of UHMWPE. In fact, it seems that high pressure causes higher shear stress, which separates the hot core from the cold skin during packing, thus making the delamination layer even more apparent.

4.5. Conclusion

In this study, the injection molding of UHMWPE powder was performed using conventional injection molding with different mold cavity thicknesses, as well as with the injection–compression molding technique. The feeding of the powder UHMWPE was accomplished by selecting the proper machine type and optimized processing conditions, such as the back pressure and rotational speed (4 MPa and 300 rpm, respectively). DMA and impact tests showed that there is possible crosslinking during the melt processing of the UHMWPE and no measurable

oxidative and thermal oxidation was detected by FTIR and DMA. Tensile test and impact test results showed that ICM samples led to better sample properties free of a delamination layer, while IM samples suffered from delamination layer formation. It was also found that increasing the cavity thickness in IM samples from 2.5 mm to 3.5 mm may might improve the mechanical and impact properties. However, doing so did not suppress the undesirable delamination layer, which was likely due to the material separation between the frozen layer and the highly entangled moving melt in the hot core of IM samples during the packing phase. It was found that the UHMWPE melt entered the mold as an irregular porous structure and then became less porous when more material was injected, and the cavity pressure built up. The ICM technique and a larger cavity thickness were found to minimize the injection pressure requirement, improve the packing efficiency, and mechanical properties of the molded parts.

4.6. Acknowledgements

The authors would like to thank the Wisconsin Institute for Discovery (WID), the College of Engineering (COE), the Vice Chancellor for Research and Graduate Education (VCRGE), and the Kuo K. and Cindy F. Wang Professorship at the University of Wisconsin–Madison for their support. The authors would also like to acknowledge the Celanese Corporation for the material donation.

5. INJECTION MOLDING OF DELAMINATION-FREE ULTRA-HIGH MOLECULAR WEIGHT POLYETHYLENE

5.1. Abstract

When ultra-high molecular weight polyethylene (UHMWPE) in powder form is injection molded, the so-called delamination layering occurs near the skin of the parts. This layering defect hampers UHMWPE's superior wear resistance property and part surface quality. The delamination layer was caused by a combination of excessive shear stress near the part surface and high degree of molecular entanglement of UHMWPE. A mold insulation method that delays the rapid cooling of UHMWPE to reduce the shear stress and improve polymer chain "interdiffusion" across the entangled chain bundles was used to eliminate the delamination layer. When the insulation layer thickness and mold temperature were optimized, the delamination layer was eliminated completely while still maintaining a reasonable cooling/cycle time. The delamination-free parts were found to regain UHMWPE's superior impact resistance and tensile properties.

5.2. Introduction

Ultra-high molecular weight polyethylene (UHMWPE) is one of the specialty thermoplastics due to its extremely high molecular weight that gives UHMWPE all of its special properties. On the other hand, the high molecular weight structure increases the degree entanglement of the polymer chains and the viscosity, which causes very poor melt processability [4].

UHMWPE has been used in two well-known applications—high-performance synthetic fibers [81] and the bearing components of joint prostheses [82]—thanks to its characteristic

properties including high abrasion resistance [83], low friction coefficient, great chemical inertness, very high impact strength [84], and inherent biocompatibility [85].

Injection molding technology can be very economical when detailed part designs are needed at high manufacturing rates [14]. Any product design that requires one of UHMWPE's superior properties and a high rate of manufacturing can be a potential application for UHMWPE molding.

Injection molding of UHMWPE is a challenging task because UHMWPE lacks fluidity**.** In one of our previews studies [67], UHMWPE was processed with the aids of a super critical fluid (SCF); namely, super critical nitrogen (scN_2) or super critical carbon dioxide ($scCO_2$), as a plasticizer. The reduced injection pressure and thermal degradation suggested that the processability of UHMWPE in injection molding can be improved by introducing a SCF via a special full-shot option of microcellular injection molding (MIM) [53]. It was found that the highly viscous UHMWPE has a unique flow behavior that does not show a smooth and progressive melt front, nor the fountain-flow behavior, contrary to typical engineering plastics. Instead, it enters the cavity in the form of an irregular porous structure as a result of severe melt fracture.

In another study, we reported that a powder UHMWPE resin was processed with regular injection molding, as well as a special process called injection–compression molding (ICM). For the regular injection molding of UHMWPE powder, the so-called delamination layer problem was observed [66]. This persistent layering problem occurred near the surface of the part by delamination of the skin from the core. When the part was bent or twisted by hand, this skin popped out and could be easily peeled away from the core. When considering UHMWPE's high

abrasion resistance characteristic, this delamination layer hampers the product's success and must be solved.

The delamination of UHMWPE is a well-known concern in the components of total joint prostheses. This delamination issue has been attributed to the oxidation of UHMWPE during gamma air sterilization [86], [87]. If not done properly, the melt processing of UHMWPE in injection molding can also cause an oxidation risk for melt-processed UHMWPE. However, oxidation alone does not explain the entire delamination mechanism in injection molding.

The delamination layer can be attributed to two major factors during injection molding. The first factor is the excessive shear stress during the filling and packing stages. This high shear stress, especially at the interface of the frozen layer, can be related to the high viscosity of the material and the fast cooling of the skin [14]. The second factor can be attributed to UHMWPE's own inherent conditions that encourage easy layering. These inherent conditions are due to the high entanglement degree of molecular chains and slow polymer chain "interdiffusion" across the entangled chain bundles. Separate entangled chain bundles, especially those across the highly sheared layer near the frozen part surface, require a longer time and higher temperature to fuse to the core during the packing cycle [72], [88]. Increasing the packing pressure alone does not eliminate the delamination layer, rather it makes the delamination problem worse [66].

A method proposed here is using a thin layer of low-conductive material surface coating to eliminate the delamination problem. This coating method can delay the cooling on the skin of the UHMWPE melt during the filling and packing stages, which can promote chain "interdiffusion" and thus eliminate the delamination layer formation. In the literature, mold-cavity insulation coatings have been used for improving surface quality, reducing residual stress, improving

polymer flow, and eliminating weld lines in molded parts [89], [90]. According to the literature, difficult-to-flow polymers such as polycarbonate can benefit from this method [69]. These benefits can also be applied to molding UHMWPE considering its high viscosity, shear stress, and degree of molecular entanglement.

One concern with mold insulation might be the increased cooling cycle time. In general, the cooling stage accounts for at least two-third of the overall cycle time and having a longer cooling time will increase the overall cycle time and cost of manufacturing [14]. Therefore, the insulation thickness needs to be kept at a minimum. Traditionally, regular injection molding of UHMWPE requires relatively high mold temperatures, such as 80 °C. In the present approach, a lower mold temperature can be used with mold insulation. In this way, the ejection can take place sooner thanks to more efficient cooling in the cooling stage, despite a warmer mold surface temperature during mold filling and packing stages. If special molding heating and cooling techniques, such as rapid mold temperature control, rapid heat cycle molding (RHCM), or highly engineered cooling channels, can be employed [91], [92], the overall cycle time can be improved even more.

The aim of this study is to provide a robust molding solution for eliminating the delamination problem of powder UHMWPE by manipulating mold cooling via a low-conductive coating on mold cavity surface. Herein, the method for mold coating, along with a variety of mold temperature settings, will be presented. Results of impact tests, tensile tests, and differential scanning calorimetry (DSC) were used to characterize how the delamination layer or the lack of it affected part quality. SEM imaging was performed on the fracture surfaces to explore delamination formation. Both one-dimensional transient heat conduction and three-dimensional injection molding simulations were used to analyze and optimize the effect of mold coating on the cooling of the UHMWPE melt.

5.3. Methods and Experiments

5.3.1. Materials

A pure UHMWPE powder, GUR® 4120, was used as received from the Celanese Corporation. The calculated molecular weight was 5.0 million g/mol and the true density was 0.93 g/cm^3. More details about the material can be found in our previous study [66]. The melting point of UHMWPE is around 135 °C, although it changes a lot depending on the degree of crystallinity.

A clear epoxy resin without any filler (West System 105A with 205A hardener) was used for mold insulation coatings. The thermal conductivity of the cured clear epoxy resin was low and consistent at 0.20 W/m·K [93], [94].

A custom-made aluminum mold insert was used for the mold cavity surface coating and molding experiments. Table 5.1 shows the thermal conductivity of related materials.

5.3.2. Epoxy Coating

The epoxy coating was applied to clean aluminum mold surfaces at room temperature for complete coverage of the cavity surfaces, except for the sprue bushing. For a more ideal case, the sprue should be coated too, or a hot runner design should be used. Coated mold halves were stored for at least 48 hours for complete curing.

It should be noted that the clear epoxy resin may might not be durable enough for molding numerous parts in commercial production. However, for experimental purposes and proof of concept, the epoxy resin was convenient to use as it yielded an easy, adaptive, and repeatable coating process without any special tools.

Table 5.1. Material properties. Parameter k is the conductivity coefficient, c_p is the heat capacity, and ρ is density. These properties were used in the computer simulation.

Material	**k (W/m·K)**	**c_p J/(kg·K)**	**ρ (g/cm^3)**	**Grade and reference**
UHMWPE melt	0.4	3000	0.77	Powder type, 4120 Moldex3D
Cured epoxy	0.2	1400	1.2	Clear
Aluminum	154.2	890	2.7	6061 COMSOL

Table 5.2. Sample types based on coating level and coolant temperature.

Label of samples	**Coolant temperature (°C)**	**Coating thickness, nominal (µm)**	**Coating thickness, actual (µm)**
0-16	16	N/A	N/A
0-85	85	N/A	N/A
1-16	16	125	124 ±10
1-85	85		
2-16	16	250	259 ±12
2-85	85		

5.3.3. Sample Types and Processing Parameters

The injection molded sample types, which were labelled based on epoxy coating layers (and thickness) and coolant (mold) temperature, can be seen in Table 5.2. As will be discussed below, the nozzle temperature and injection speed were kept the same for all sample types. In the label of the samples, the initial number from 0 to 2 defines the coating level: “0” means no coating, “1” means one layer of coating, and “2” means two layers of coating. The last two numbers refer to the coolant temperature of the sample in degrees Celsius. The mold temperature will be treated to be the same as the coolant temperature.

Table 5.3. Processing parameters used in injection molding experiments for all sample types.

Processing Parameters	Value
Injection speed	20 cm^3/s
Injection volume	10.8 cm^3
Cooling time	20 s
Back pressure	4 MPa
Dosage speed (Screw RPM)	300 rpm
Packing pressure and time	100 MPa for 6 s
Barrel temperature profile	18 – 130 – 210 – 235 – 235 °C

The resulting coating thickness of samples was adjusted based on some preliminary experiments. After the epoxy was cured, the thickness of the coating was measured with a precision height gauge.

5.3.4. Injection Molding Experiments

A 350 kN injection molding machine (Arburg Allrounder 270A) with an 18 mm diameter screw was used for the molding experiments. A technical drawing of the aluminum mold inserts is provided in Figure 5.1. The coating, as highlighted with the blue lines, reduced the cavity thickness slightly. This change was neglected in simulations for simplicity.

The processing parameters are provided in Table 5.3. These parameters were used in injection molding experiments for all samples and were selected according to our previous study [66]. The temperature of the hopper throat was adjusted lower than the room temperature at 18 °C to have continuous and reliable powder feeding through the hopper. Based on those prior experiments, the typical delamination layer thickness was found to be around 300 μm, which will be used as a reference freeze-off thickness in the computer simulation.

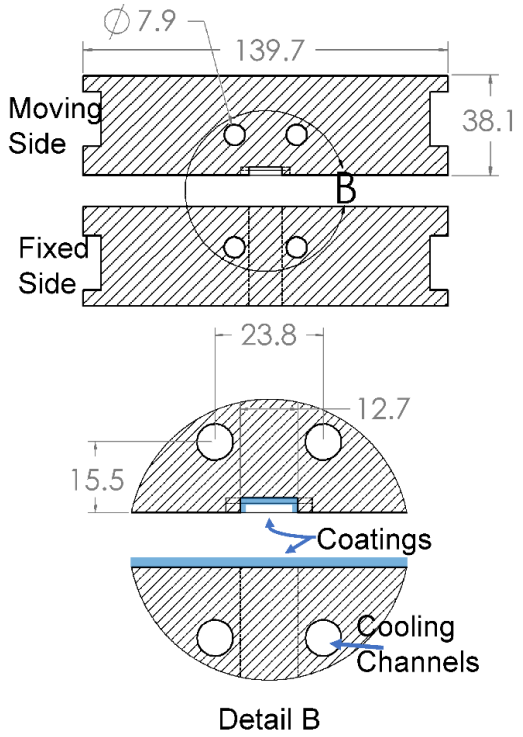

Figure 5.1. Technical drawing of aluminum mold inserts. The epoxy coating is highlighted with blue lines in the Detail B view. The dimensions are in mm.

5.3.5. Differential Scanning Calorimetry (DSC) Analysis

DSC analysis of UHMWPE was performed according to the ASTM F2625-10A standard method. Three random samples from each type were tested by heating samples from 30 to 200 °C, at a heating rate of 10 °C/min, with a weight range of 5 to 9 mg. The percentage of crystallinity was calculated as the standards indicated using the heat of fusion of 100 % crystalline polyethylene, 289.3 J/g. A leather punch was used to cut a cylindrical disk from the middle of the injection molded tensile bar. The skin of the samples was removed from both sides of the sample, leaving a core disk shape approximately 1.5 mm thick. The skin layer of the molded parts was not characterized in this study because of the difficulty of working with the large crystallinity gradient of the skin, as well as issues related to irregularities and oxidation in the delamination layer.

5.3.6. Tensile Tests

Tensile tests were performed following the ASTM D638-14 standard on an Instron 5967 test machine equipped with a 30 kN load cell. Five randomly selected specimens were tested for each sample type. The mold cavity was designed by conforming to the standard's type 1 specimen geometry except that the part thickness was slightly different due to the additional width added by the coatings. The part thickness and width were measured by a micrometer and updated each time before performing the test. The crosshead speed was set at 50 mm/min to produce rupture within 5 minutes as dictated by ASTM D638-14.

5.3.7. Impact Tests

The ASTM D4020 standard has been devoted to the characterization of UHMWPE. One of the scopes of the standard covers a method for impact strength testing of UHMWPE, which is similar to the common test method in ASTM D256, but uses a much higher impact concentration via a sharper double-notching procedure.

The impact test specimens were trimmed from the wider ends of the molded tensile bars to have a 63.5 mm long section from the middle of the bar. Specimens' tapered edges were milled gently to create flat surfaces for reliable notching and clamping on the impact tester. Specimens were notched on both sides by a single-edge razor blade (0.23 mm thick) mounted on a milling vise with a custom-made blade holder.

Five specimens for each molded sample type were tested on a standard Izod impact test device from Custom Scientific Instruments Company with a 5.4 J pendulum capacity. A few samples with a non-break type of failure were excluded since most of the samples showed a complete or hinge break. The accuracy of the notch geometry and the area of the un-notched

cross section were verified using a caliper and an optical microscope with a digital camera (Leica DM750).

5.3.8. Scanning Electron Microscopy (SEM)

The fracture surfaces from impact tests were coated using a Leica ACE600 coating system to achieve a 5 nm thick platinum sputter coating. SEM images were taken with a JEOL 6500 SEM with an accelerating voltage of 10 kV at the high vacuum setting.

5.3.9. Simulation of the Injection Molding Process

A commercial injection molding simulation software package, Moldex3D R16, was used for the mold filling analysis of the molded samples. The In-Mold Decoration (IMD) feature of the software package was used to mimic the presence of the epoxy coating on mold surface. In the IMD process, a film or coating can be defined as a boundary condition with a specified coating material and thickness. The mold base and cooling channels were included in the simulations according to the actual 3D design of the mold.

Table 5.4. Geometry and initial temperature condition used in the computer simulation.

Material	**Thickness Dimension (mm)**	**Initial Condition**
UHMWPE melt	1.65 (half of the part thickness)	240 °C, uniform
Cured epoxy	Changing depending on coating layers	Equal to the mold temperature
Aluminum	15	Mold temperature

To fully investigate the delamination problem, COMSOL Multiphysics 5.2 was selected for quickly analyzing the coating thickness and mold temperature relationship through a fast 1D transient heat conduction analysis, without running the full 3D simulation with every small step

change in the coating thickness and/or mold temperature. The program has a parametric sweep feature that allows users to change the coating thickness and mold temperature automatically for a wide range of parametric scans with small increments. In Figure 5.2, the 1D model can be seen. The geometric dimensions and initial temperature condition used in the 1D simulation are tabulated in Table 5.4.

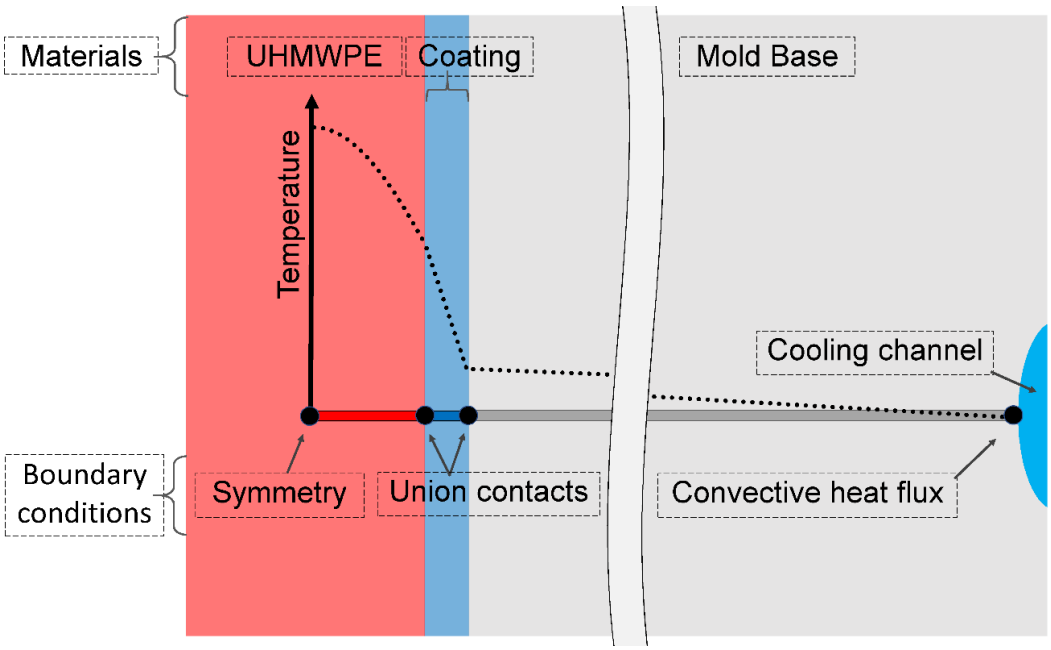

Figure 5.2. 1D transient heat transfer model used in COMSOL with representative temperature profile. Coating thickness was enlarged for easy viewing.

One major assumption of the 1D simulation was that the contact resistance at the epoxy-UHMWPE and epoxy-aluminum interfaces can be neglected due to the high cavity pressure. Another assumption—thanks to the simple part geometry, the high viscosity of UHMWPE, and the very short filling time—was that the heat transfer in the UHMWPE melt could be simulated through conduction rather than convection.

In COMSOL, an initial melt temperature of 240 °C was used. It was adjusted to be 5 degrees higher than the melt temperature to account for viscous heating during filling. The cooling

channel heat transfer coefficient was 50000 W/(m^2K). A constant melt density of UHMWPE was set as 0.77 g/cm^3 based on a pvT diagram from the Moldex3D library for an average pressure and temperature of 10 MPa and 180 °C, respectively.

The parametric sweep feature of COMSOL was used to apply the increasing coating thickness from no coating to 700 μm thick, in 50 μm increments. For each coating thickness, the four mold temperature settings were used: 16, 39, 62, and 85 °C. The time to reach the melting point of UHMWPE (~135 °C) on the delamination layer (300 μm inside from the surface) was named as "layer freezing time".

5.4. Results and Discussion

5.4.1. Impact Strength and Fracture Surface

UHMWPE's extraordinary impact strength was observed via the dedicated standard method (ASTM D4020). An extreme impact concentration via the sharp double-notching method was employed. A lower impact strength of injection molded UHMWPE can indicate excessive thermal degradation and/or delamination damage on the part.

Figure 5.3 shows the average impact strengths of the specimens for each of the six sample types. The 2-85 sample had the highest average impact strength of 119.0 ± 6.3 kJ/m^2, which was comparable to the reference value of 128.0 ± 6.5 kJ/m^2 (compression-molded samples) from ASTM D4020. The high impact strength of the 2-85 sample not only indicated that the molding process was satisfactory via optimal coating thickness and mold temperature settings, it also indicated that the plasticizing process (the dosage cycle) in the injection molding barrel was done properly and the thermal degradation is minimized.

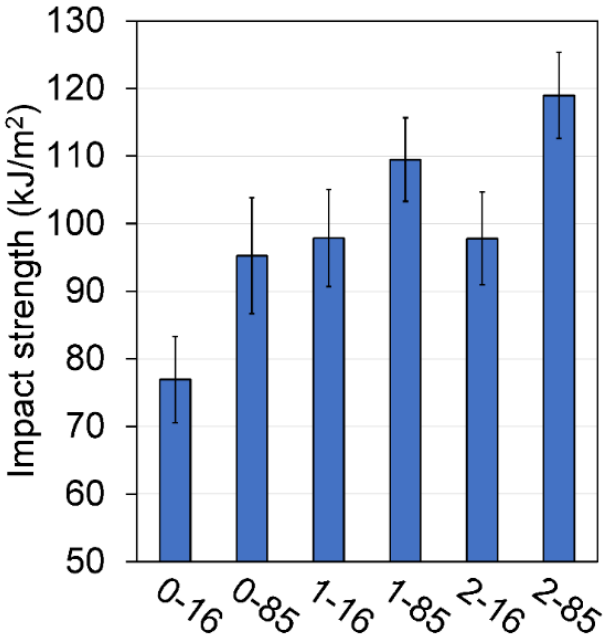

Figure 5.3. Izod Impact strengths of samples.

Since the dosage cycle was kept the same for all sample types, the weakness of the other samples can be attributed to molding-related issues such as a delamination layer and/or insufficient packing. The 0-16 sample had the lowest impact strength, which can be attributed to the fastest cooling time. On the one hand, the similar impact strengths of the 1-16 and 2-16 samples could be due to the insulating effect of the different coating levels, which were similar when the mold temperature was very low (16 °C). On the other hand, there was a notable improvement by increasing the coating thickness at the high mold temperature setting (85 °C). This suggests that the mold temperature should be adjusted accordingly in conjunction with the coating thickness for good quality parts.

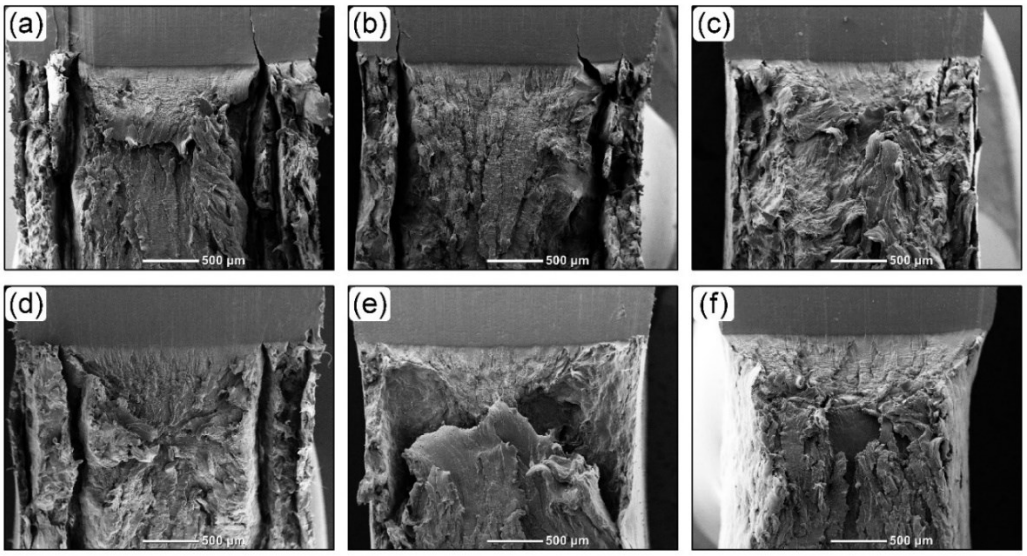

Figure 5.4. SEM images of the impact test fracture surfaces of samples: (a) 0-16, (b) 1-16, (c) 2-16, (d) 0-85, (e) 1-85, and (f) 2-85. The notch area from one of the double notches can be seen at the top of the images.

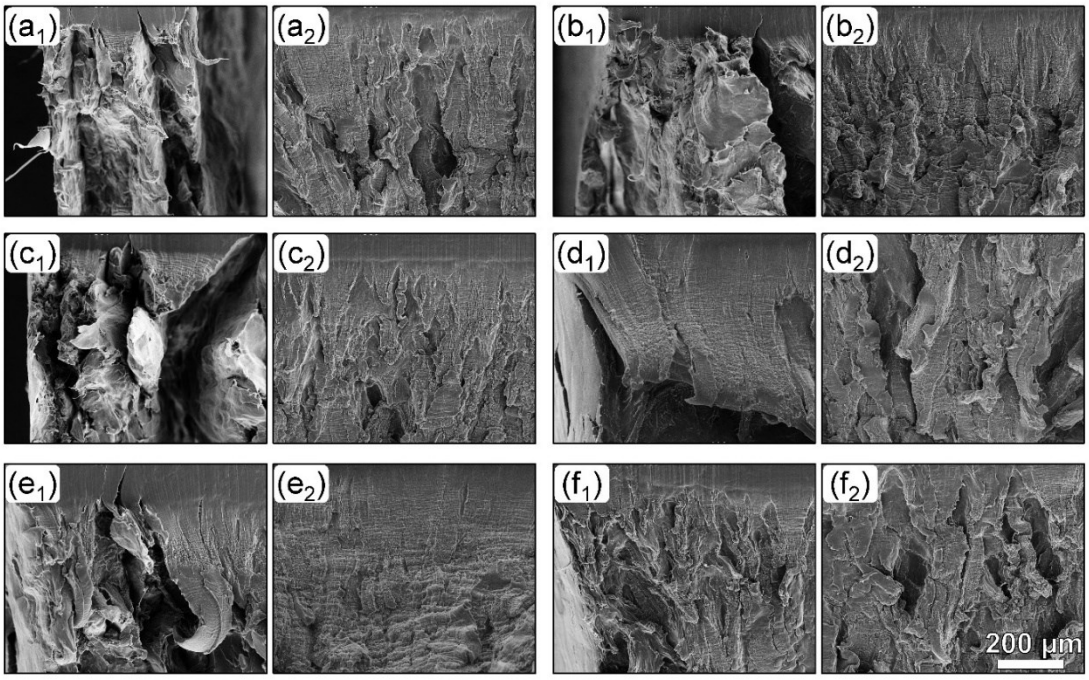

Figure 5.5. SEM images of the impact test fracture surfaces of samples at higher magnification: (a) 0-16, (b) 0-85, (c) 1-16, (d) 1-85, (e) 2-16, and (f) 2-85. The notched ends can be seen at the top. Subscript number 1 shows the skin and number 2 shows the core location. The 200 µm scale bar in (f_2) applies to all images.

In Figure 5.4, the impact test fracture surfaces of the molded samples are shown. The delamination layers of samples (a), (b), and (d) can be seen on both sides of the molded samples. These layers appeared flat and usually separated from the core as a result of the impact force, which suggested a brittle fracture on the delamination layer. Samples (c) and (e) showed some improvement. However, sample (f)—the 2-85 sample—was completely delamination free. Unlike the other samples, the side walls of 2-85 were pulled inwards due to ductile fracture. When present, the brittle delamination layer can be easily peeled away from the core, negatively affecting both the part surface quality and the mechanical properties of the part.

In Figure 5.5, the higher magnification of the fracture surfaces of all sample types is provided. In particular, the worst and best performing samples, 0-16 and 2-85, respectively, are worthy of comparison. Images from the core section for both samples in (a_2) and (f_2) seemed identical, with some wavy and elongated bundles as a result of ductile fracture under the impact force. However, unlike the flat and brittle looking delaminated skin in Figure 5.5 (a_1), the skin of the 2-85 sample (f_1) looks similar to the stretched bundles of its core morphology (f_2) as a result of its delamination-free and ductile structure.

5.4.2. DSC Analysis

The average percentage of sample crystallinities, including the raw, as-received UHMWPE powder, is plotted in Figure 5.6 for the 1st and 2nd heating cycles. Figure 5.7 shows the representative thermograms of both heating cycles. The higher core crystallinity of the samples reflects longer cooling time histories. For the 1st heating thermograms, samples exhibited two kinds of % crystallinity: one low at around 58.2 ± 0.3% for 16 °C samples, and one high at around 61.3 ± 0.5% for 85 °C samples. This separation in the two groups suggests that the mold temperature has a stronger effect on the cooling behavior of the samples than the coating level.

This phenomenon also suggests that the insulating effect of the coating layer is limited to the skin layers of the molded samples.

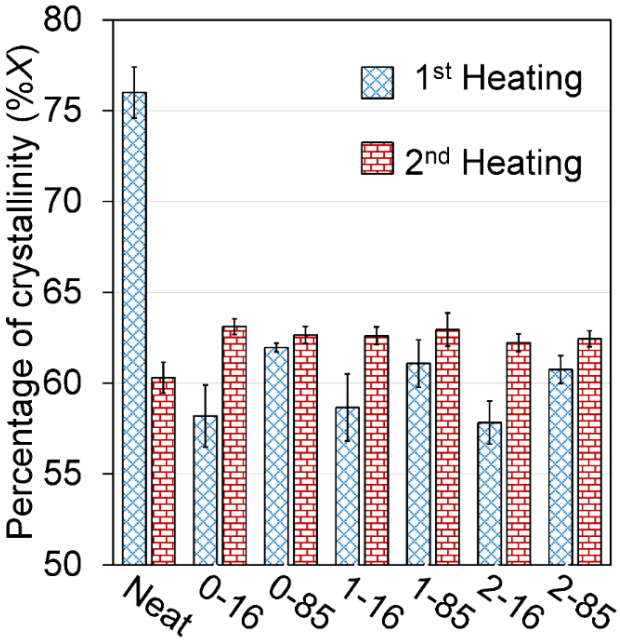

Figure 5.6. The average percentage of crystallinity of samples from the 1st and 2nd heating scan thermograms.

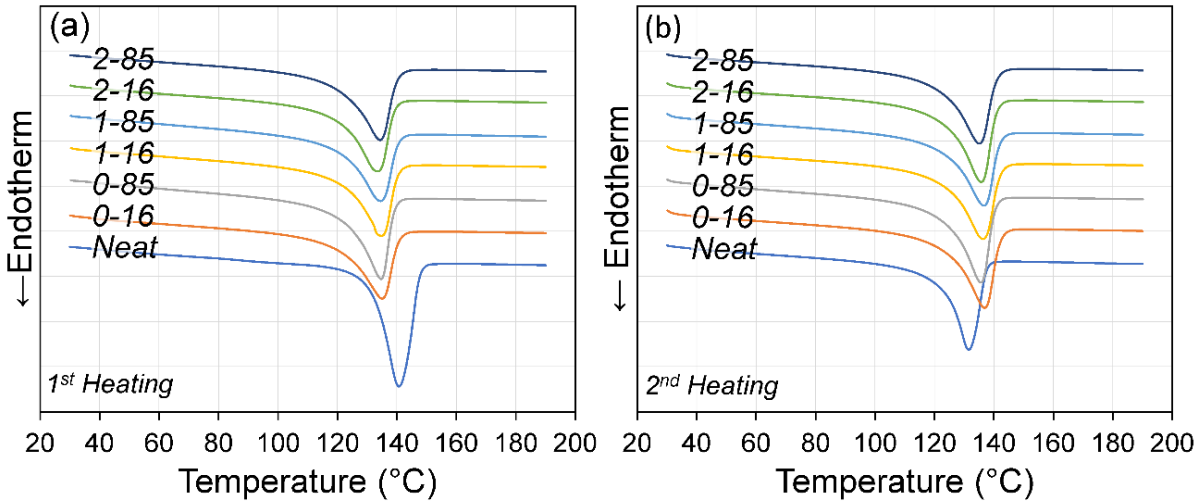

Figure 5.7. DSC heating thermograms of samples showing (a) first heating and (b) second heating scans.

Figure 5.6 includes the % crystallinity of the samples from the second heating cycle. As expected, all injection molded samples had similar % crystallinities, with an average of 62.4 ± 0.33%, with no significant difference among the samples. This was slightly above the as-received powder's % crystallinity of 60.3 ± 0.85%.

In the Figure 5.7 (a), the melting point of the injection molded samples did not exhibit a significant difference at 134.9 ± 0.8 °C, while the raw sample exhibited a much higher melting point at 140.6 ± 1.2 °C. After equalizing the thermal history, the second heating reversed the situation. The neat sample exhibited a lower melting point at 131.6 ± 0.8 °C, while the injection molded samples had a higher melting point of 136.5 ±0.4 °C.

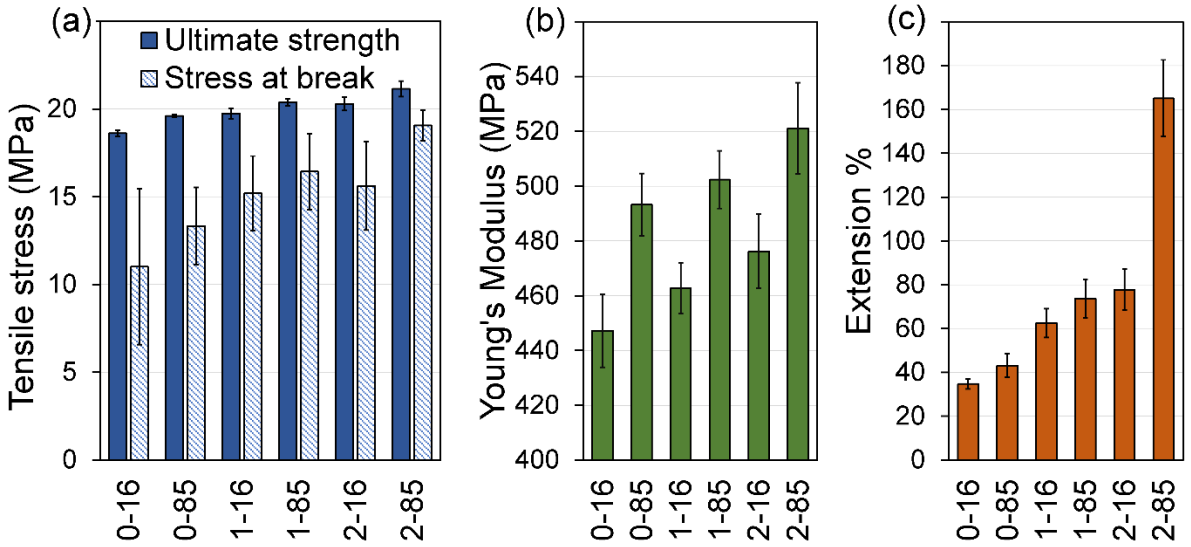

Figure 5.8. Tensile test results: (a) tensile stress, (b) Young's moduli, and (c) extension percent.

The difference of melting points and % crystallinities between injection molded and raw samples is likely due to the material degradation of UHMWPE, such as chain scission from melt processing. However, the degree of degradation should be minimal since the impact tests did not reflect any noticeable reduction in strength.

5.4.3. Tensile Properties

The average tensile properties of all samples are plotted in Figure 5.8, and the same data are tabulated in Table 5.5. Besides the tensile test results, the part weights are also provided in Table 5.5. As expected, the extra coating layer(s) reduced the effective cavity thickness and, thereby, the overall part weight.

Table 5.5. Tensile test results of samples.

Sample type	**Ultimate strength (MPa)**	**Stress at break (MPa)**	**Young's Modulus (MPa)**	**Area under curve (J)**	**Extension (%)**	**Part weight (g)**
0-16	18.6 ± 0.2	11.0 ± 4.4	447.2 ± 13.4	13.7 ± 1.1	34.8 ± 2.4	8.56 ± 0.03
0-85	19.6 ± 0.1	13.3 ± 2.2	493.3 ± 11.3	18.0 ± 2.3	43.1 ± 5.3	8.52 ± 0.07
1-16	19.7 ± 0.3	15.2 ± 2.1	462.8 ± 9.2	22.9 ± 2.3	62.5 ± 6.6	7.97 ± 0.02
1-85	20.4 ± 0.2	16.4 ± 2.2	502.4 ± 10.5	29.6 ± 3.6	73.7 ± 8.7	7.89 ± 0.02
2-16	20.3 ± 0.4	15.6 ± 2.5	476.2 ± 13.5	28.8 ± 3.5	77.8 ± 9.4	7.70 ± 0.03
2-85	21.2 ± 0.4	19.1 ± 0.9	521.1 ± 16.7	63.5 ± 6.7	165.1 ±17.5	7.74 ± 0.02

It is known that UHMWPE tends to exhibit strain hardening behavior unless the structure contains defects resulting from poor melt processing and/or a delamination layer [66]. Therefore, the improvement in ultimate strength in Figure 5.8 (a), particularly for the 2-85 samples, can be attributed to the elimination of the delamination layer and improved molding due to delayed cooling. These process-related improvements contributed to the percent of extension the most. The percent of extension of the 2-85 samples was more than twice that of the other samples, as shown in Figure 5.8 (c).

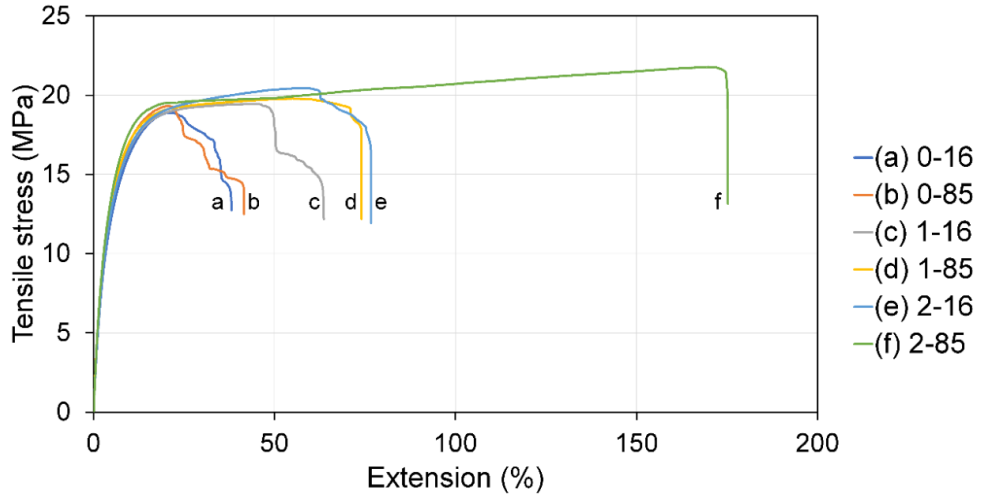

Figure 5.9. Engineering stress vs. extension plots of representative samples for each sample type.

The Young's moduli of samples in Figure 5.8 (b) increased gradually as the coating thickness and mold temperature increased. As a well-known effect, the longer cooling time of samples can increase the Young's modulus due to the increased crystallinity [61]. For example, the similar Young's moduli of the 0-85 and 2-16 samples, 493 and 476 MPa, respectively, can be attributed to their similar cooling histories. Similarly, 16 °C samples had smaller moduli than 85 °C samples as a result of the different thermal histories of the samples based on the two different mold temperature settings of 16 and 85 °C.

The difference between the ultimate strength and the stress at break of the 2-85 samples was the smallest among the sample types, as shown in Figure 5.8 (a). However, other samples lost a considerable amount of stress before failure, likely as a result of yielding from pealed delamination layer(s) during tensile load. This phenomenon can be seen in the plots of representative samples in Figure 5.9. While the 2-85 samples exhibited a sudden break, other samples showed decaying stress until rupture.

5.4.4. Computer Simulation of the Injection Molding Process

Although UHMWPE's unique flow behavior might be difficult to simulate, contemporary injection molding CAE programs are highly sophisticated when predicting the molding process [14]. For this purpose, we created a model based on the actual mold design and Moldex3D's IMD module was used to account for the insulation effect of the epoxy coatings.

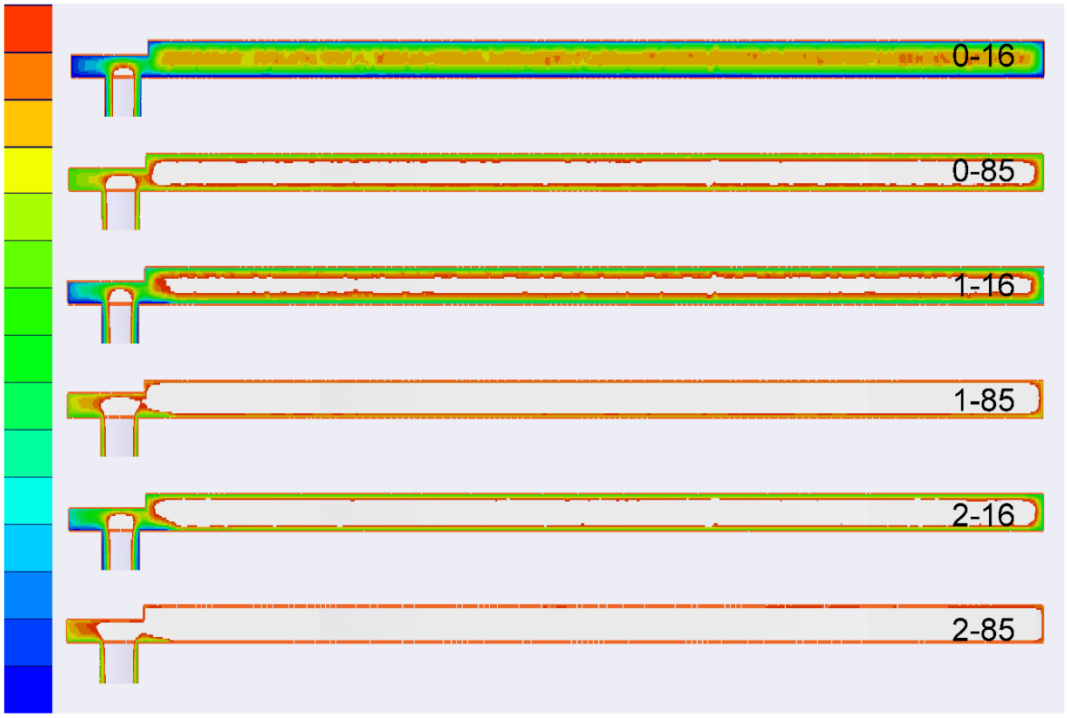

Figure 5.10. End of the packing temperature distribution from the center section view of the parts. The gates are on the left. The thickness of the part was magnified two times for ease of visualization; the actual size of the parts is thinner. The bar thickness is 3.3 mm and bar length without gate is 165.1 mm. For all color images, the upper and lower limits of the color range were set at 135 °C (red) and 16 °C (dark blue), respectively.

The primary interest in this 3D simulation is to obtain the predicted temperature distribution in the part, especially at the end of packing stage, to search for the cause of delamination layer. Due to the high viscosity of UHMWPE, the material is under very high shear stress during the filling stage. It has been found that the delamination layer and part core separation occurred at around 300 μm from the un-coated part surface and the shear stress from the packing stage only

exacerbated delamination layer formation [66]. If the temperature of the skin can be kept above the melting point of UHMWPE (135 °C) until the packing stage is done, delamination layer formation can be avoided.

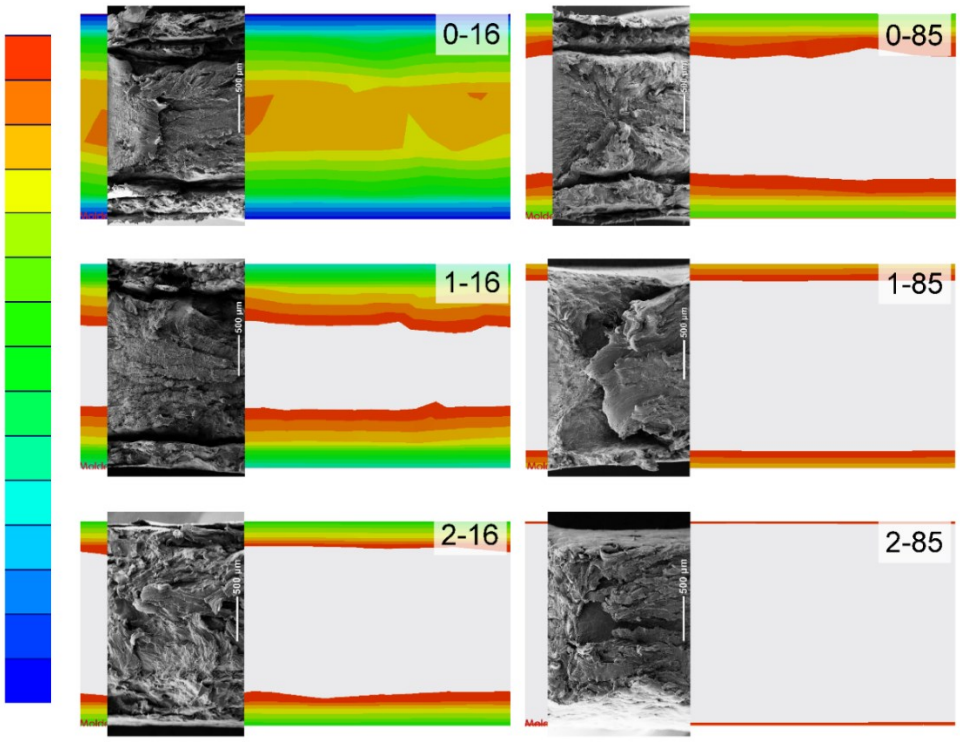

Figure 5.11. Zoomed in images from the center section views of the parts with inset impact fracture SEM images.

Figure 5.10 shows the temperature distribution at the end of the packing stage (6.54 s) from the center section view of the parts. The color bar was selected to be from the lowest mold temperature of 16 °C to the reference melting temperature of UHMWPE (135 °C). With that, the colored area shows the frozen layer and any area in light gray inside the part contour indicates that the temperature was above 135 °C. With the exception of sample 0-16, samples had a hot core (unfrozen) at various thicknesses. Sample 2-85 had the thickest hot core and the thinnest frozen layer. Across each sample type, the hot core and frozen layer thickness seemed unchanged due to the short filling stage and simple part geometry.

In Figure 5.11, the images were created by zooming in on the center of the section views from Figure 5.10, inset with SEM images from the impact tests. The different thicknesses of the frozen layers as a result of different cooling rates can be correlated with delamination formation in the SEM images. Sample 2-85 had the thinnest frozen layer and no delamination layer. Sample 1-85 had a frozen layer slightly thinner than sample 2-16. Although samples 1-85 and 2-16 did not show as clear of a delamination layer crack, their skins were still brittle and a thin detached skin layer was still present. The severe delamination layers of samples 0-16 and 0-85 corresponded to their relatively thick frozen layers.

Although the 3D simulation clearly shows the effect of coating thickness and mold temperature, the long execution time and some IMD design features prevented it from being used to give a detailed local view of how the cooling of the polymer was affected by applying a large number of different coating thicknesses and mold temperatures.

For the comparison of the 1D model with the 3D results, the temperature profiles of the samples at the end of the packing phase (6.54 s) are plotted in Figure 5.12. It is obvious that the 3D results had a viscous heating peak near the part surface where the shear is highest. Furthermore, the predicted center-line temperature from the 3D simulation was slightly lower than the 1D model, despite having viscous heating. Nonetheless, the surface and center temperatures of the 1D and 3D models agreed well. For example, the 1D model was able to capture the coating thickness and mold temperature interrelation on the cooling history as shown in the 3D results.

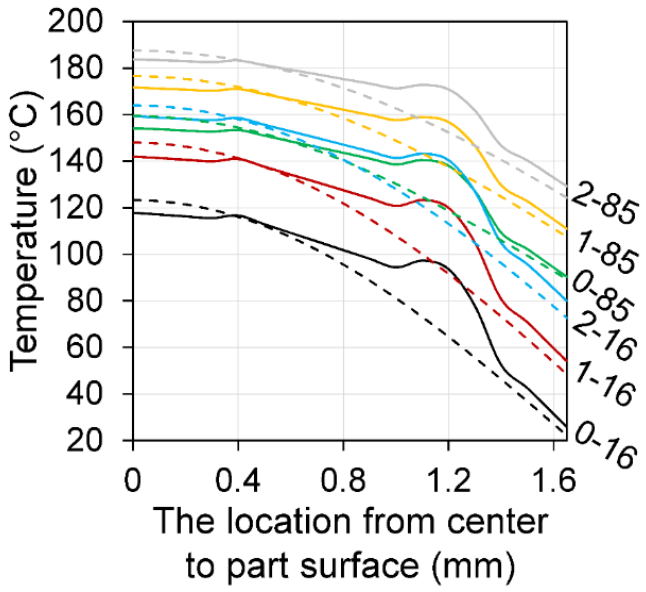

Figure 5.12. Temperature profile comparison from the center to the part surface at the end of packing; 1D model (dashed lines) and Moldex3D (solid lines).

Figure 5.12 shows that the temperature profile histories of the 2-16 and 0-85 samples are similar. This suggests that increasing the mold temperature from 16 to 85 °C (from 0-16 to 0-85 samples), and increasing the coating thickness from 0 to 250 μm (from 0-16 to 2-16 samples), have a similar influence on the cooling delay.

As we know, only the 2-85 samples are free of a delamination layer. The 2-16 samples with the same coating thickness had the delamination layer problem. This means that, at an unknown transition temperature that is between 16 and 85 °C, the delamination layer was eliminated for the two-layer (250 μm) coating.

From the 1D simulation results, the layer freezing time for the 2-85 sample was 8.44 s. Figure 5.13, which is based on the parametric sweep feature over a wide range of coating thicknesses and mold temperatures, has a horizontal line marking this time corresponding to the 250 μm coating thickness and a mold temperature of 85 °C.

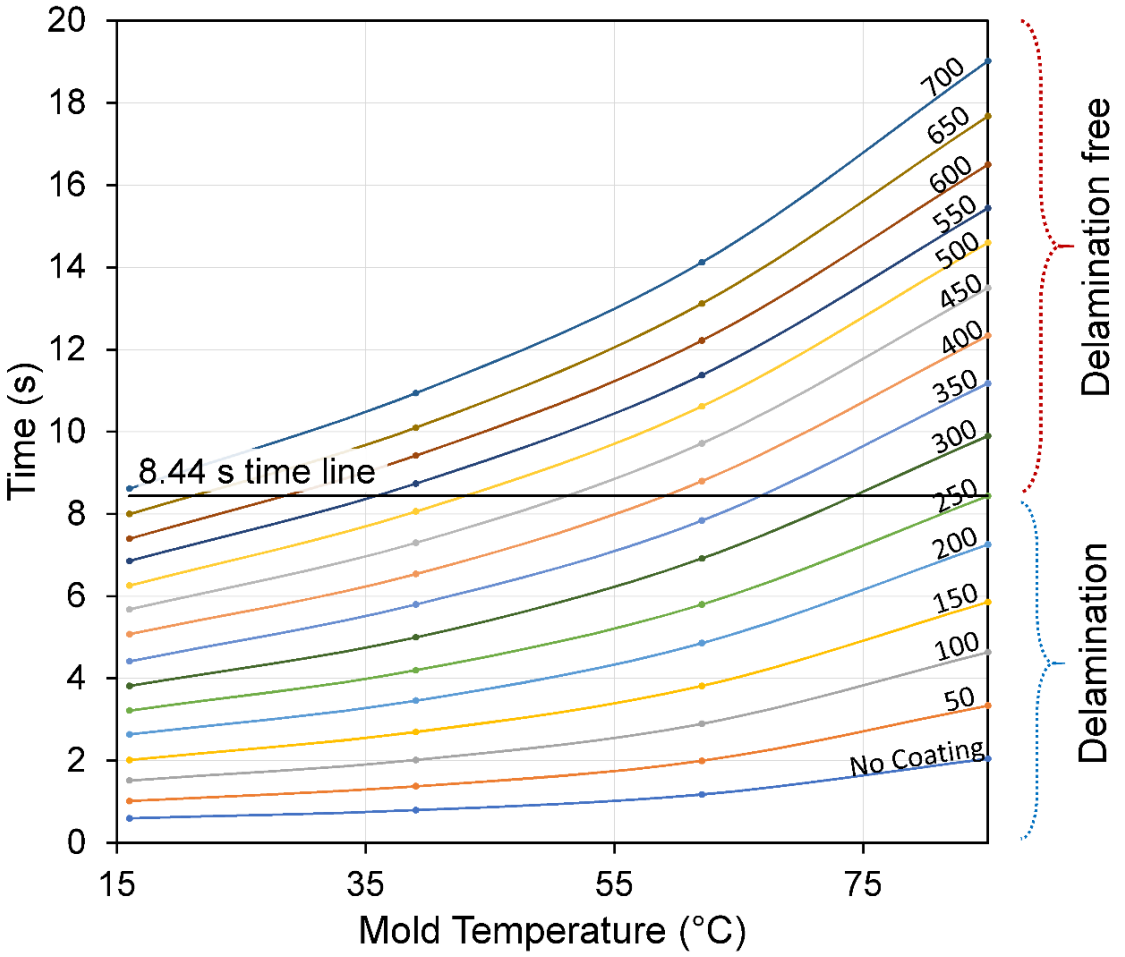

Figure 5.13. The layer freezing time based on the mold temperature and coating thickness (in μm).

The assumption based on the 2-85 samples is that any coating and mold temperature combination that has a layer freezing time equal to or greater than 8.44 s would be completely delamination free. This time assumption, in combination with a two-layer coating, can be refined by finding the actual transition temperature. However, for simplicity, we will keep using the time of 8.44 s at the 85 °C mold setting. By using the 8.44 s line in Figure 5.13, we found the corresponding mold temperature for each coating level above 250 μm; this is plotted in Figure 5.14. One can see the linear relationship and competing effect between decreasing the mold temperature and increasing the coating thickness.

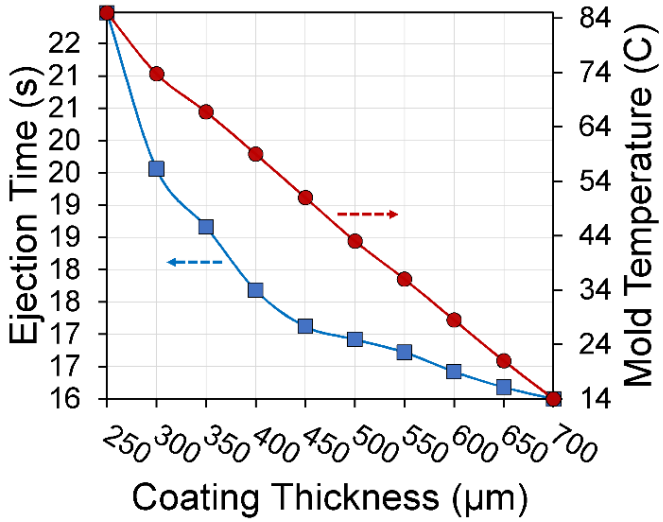

Figure 5.14. The corresponding mold temperature for each coating level, and the ejection time for increasing coating thickness.

Optimization of the ideal mold coating thickness and mold temperature can be determined based on two conflicting objectives. The first objective is having a minimum 8.44 s of layer freezing time to create a similar cooling history as the 2-85 samples. The second objective is that the part should be cooled as quickly as possible for cost savings. In this study, we assumed that the part could be ejected when the temperature at the delamination layer (300 μm from the part surface) was below 100 °C. (This value is well below the recrystallization temperature of UHMWPE, which is 117 °C).

In Figure 5.15, the cooling history at the delamination layer for ideal mold temperature (obtained from Figure 5.13) and the corresponding coating thicknesses (to reach an 8.44 s layer freezing time) are plotted. A vertical time of 8.44 s and two horizontal lines for the layer freezing temperature (135 °C) and ejection temperature (100 °C) were added for ease of reading. As expected, the layer temperature came down to 135 °C at 8.44 s (the intersection points of the two lines) for all sets. Then, the cooling behavior of the sets started to diverge and crossed the ejection temperature line at different times. These time values are plotted in Figure 5.14. As one

can see, increasing the coating thickness and decreasing the mold temperature is beneficial for reducing the ejection time. This reduction shows a diminishing effect in cooling time reduction, especially for a coating thickness above 500 µm and a mold temperature less than 25 °C.

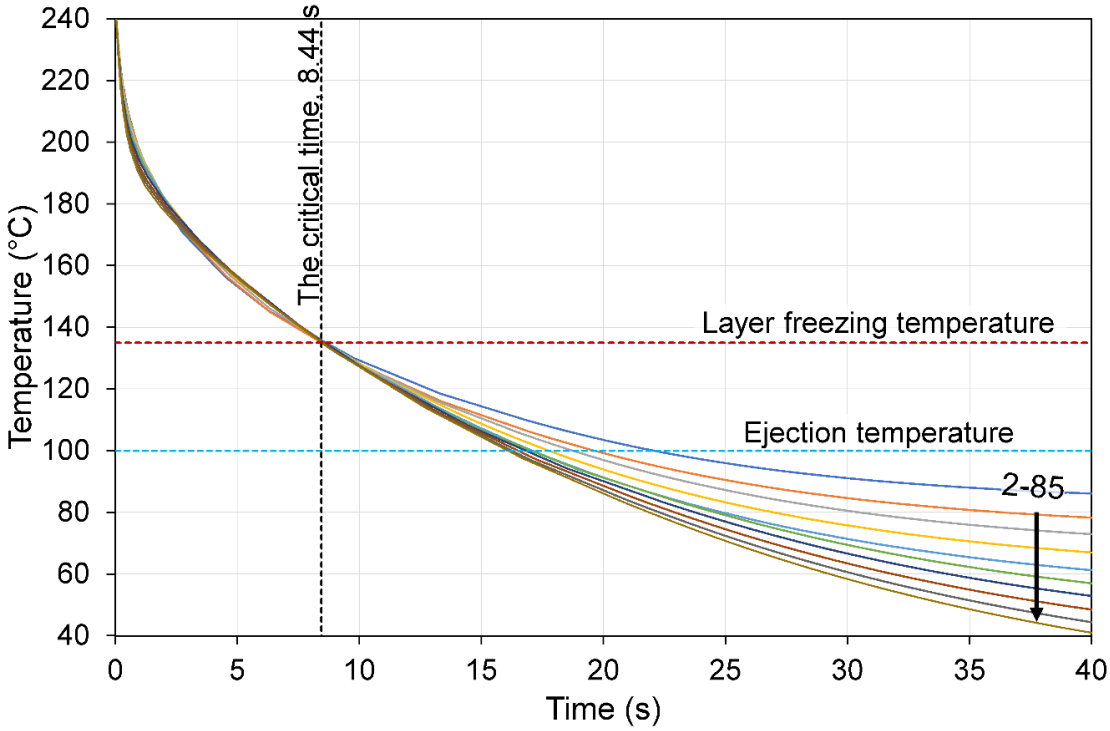

Figure 5.15. The cooling history of the delamination layer for the ideal mold temperature and coating sets. The black arrow shows the cases with increasing coating thickness and decreasing mold temperature.

5.5. Conclusions

A mold insulation method using a low-conductive coating was employed successfully to eliminate the UHMWPE powder delamination problem in injection molding. SEM images from impact tests showed that only the 250 µm thick coating, in conjunction with an 85 °C mold temperature, yielded a sample (2-85) free of a delamination layer. The tensile tests showed that the 2-85 sample exhibited more than twice as much extension as compared to other samples tested. Moreover, the 2-85 sample showed an instant break at the longest extension, while others

had a prolonged period of stress yielding as a result of the delamination layer peeling. Although the increase in the second heating % crystallinity of the samples compared to as-received powder indicated some thermal degradation, the high impact strength of the 2-85 sample suggested that the overall processing method and mold coating method together were very effective for creating high-quality UHMWPE injection molded parts with minimal thermal degradation. Computer simulations for a transient 1D model and a full 3D model matched well for the cooling history of the samples. Using parametric sweep 1D simulations, optimization of the cooling time, while avoiding delamination formation, was performed. It was found that using a thicker coating and lower mold temperatures yielded the best results in terms of part quality and overall cycle time. From the 3D simulations, it was found that delaying delamination layer freezing beyond the packing time was beneficial for avoiding delamination.

5.6. Acknowledgements

The authors would like to thank the Wisconsin Institute for Discovery at the University of Wisconsin–Madison for providing the research environment. The authors would like to thank the Celanese Corporation for their material donation.

CONCLUSION

In the first part, UHMWPE pellets were processed with scN_2 and $scCO_2$ as a reversible plasticizer via injection molding. Compared with regular injection molded samples, successful processing of UHMWPE was achieved by using scN_2 and $scCO_2$ to effectively reduce the required injection pressure and thermal degradation. In the second part, further studies were conducted on scN_2 for a box-shaped mold with varying wall thickness. The results showed that using scN_2 helped solve the challenging problem of short shots of UHMWPE parts. It was also beneficial for improving the dimensional accuracy of the final part by reducing the shrinkage.

Regardless of the use of SCFs, a characteristic flow pattern of UHMWPE was observed on short shot samples. UHMWPE failed to demonstrate typical fountain flow behavior; instead, it entered the mold cavity with a porous structure due to severe melt fracture. In regular injection molded samples of UHMWPE, short shot images showed that the porous structure solidified at a certain flow length when enough material had accumulated in front of the melt, which occurred before the mold filled completely. This led to an undesirable pressure increase and some delamination defects on the part's surface. However, this solidification process was delayed up to the packing cycle when scN_2 or $scCO_2$ was employed. This suggests that UHMWPE can be injection molded at even longer flow lengths without reaching unreasonable injection pressure values during the filling cycle.

In the third part, a more common grade of UHMWPE powder, which was more challenging, was used in injection molding with the injection–compression molding (ICM) method. Quality UHMWPE parts with minimal thermal degradation and surface defects were produced via processing parameter optimization, proper machine type, and a more suitable molding method with ICM capability.

In the last part, a robust and feasible mold coating method was implemented to solve the delamination problem. A 250 μm thick insulation coating, in conjunction with an 85 °C mold temperature, eliminated the delamination layer completely. Therefore, delamination-free samples retained UHMWPE's expected qualities in terms of very high impact strength and tensile extension. A transient 1D model and a full 3D model were used successfully to simulate the cooling history of the samples, with the result that the delamination layer could be avoided by delaying the cooling of the part skin.

FUTURE WORK

Several improvements on the injection molding of UHMWPE have been demonstrated in this thesis by way of bringing this technology into the real world. However, for accelerated implementation, there are still many aspects to explore for the molding of this special polymer, including those described below.

Understanding UHMWPE's Flow Characteristics and the SCF Effect

UHMWPE has unique flow characteristics and more work is needed to understand its nature. In-situ mold visualization techniques supported by pressure and temperature sensors could be used to further investigate UHMWPE mold filling from the inside. In particular, understanding the stick–slip behavior and frictional force between the UHMWPE melt and mold surface could be the target of future research projects. In addition, the injection pressure requirement of UHMWPE molding could be extremely high due to its high viscosity and the fast cooling requirement of the injection molding concept.

For a typical polymer (e.g., HDPE) experiencing typical processing settings, the slip of the melt on the mold surface is less likely. As such, a typical D-shape flow pattern called fountain flow in the mold slit occurs. As concluded in Chapters 2 and 3, the UHMWPE melt tends to slip on the mold surface at the early stages of mold filling, contrary to common polymers. This completely different flow type is called plug flow and requires a different (and presumably lower) pressure to overcome the surface friction to fill the cavity than typical fountain flow. However, the UHMWPE melt cannot maintain plug flow behavior beyond the early filling stages. Thus, promoting plug flow for an extended time could be an interesting way of increasing the ease of processing.

Employing SCFs can introduce lower friction via a gas buffer layer on the melt–mold interface during filling, thus promoting slipping of the plug flow behavior over a longer time and flow length. Further investigation is required to promote plug flow by SCFs. In addition, tuned processing settings and a better understanding of SCF behavior could allow for a very low injection pressure requirement.

Today's sophisticated computer simulation tools for plastic injection molding processes allow for time and money savings, as well as the ability to achieve better designs and more optimized processing parameters. However, current commercial software packages do not provide any material model for UHMWPE's flow type, which experiences severe melt fracture and high chain entanglement. As such, simulation code specific to UHMWPE's unique flow behavior has the potential to enable breakthroughs on the processing front.

Mold Technologies and New Applications

As indicated earlier in this thesis, injection molded UHMWPE is vulnerable to a delamination layer. It was found that some molding techniques—namely, ICM and the mold insulation method—have the ability to eliminate the delamination layer. For the ICM method, the optimum mold thickness, as well as the flow and compression ratios, is important to study in terms of the delamination formation. For larger flow ratios and lower compression ratios, the delamination layer is likely to re-occur. However, for larger compression ratios, the hesitation of the flow might be induced, especially for complex geometries. Therefore, further analysis of the relationship between delamination layer and compression ratio in the ICM method is necessary, especially for complex part designs.

As concluded in Chapter 3, UHMWPE tends to shrink a lot. The high shrinkage rate can easily cause visual and functional flaws. Therefore, further studies are necessary for predicting and reducing the shrinkage. Understanding how better processing conditions and mold design can reduce the shrinkage would likely yield better quality parts.

For the mold insulation method, an aluminum mold with an epoxy coating was used in this study for simplicity and proof-of-concept. However, in industry, steel molds and more durable coatings, such as PTFE-based coatings, are more common due to their durability. More work is needed to understand how different mold materials and coating material technologies can be used for the elimination of the delamination layer. Moreover, some mathematical models are needed to quickly evaluate how changing mold insulation thickness, mold temperature, and melt temperature affect the formation of a delamination layer. Moreover, these models are crucial in the mold design process.

UHMWPE is a versatile material that can be used to replace polyamides (PA) when moisture absorption, very cold weather environments, and/or higher friction of running parts are issues for PA. It can also be used to replace polytetrafluoroethylene (PTFE) when high abrasion rates and molding costs are an issue for PTFE. The major drawback of using UHMWPE, as compared to PTFE and PA, is the softening and melting point that occurs at a much lower temperature in UHMWPE. So far, only experimental parts have been produced. By utilizing the knowledge from this thesis, real parts can be produced and tested in real working environments. For example, UHMWPE could be beneficial for resistance impellers, bearings, sliding components, pump components, marine applications (to replace bronze parts), and in the medical field, where parts are required to be maintenance-free and lubrication-free.

REFERENCES

[1] J. B. P. Soares and T. F. L. McKenna, *Polyolefin Reaction Engineering*. Weinheim, Germany: Wiley-VCH, 2012.

[2] R. Geyer, J. R. Jambeck, and K. L. Law, "Production, use, and fate of all plastics ever made," *Science Advances*, vol. 3, no. 7, p. 1700782, Jul. 2017.

[3] A. J. Peacock, *Handbook of Polyethylene: Structures, Properties and Applications*. New York, NY, USA: Marcel Dekker, 2000.

[4] S. M. Kurtz, *The UHMWPE Biomaterials Handbook: Ultra-High Molecular Weight Polyethylene in Total Joint Replacement and Medical Devices*, 2nd ed. Burlington, MA, USA: Academic Press, 2009.

[5] A. A. Edidin and S. M. Kurtz, "Influence of mechanical behavior on the wear of 4 clinically relevant polymeric biomaterials in a hip simulator," *The Journal of Arthroplasty*, vol. 15, no. 3, pp. 321–331, Apr. 2000.

[6] M. P. Gispert, A. P. Serro, R. Colaço, and B. Saramago, "Friction and wear mechanisms in hip prosthesis: Comparison of joint materials behaviour in several lubricants," *Wear*, vol. 260, no. 1–2, pp. 149–158, Jan. 2006.

[7] R. Schaller, K. Feldman, P. Smith, and T. A. Tervoort, "High-performance polyethylene fibers 'Al dente': Improved gel-spinning of ultrahigh molecular weight polyethylene using vegetable oils," *Macromolecules*, vol. 48, no. 24, p. 24, 2015.

[8] "Webpage: What-is-UHMW-PE." [Online]. Available: https://www.celanese.com/engineered-materials/products/GUR-UHMW-PE/What-is-UHMW-PE.aspx. [Accessed: 13-Dec-2018].

[9] "Webpage: Endumax® | Teijin Aramid." [Online]. Available: https://www.teijinaramid.com/en/products/endumax/. [Accessed: 13-Dec-2018].

[10] P. Ciselli, R. Zhang, Z. Wang, C. T. Reynolds, M. Baxendale, and T. Peijs, "Oriented UHMW-PE/CNT composite tapes by a solution casting-drawing process using mixed-solvents," *European Polymer Journal*, vol. 45, no. 10, pp. 2741–2748, Oct. 2009.

[11] S. Uma Sankar and S. S. R. Gandham, "Easily processable ultrahigh molecular weight polyethylene and a process for preparation," US9624363B2, 2017.

[12] A. Sano, M. Oka, T. Kuroishi, and K. Matsuura, "Molding composition," US4786687A, 21-Apr-1986.

[13] T. Wyatt, Y. Deng, and D. Yao, "Fast solvent removal by mechanical twisting for gel spinning of ultrastrong fibers," *Polymer Engineering & Science*, vol. 55, no. 4, pp. 745–752, Apr. 2015.

[14] T. A. Osswald, L.-S. Turng, and P. J. Gramann, *Injection Molding Handbook*, 2nd ed. München, Germany: Hanser, 2008.

[15] T. A. Osswald, E. Baur, S. Brinkmann, K. Oberbach, and E. Schmachtenberg, *International Plastics Handbook*. München, Germany: Hanser, 2006.

[16] S. Gorden, H. van Laak, and H. Schmitz, "Process for the production of porous moldings," US5494629A, 1994.

[17] H. Chanzy, B. Rotzinger, and P. Smith, "Production of substantially linear highly crystalline polyolefins," 1991.

[18] D. Hofmann *et al.*, "Tailored nanostructured HDPE Wax/UHMWPE reactor blends as additives for melt-processable all-polyethylene composites and in situ UHMWPE fiber reinforcement," *Macromolecules*, vol. 50, no. 20, pp. 8129–8139, 2017.

[19] S. S. R. Gandham, A. B. Mathur, U. S. Satpathy, K. R. Sarma, and R. V. Jasra, "Disentangled ultra high molecular weight polyethylene graft co-polymers and a process for preparation thereof," WO2014045303A2, 10-Sep-2013.

[20] Y.-F. Huang *et al.*, "Melt processing and structural manipulation of highly linear disentangled ultrahigh molecular weight polyethylene," *Chemical Engineering Journal*, vol. 315, pp. 132–141, May 2017.

[21] G. Forte and S. Ronca, "Synthesis of disentangled ultra-high molecular weight polyethylene: Influence of reaction medium on material properties," *International Journal of Polymer Science*, vol. 2017, pp. 1–8, May 2017.

[22] K. T. Okamoto, *Microcellular Processing*. München, Germany: Hanser, 2003.

[23] J. Xu, *Microcellular Injection Molding*. Hoboken, NJ, USA: Wiley, 2010.

[24] I. Kikic, "Polymer-supercritical fluid interactions," *Journal of Supercritical Fluids*, vol. 47, no. 3. pp. 458–465, 2009.

[25] X. Sun and L. S. Turng, "Novel injection molding foaming approaches using gas-laden pellets with N2, CO2, and N2 + CO2 as the blowing agents," *Polymer Engineering and Science*, vol. 54, no. 4, pp. 899–913, Apr. 2014.

[26] D. L. Tomasko *et al.*, "Development of CO2 for polymer foam applications," *The Journal of Supercritical Fluids*, vol. 47, no. 3, pp. 493–499, Jan. 2009.

[27] M. J. Wingert, J. Shen, P. M. Davis, L. J. Lee, D. L. Tomasko, and K. W. Koelling, "Rheological studies of polymers under high pressure carbon dioxide," in *ANTEC*, 2005, pp. 1143–1147.

[28] J. Ehlers, N. Freisler, and H. van Laak, "Polyethylene composition for injection molding," US5658992A, 1997.

[29] W. Payer, M. Onallan, W. Materne, and A. Sobbe, "Process for pelleting ultra-high molecular weight polyethylene," US5393473A, 1993.

[30] L. Meinhard, G. Stanislaw, and H. Kerstin, "Filled granulates consisting of high or ultra-high molecular weight polyethylenes," US20050127555A1, 2005.

[31] H. A. Scheetz and R. C. Gilles, “Melt processable UHMWPE,” US4281070A, 1980.

[32] H.-P. Heim, *Specialized Injection Molding Techniques*, 1st ed. Oxford, UK: William Andrew, 2015.

[33] H. C. Kuo and M. C. Jeng, “The influence of injection molding on tribological characteristics of ultra-high molecular weight polyethylene under dry sliding,” *Wear*, vol. 268, no. 5–6, pp. 803–810, 2010.

[34] T. Shiraki, S. Hieda, and T. Ninomiya, “Injection molding of ultra high molecular weight polyethylene,” US4164531A, 1977.

[35] J. Beaumont, *Runner and Gating Design Handbook. Tools for succesful Injection Molding*. München, Germany: Hanser, 2007.

[36] H. McKellop, F. Shen, B. Lu, P. Campbell, and R. Salovey, “Development of an extremely wear-resistant ultra high molecular weight polythylene for total hip replacements,” *Journal of Orthopaedic Research*, vol. 17, no. 2, pp. 157–167, Mar. 1999.

[37] A.-H. I. Mourad, H. Fouad, and R. Elleithy, “Impact of some environmental conditions on the tensile, creep-recovery, relaxation, melting and crystallinity behaviour of UHMWPE-GUR 410-medical grade,” *Materials & Design*, vol. 30, no. 10, Dec. 2009.

[38] M. M. Xu, G. Y. Huang, S. S. Feng, G. J. McShane, and W. J. Stronge, “Static and dynamic properties of semi-crystalline polyethylene,” *Polymers*, vol. 8, no. 4, p. 77, Mar. 2016.

[39] B. D. M. Bryce, *Plastic Injection Molding Vol I: Manufacturing Process Fundamentals*, vol. I. Dearborn, MI, USA: Society of Manufacturing Engineers, 1996.

[40] H. C. Kuo and M. C. Jeng, “The influence of injection molding and injection compression molding on ultra-high molecular weight polyethylene polymer microfabrication,” *International Polymer Processing*, vol. 26, no. 5, 2011.

[41] S. P. Nalawade, F. Picchioni, and L. P. B. M. Janssen, “Supercritical carbon dioxide as a green solvent for processing polymer melts: Processing aspects and applications,” *Progress in Polymer Science*, vol. 31, no. 1, pp. 19–43, Jan. 2006.

[42] M. Garcia-Leiner, J. Song, and A. J. Lesser, “Drawing of ultrahigh molecular weight polyethylene fibers in the presence of supercritical carbon dioxide,” *Journal of Polymer Science Part B: Polymer Physics*, vol. 41, no. 12, pp. 1375–1383, Jun. 2003.

[43] E. Kiran, “Supercritical fluids and polymers - The year in review - 2014,” *Journal of Supercritical Fluids*, vol. 110. Elsevier, pp. 126–153, 01-Apr-2016.

[44] T. Ellingham, L. Duddleston, and L.-S. Turng, “Sub-critical gas-assisted processing using CO2 foaming to enhance the exfoliation of graphene in polypropylene + graphene nanocomposites,” *Polymer*, vol. 117, pp. 132–139, 2017.

[45] M. D. Wilding, D. G. Baird, and A. P. R. Eberle, “Melt Processability and Foam

Suppression of High Molecular Weight Polyethylenes Plasticized with Supercritical Carbon Dioxide," *International Polymer Processing*, vol. 23, no. 2, pp. 228–237, May 2008.

[46] C.-L. Hsu, L.-S. Turng, T. A. Osswald, N. Rudolph, E. Dougherty, and P. Gorton, "Effects of pressure and supercritical fluid on melt viscosity of LDPE in conventional and microcellular injection molding," *International Polymer Processing*, vol. 27, no. 1, pp. 18–24, Mar. 2012.

[47] X. Sun, H. Kharbas, J. Peng, and L. S. Turng, "A novel method of producing lightweight microcellular injection molded parts with improved ductility and toughness," *Polymer (United Kingdom)*, vol. 56, pp. 102–110, 2015.

[48] C. Hsu, L. Turng, and T. Osswald, "Effects of pressure and supercritical fluid on melt viscosity of LDPE in conventional and microcellular injection molding," *International*, 2012.

[49] H. A. Kharbas, "Developments in microcellular injection molding technology," University of Wisconsin - Madison, 2003.

[50] L.-S. Turng and H. Kharbas, "Development of a Hybrid Solid-Microcellular Co-injection Molding Process," *International Polymer Processing*, vol. 19, no. 1, pp. 77–86, Mar. 2004.

[51] H. Kharbas, T. Ellingham, and L.-S. Turng, "Use of core retraction to achieve low density foams in microcellular injection molded polypropylene parts," in *ANTEC 2016*, 2016, pp. 1285–1290.

[52] S. Gong, M. Yuan, A. Chandra, H. Kharbas, A. Osorio, and L. S. Turng, "Microcellular Injection Molding," *International Polymer Processing*, vol. 20, no. 2, pp. 202–214, May 2005.

[53] V. Shaayegan, G. Wang, and C. B. Park, "Effect of foam processing parameters on bubble nucleation and growth dynamics in high-pressure foam injection molding," *Chemical Engineering Science*, vol. 155, pp. 27–37, Nov. 2016.

[54] V. Shaayegan, C. Wang, F. Costa, S. Han, and C. B. Park, "Effect of the melt compressibility and the pressure drop rate on the cell-nucleation behavior in foam injection molding with mold opening," *European Polymer Journal*, vol. 92, pp. 314–325, 2017.

[55] B. Wunderlich and C. M. Cormier, "Heat of fusion of polyethylene," *Journal of Polymer Science Part A-2: Polymer Physics*, vol. 5, no. 5, pp. 987–988, Sep. 1967.

[56] T. A. Osswald and N. Rudolph, *Polymer Rheology: Fundamentals and Applications*. Munich, Germany: Hanser, 2015.

[57] W. Pang, Z. Ni, G. Chen, G. Huang, H. Huang, and Y. Zhao, "Mechanical and thermal properties of graphene oxide/ultrahigh molecular weight polyethylene nanocomposites," *RSC Adv.*, vol. 5, no. 77, pp. 63063–63072, Jul. 2015.

[58] M. Yasuniwa, S. Tsubakihara, and C. Nakafuku, “Molecular weight effect on the high pressure crystallization of polyethylene,” *Polymer Journal*, vol. 20, no. 12, pp. 1075–1082, Dec. 1988.

[59] J. Kubaut, J.-A. Manson, and M. Rigdahl, “Influence of mold design on the mechanical properties of high-pressure injection—molded polyethylene,” *Polymer Engineering and Science*, vol. 23, no. 16, pp. 877–882, Nov. 1983.

[60] G. Kalay, R. A. Sousa, R. L. Reis, A. M. Cunha, and M. J. Bevis, “The enhancement of the mechanical properties of a high-density polyethylene,” *Journal of Applied Polymer Science*, vol. 73, no. 12, pp. 2473–2483, Sep. 1999.

[61] T. A. Osswald and G. Menges, *Material science of polymers for engineers*. München, Germany: Hanser, 2012.

[62] M. Sauceau, J. Fages, A. Common, C. Nikitine, and E. Rodier, “New challenges in polymer foaming: A review of extrusion processes assisted by supercritical carbon dioxide,” *Progress in Polymer Science*, vol. 36, no. 6, pp. 749–766, Jun. 2011.

[63] P. M. Joseph and R. D. Spital, “The exponential edge-gradient effect in x-ray computed tomography.,” *Physics in medicine and biology*, vol. 26, no. 3, pp. 473–87, May 1981.

[64] A. B. Strong, *Plastics : Materials and Processing*, 3th ed. Pearson Prentice Hall, 2006.

[65] H.-C. Kuo and M.-C. Jeng, “Effects of part geometry and injection molding conditions on the tensile properties of ultra-high molecular weight polyethylene polymer,” *Materials & Design*, vol. 31, no. 2, 2010.

[66] G. Yilmaz, T. Ellingham, and L. S. Turng, “Injection and injection compression molding of ultra-high-molecular weight polyethylene powder,” *Polymer Engineering and Science*, vol. 59, no. s2, pp. E170–E179, Dec. 2019.

[67] G. Yilmaz, T. Ellingham, and L.-S. Turng, “Improved processability and the processing-structure-properties relationship of ultra-high molecular weight polyethylene via supercritical nitrogen and carbon dioxide in injection molding,” *Polymers*, vol. 10, no. 1, p. 36, Dec. 2017.

[68] S. Kurtz, O. Muratoglu, M. Evans, and A. Edidin, “Advances in the processing, sterilization, and crosslinking of ultra-high molecular weight polyethylene for total joint arthroplasty,” *Biomaterials*, 1999.

[69] B. Kim and M. Niemeyer, “Insulated mold structure for injection molding of optical disks,” US5458818A, 1993.

[70] Y. F. Huang *et al.*, “Melt processing and structural manipulation of highly linear disentangled ultrahigh molecular weight polyethylene,” *Chemical Engineering Journal*, vol. 315, May 2017.

[71] J. Fisher, H. M. J. McEwen, P. I. Barnett, C. Bell, M. H. Stone, and E. Ingham, “Influences of sterilising techniques on polyethylene wear,” *The Knee*, vol. 11, no. 3, Jun.

2004.

[72] L. Costa, K. Jacobson, P. Bracco, and E. M. Brach del Prever, “Oxidation of orthopaedic UHMWPE,” *Biomaterials*, vol. 23, no. 7, Apr. 2002.

[73] J. V. Gulmine, P. R. Janissek, H. M. Heise, and L. Akcelrud, “Polyethylene characterization by FTIR,” *Polymer Testing*, vol. 21, no. 5, Jan. 2002.

[74] A. Kömmling, K. von der Ehe, D. Wolff, and M. Jaunich, “Effect of high-dose gamma irradiation on (U)HMWPE neutron shielding materials,” *Radiation Physics and Chemistry*, vol. 142, Jan. 2018.

[75] H. Hinsken, S. Moss, J.-R. Pauquet, and H. Zweifel, “Degradation of polyolefins during melt processing,” *Polymer Degradation and Stability*, vol. 34, no. 1–3, Jan. 1991.

[76] S. K. Bhateja and E. H. Andrews, “Thermal, mechanical, and rheological behavior of blends of ultrahigh and normal-molecular-weight linear polyethylenes,” *Polymer Engineering and Science*, vol. 23, no. 16, Nov. 1983.

[77] M. Deng and K. E. Uhrich, “Viscoelastic behaviors of ultrahigh molecular weight polyethylene under three-point bending and indentation loading,” *Journal of Biomaterials Applications*, vol. 24, no. 8, 2010.

[78] F. J. Medel, P. Peña, J. Cegoñino, E. Gomez-Barrena, and J. A. Puértolas, “Comparative fatigue behavior and toughness of remelted and annealed highly crosslinked polyethylenes,” *Journal of Biomedical Materials Research - Part B Applied Biomaterials*, vol. 83, no. 2, Nov. 2007.

[79] J. Fu, B. W. Ghali, A. J. Lozynsky, E. Oral, and O. K. Muratoglu, “Ultra high molecular weight polyethylene with improved plasticity and toughness by high temperature melting,” *Polymer*, vol. 51, no. 12, May 2010.

[80] J. F. Vega, S. Rastogi, G. W. M. Peters, and H. E. H. Meijer, “Rheology and reptation of linear polymers. Ultrahigh molecular weight chain dynamics in the melt,” *Journal of Rheology*, vol. 48, no. 3, May 2004.

[81] A. J. Hsieh, T. L. Chantawansri, W. Hu, J. Cain, and J. H. Yu, “New insight into the influence of molecular dynamics of matrix elastomers on ballistic impact deformation in UHMWPE composites,” *Polymer*, vol. 95, pp. 52–61, Jul. 2016.

[82] M. Merola and S. Affatato, “Materials for hip prostheses: A review of wear and loading considerations,” *Materials*, vol. 12, no. 3, p. 495, Feb. 2019.

[83] J. Fu, B. N. Doshi, E. Oral, and O. K. Muratoglu, “High temperature melted, radiation cross-linked, vitamin E stabilized oxidation resistant UHMWPE with low wear and high impact strength,” *Polymer*, vol. 54, no. 1, pp. 199–209, Jan. 2013.

[84] B. G. Liu, K. Kandan, H. N. G. Wadley, and V. S. Deshpande, “Deep penetration of ultra-high molecular weight polyethylene composites by a sharp-tipped punch,” *Journal of the Mechanics and Physics of Solids*, vol. 123, pp. 80–102, Feb. 2019.

[85] Y. Chen, Y. Qi, Z. Tai, X. Yan, F. Zhu, and Q. Xue, “Preparation, mechanical properties and biocompatibility of graphene oxide/ultrahigh molecular weight polyethylene composites,” *European Polymer Journal*, vol. 48, pp. 1026–1033, 2012.

[86] C. J. Bell, P. S. Walker, M. R. Abeysundera, J. M. H. Simmons, P. M. King, and G. W. Blunn, “Effect of oxidation on delamination of ultrahigh-molecular-weight polyethylene tibial components,” *The Journal of Arthroplasty*, vol. 13, no. 3, pp. 280–290, Apr. 1998.

[87] V. Saikko, “Effect of shelf versus accelerated aging of UHMWPE on delamination in knee wear simulation,” *Tribology International*, vol. 73, pp. 10–16, May 2014.

[88] P. Gao and M. R. Mackley, “The structure and rheology of molten ultra-high-molecular-mass polyethylene,” *Polymer*, vol. 35, no. 24, pp. 5210–5216, 1994.

[89] J. Lee and L.-S. Turng, “Improving surface quality of microcellular injection molded parts through mold surface temperature manipulation with thin film insulation,” *Polymer Engineering & Science*, vol. 50, no. 7, pp. 1281–1289, Jul. 2010.

[90] S.-C. Chen, Y. Chang, Y.-P. Chang, Y.-C. Chen, and C.-Y. Tseng, “Effect of cavity surface coating on mold temperature variation and the quality of injection molded parts,” *International Communications in Heat and Mass Transfer*, vol. 36, no. 10, pp. 1030–1035, Dec. 2009.

[91] P. Xie *et al.*, “Carbide-bonded graphene coating of mold insert for rapid thermal cycling in injection molding,” *Applied Thermal Engineering*, vol. 122, pp. 19–26, Jul. 2017.

[92] G. Wang, Y. Hui, L. Zhang, and G. Zhao, “Research on temperature and pressure responses in the rapid mold heating and cooling method based on annular cooling channels and electric heating,” *International Journal of Heat and Mass Transfer*, vol. 116, pp. 1192–1203, Jan. 2018.

[93] S. Ganguli, A. K. Roy, and D. P. Anderson, “Improved thermal conductivity for chemically functionalized exfoliated graphite/epoxy composites,” *Carbon*, vol. 46, no. 5, pp. 806–817, Apr. 2008.

[94] J. Gu, Q. Zhang, J. Dang, and C. Xie, “Thermal conductivity epoxy resin composites filled with boron nitride,” *Polymers for Advanced Technologies*, vol. 23, no. 6, pp. 1025–1028, Jun. 2012.